Al- Farabi Kazakh National University

UDC 621.376.234

JAPASHOV NURSULTAN

Development of high- sensitive detection system based on large- sized silicon lithium structures

6D071900 - Radio engineering electronics and telecommunications

Dissertation is submitted in fulfillment of the requirements for the degree of the Doctor of Philosophy (PhD)

Scientific consultants:

PhD, Saymbetov A. K.
Department of Physics and Technology,
Al- Farabi Kazakh National University,
Almaty, Kazakhstan

Prof. Shur M. S., PhD
Rensselaer Polytechnic Institute,
Troy, New York, US

Republic of Kazakhstan
Almaty, 2018

CONTENT

SYMBOLS AND ABREVIATIONS:

SCD	semiconductor detectors
SD	silicon detectors
PD	pixel detectors
MSD	microstrip detectors
DSSD	double sided silicon detector
LHC	*Large Hadron Collider*
LHCb	Large Hadron Collider beauty experiment
SPS	Super Proton Synchrotron
CERN	European Organization for Nuclear Research
ALICE	A Large Ion Collider *Experiment*
PHENIX	Pioneering High Energy Nuclear Interaction experiment
RHIC	relativistic heavy ion collider
CMS	Compact Muon Solenoid
KEKW	High Energy Accelerator Research Organization
STAR	Solenoidal tracker (detector at *Large Hadron Collider*)
e^-	electron
p	proton
eV	electron Volt
h^+	hole

INTRODUCTION

The general characteristics of the study

The thesis is devoted to the development, research and application of spectrometric instruments for registration of X- ray radiation. Special attention was paid to the development of semiconductor detector and readout electronics for this. In the framework of this work, it was proposed a new method for double sided diffusion and double sided drift of lithium ions into a mono- crystalline silicon wafer for the further fabrication of Si (Li) p-i-n nuclear radiation detectors with a diameter of the sensitive area more than 110 mm and with a thickness of the sensitive region more than 4 mm. The theoretical assumptions and experimental characteristics of double sided diffusion are considered. To obtain the structure, dislocation-free p-type mono-crystal silicon grown by the Czochralski method and crystal silicon obtained by float-zone method were taken as the initial materials. Also, an optimized, fast-acting, low-noise read-out electronics was developed, an algorithm and a block diagram of the detecting system were proposed.

Actuality of the study

Today, silicon detection systems are widely used in the field of registration of various types of particles and radiations. One of the main advantages of this kind of detector systems is low energy, high efficiency of statistics collection, good radiation resistance. Due to such characteristics, silicon detection systems are the object of research and products of various laboratories from around the world. One of them is CANBERRA - which develops and manufactures silicon detectors and spectrometers for research and industrial needs. One of the leaders in the design and production of ionizing radiation detection systems is the industrial organization ORTEC. There are many worldwide laboratories, such as the Brookhaven National Laboratory, the laboratory of semiconductor detectors of the Institute of High Energy Physics, etc. who are engaged in research and development of semiconductor detectors and spectrometers.

At the same time, the registration of various types of particles and radiation continues to be a special task of science and technology. Among them, a special place is occupied by detection systems, based on nuclear radiation with high energy, good positional resolutions, signal linearity in a wide range of energy for various types of ionizing particles. One of the important technological, scientific and technical stages of obtaining highly efficient detection systems is the correct understanding of physical, technological and structural solutions. As the detector is an integral part of spectrometric systems, the process of formation of detector structures, plays very important role in development of spectrometric systems. The high energy resolution of the detector, the linearity of the output signal and the high operating ability of the detector ensures the successful operation of the whole system. In this matter, a special place is occupied by the quality of the initial crystal material for the detectors. In our study, monocrystalline

silicon was chosen as the initial material. Comparing with other materials Silicon meets all of the above requirements.

It is well known that the Ge-detectors have the highest functional characteristics, but they work under temperature T≤77K, so they need cooling system with liquid nitrogen during the work process. The technologies of production of monocrystals, such as - GaAs, CdTe and CdZnTe, as initial material for detector manufacturing have low efficiency of detection and small energy resolution.

Nowadays, in the world practice detectors with relative small size are well developed. Simultaneously, the development of silicon detectors with big size is necessary. In comparison with other semiconductor devices, such as diodes, transistors, thyristors and etc., the structures of detector should correspond with high requirements related to their current, charge, capacitance, noise, spectrometric and time characteristics, also with the sameness of identification of ionizing radiation regardless of its contact with any part of the sensitive area of the detector. In this regard, it is important to study the technological issues caused by effects of big size semiconductor crystals for forming required detector structures with p-n and p-i-n junctions.

There is a need to increase the information taken from the spectrometer, both about the particle itself and about the processes occurring in the detector at the time of its registration. This statement is trivial, but its implementation by analog electronic methods is very problematic, since almost all the available resources are already involved. With the digital method of signal analysis, it becomes possible to use powerful mathematical methods inaccessible to analog electronics. This allows a new level to analyze the pulse shape and extract additional information from it.

Improving the stability of the spectrometers. The properties of electronic components that make up analog spectrometers vary with environmental conditions (temperature, humidity, mains voltage, etc.). Despite the widely developed systems of stabilization and compensation, the problem remains relevant for almost any experiments. In digital signal processing, much of the work done by electronic modules is transferred to computer programs. Therefore, the stability of the entire system increases.

Achieve better resolution of spectrometers. The task of improving the resolution of the spectrometer is always relevant. There are known effects that interfere with its improvement (ballistic defect, non-optimal filtering of signals, etc.); however, this is difficult to implement using analog electronics. Means of digital signal processing can restore the signals and thereby reduce the effects of a ballistic defect. In addition, it is possible, before starting processing a particular signal, taking into account the peculiarities of its shape, to design an individual filter that optimally matches this signal.

The purpose of research - in order to construct high efficient, low cost spectrometer for X – ray radiation it is needed to develop technology of manufacturing of Si(Li) p-i-n detectors of large size and create suitable electronics for these detectors.

To achieve this purpose, the following tasks were set:

-To chose suitable initial materials for detectors.

-To study experimentally electro-physical characteristics of initial material for detectors.

-To develop the technological modes of double-sided diffusion of lithium atoms in silicon wafers of large sizes;

- To develop the technological modes of double-sided drift of lithium ions in silicon wafers of large sizes;

- To develop suitable and high efficient readout electronics for large size Si(Li) p-i-n detectors;

- Hardware implementation for highly efficient spectrometric system based on large size Si(Li) p-i-n detectors;

Objects of research:

Object is a highly sensitive X-ray detection system and Si (Li) p-i-n structured detectors.

Subject of study

Subjects of the research is the physical mechanisms and technology for the development of both detectors and detection systems.

The main provision for the defense

- The optimal regime for lithium diffusion into large-diameter silicon (≥110 mm) with a thickness of the sensitive region W ≥ 4 mm is at a temperature T = (450 ± 20) ^{0}C, t = 3 min, h_{Li} = (300 ± 10) μm.

- The method of conducting a double sided drift of lithium ions into a silicon monocrystal is performed by a synchronous stepwise increase in temperature from 55 ^{0}C to 100 ^{0}C and a reverse bias voltage from 70V to 200V.

- The technology of double-sided drift of lithium ions into a silicon monocrystal improves spectrometric characteristics, increases the efficiency of the detection system and reduces the time to manufacture the detector.

- The charge-sensitive preamps for silicon detectors have high speed (rise time no more than 5 ns), low sensitivity to the input capacitance, which ensures, as a result, a low-noise amplifier with a level of 0.45 nV/Hz$^{1/2}$ and its stability, and the possibility of matching the impedance of the connected line and the input of the amplifier.

Scientific novelty

- Experimentally, it was found the regimes of diffusion of lithium atoms in a silicon single crystal were detected, for the manufacture of a detector with a sensitive area greater than 110 mm^2 and a thickness of 4 mm.

-Technological regimes of double-sided drift of lithium ions into monocrystalline silicon were experimentally determined, including a synchronous step change in temperature and reverse bias voltage leading to a reduction in the drift path of penetration of lithium ions and to a more homogeneous detector structure, thereby reducing the energy resolution of the detector for beta particles by 5 keV and for alpha particles at 7 keV.

- Theoretical calculations and experimental data showed that the technology of double-sided drift reduces the manufacturing time of the Si (Li) p-i-n structure by four times.

- The developed charge-sensitive preamplifier for a Si (Li) p-i-n structured detector showed a low noise level; for detectors with an output capacitance of 300 pF, the mean square deviation of the noise current is 45 nA and the minimum delay time is up to 8 ns. Also, it is established that the preamplifier is fully compatible with other, alternative, silicon detectors with an output capacitance from 10 to 1300 pF.

Method of research

The Si (Li) p-i-n detector structure was obtained by the method of double-sided diffusion and drift of lithium ions on a silicon wafer. The determination of the electro-physical characteristics of the detector and the entire detection system was carried out by theoretical calculation and then experimental measurements. The electronic part of the system was built by modeling, theoretical calculation, then by an experimental method.

Scientific and practical significance of the work

In the dissertation work, new theoretical and experimental features of the formation of large sized Si (Li) p-i-n structures are considered. The creation of such detector structures is associated with a more detailed and in-depth understanding of the electrical properties of the original silicon of large diameter, and the establishment of their relationship with the requirements for obtaining high-performance Si (Li) p-i-n structures. These scientific results are important for understanding the physical processes for various large-sized semiconductor devices, as well as practical implications for improving their characteristics.

Development of unique spectrometers based on Si (Li) p-i-n detectors of large sizes opens up new opportunities to conduct research in the field of science and technology to study the physics-chemical properties of environmental objects. This development will open new perspectives in the development of science and industry in improving the quality of information processing of radioactive radiation, which further allows its use in seismology, geology, medicine and. etc.

Consequently, to complete these requirements in this work it was developed digital electronics for large sized Si(Li) p-i-n structured detectors. Also, algorithm for reading digital electronics of the detecting system has been created with respect to electro-physical and radiometric characteristics of the detecting system.

Personal contribution of the author is that the author was directly involved in obtaining the main scientific results. All the results of a physical experiment, theoretical calculations, numerical analysis of models, the assembly of the detecting system were obtained personally by the author. The setting of tasks and the development of ideas were carried out in collaboration with scientific consultants. All publications on the topic of the thesis were prepared with his direct participation.

Reliability of results

- The theoretical part described in this paper is a continuation of the well-known scientific works in the field of electronics and semiconductor electronics. The results obtained are associated with the works of previous research and their logical continuation.

- The experimental and theoretical results given in the paper are in good agreement.

- The developed X-ray detection system is fully functional.

Approbation testing of thesis

The main results of the thesis were presented and discussed at the seminars of the Physics and Technology Faculty of the Al-Farabi Kazakh National University, as well as at the following international conferences:

- Fourth International Conference on Radiation and Application in Various Fields of Research (2016, Niš, Serbia);

- International scientific conference of students and young scientists "Farabi alemi" (2018, Almaty, Kazakhstan);

- The results of dissertation was implemented in household activity of LTD «Scientia Kazakhstan», for determination of radiation level of equipment.

Publications

According to the materials of the dissertational work, 11 publications were published. From which 8 are articles, 2 in an international scientific publication, having citations in Thomson Reuters database (ISI Web of Knowledge, Thomson Reuters), which is also included in the Scopus database, 6 articles in scientific publications recommended by the Committee on the Control of Education and Science of the Ministry of Education and Science of the Republic of Kazakhstan, 1 report at an abroad international conference and 2 reports at local international conference.

Structure and volume of the dissertation

The dissertation consists of an introduction, four chapters, conclusions and a list of references. It is presented on 114 pages of typewritten text, contains 56 figures, 4 tables, 148 references.

1. BASIC CONCEPTS OF SEMICONDUCTOR DETECTING SYSTEMS.

This chapter provides an overview of the current state of the radiation detection system based on silicon detectors. An analysis was made of various types of detectors, such as strip detectors, surface barrier detectors, scintillation detector, pixel detectors, etc., which are the main part of the detecting systems. It has been determined that today, in well-developed spectrometers, Si(Li) detectors are widely used to determine radiation levels. The principle of operation of semiconductor detectors is explained. Their electro-physical characteristics, spectrometric and noise characteristics are considered. The most important characteristic of detectors is the energy decay of the detector, which has different meanings for different detectors. Also, one of the main issues is the technology for obtaining detectors. It analyzed various technologies for obtaining silicon detectors, their advantages and weaknesses. The problems in the manufacture of silicon detectors and their possible solutions are shown.

In the second part of the first chapter, the electronic part of the acting detection systems is analyzed. Here the characteristics of the detector output signals are described in detail, the readout electronics of the detector output signals are described. Each part of the detector is analyzed, the electronic circuits of the detecting system and the waveforms of the corresponding circuit was given. Also, here it is made a comparative analysis of analog and digital electronics. The types of analogue-digital converters, which use in such detecting systems were shown. The existing problems in the electronics of detecting radiation was identified.

Silicon and other semiconductor detectors (SCD) appeared in the early 1960s of the previous century and occupied one of the leading places in the arsenal of devices for registration nuclear radiation. SCD possess such valuable qualities as high energetical and spatial resolution, linearity of characteristics in a wide range of energy losses absorbed by them, the possibility of providing a good geometry of the experiment, insensitivity to magnetic fields, good operability at low temperatures, compactness, mechanical strength and etc.

Description of the properties of early SCD. (60-80s) and their application in practice can be found in [1-3].

Among semiconductors, which are the basis for constructing SCD, silicon is the most widely used. Silicon detectors (SD) occupy a special place in experiments on elementary particle accelerators. Applicability of SD with their low signal amplitude in conditions of a high level of interference in such experiments firstly was demonstrated at the synchrophasotron [4], which allowed to successfully carry out a number of actual studies in various accelerators of high-energy particles in the 1970s [5].

Successes in the development of the technology of SCD production, as well as in the development of the low-noise multi-channel electronics matched with them, made it possible to create precision position-sensitive (track, or coordinate) SD and their successful use in the physics of elementary particles, astrophysics, fluoroscopy and other

fields of experimental physics and technology. Such detectors are performed on the same substrate in the form of microstrips or microcells, usually in the form of quadrilaterals (pads / pixels) [6]. The latter also include charge-coupled devices. Silicon drift detectors also have a high interest [7].

1.1 The operating principle of semiconductor radiation detectors.

Semiconductors are crystals, band structure of which is schematically shown in Fig.1.1. Electrons fully fill the valence band with energy levels $\leq E_v$. The free levels ($\geq E_c$) which situated above form a conduction band. Both zones are separated by a zone of forbidden for electrons condition with a width ΔE_g. If an electron located in the valence band is given energy exceeding ΔE_g, then it gets the opportunity to go into the conduction band. The excitation energy can arise as a result of thermal fluctuations leading to local temperature increases. The electrons that have passed into the conduction band create current. In particular, for silicon, $\Delta E_g = 1.1E_v$. Semiconductors are characterized, although not very large, but by an appreciable intrinsic electrical conductivity, due to the direct transition of electrons from the valence band to the conduction band as a result of local temperature fluctuations. Volume density of charge carriers

$$n_i \infty \exp(-\frac{\Delta E g}{2kT})$$

where k-Boltzmann constant, and T-temperature in absolute units. In silicon at room temperature, n_i=1.45×10^{10}см$^{-3}$when the temperature falls, n_i decreases, i.e the electrical conductivity decreases.

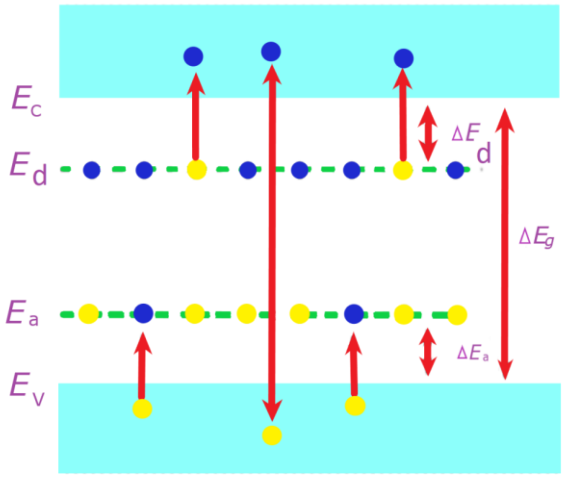

Figure 1.1 – Schematic diagram of semiconductor structure. E_c and E_v are the boundary levels of the conduction band and the valence band, respectively, and E_d and E_a are the levels of the donor and acceptor impurities, respectively.

Semiconductors always contain a certain amount of impurities of other elements whose energy levels can lie either near the conduction band (E_d) or the valence band

(E_a). In the first case, the electrons of impurity (donor) atoms freely pass into the conduction band, and in the second - on the contrary, impurity (acceptor) atoms absorb electrons from the valence band. Semiconductors with donor impurities refer to the *n* -type, while semiconductors with acceptor impurities refer to the *p* -type.

To produce detectors, usually used material, in which the density of impurities equal to – 10^{12}cm^{-3}, which is 3-4 times less, than in the material for manufacturing recording electronic devices. The resistivity of silicon ρ is inversely proportional to the amount of impurities contained in it: donor N_d or acceptor -N_a. In particular, at a concentration of $5x10^{11}$ см$^{-3}$, the resistivity ρ =10 kΩ * cm.

Semiconductors contain impurities of both types. Electrons from donor levels jump to lower acceptor levels. As a result of such recombination, the effect of impurities is compensated. The conductivity type of a semiconductor is determined by the conductivity that is present in a larger quantity. The difference in their concentration is the effective concentration of $N_{eff}=|N_d-N_a|$ determines the resulting electrical conductivity of the semiconductor resistance. In order to reduce the electrical conductivity, controlled amount of impurity, which initial concentration is lower, can be added into the semiconductor. This process is called semiconductor alloying. However, the strongest decrease in electrical conductivity is achieved by the creation of a *p*-*n*-junction in a semiconductor [8].

The formation of the *p*-*n* junction occurs in such way that to the *p*-type material, which is rich in electrons, *p*-type material is deposited, which is rich in holes (hole-absence of an electron in an atom). At the boundary of these materials, electrons will go to that direction where the amount of holes big, i.e. will penetrate into the *p*-type material, leaving behind positively charged ions. In turn, the hole is directed toward the *n* type material, which will lead to the formation of *n*-type material, which will lead to the formation of a negative charge in the *p*-type material. The resulting potential barrier will prevent further transfer of charge carriers, which eventually terminates, and at the boundary of the p and n materials a region with depleted number of charge carriers will be formed. The depth of this region can be increased, attaching to outer boundaries of *p*-*n*junction inverse bias voltage to *p* layer.

$$d, \mu m = A[(V + \varphi_0)\rho]^{1/2}, \quad (1.1)$$

whereφ_0 = 0.5B is the potential of *p*-*n* junction without an external voltage, ρ is the resistivity of the material. A = 0,53. For example, at ρ = 2000 Ω * cm and V = 150 V, we obtain d = 300 μm. Expression (1) refers to the *n*-*p*-junction, i.e. when the starting material is silicon of *p*-type, only in this case A = 0.32 [9].

1.2 Types of semiconductor detectors

Depending on the method of creating the p-n-junction, there are surface-barrier, diffusion, ion-doped semiconductor detectors, etc. [10].By topology, silicon detectors can be divided into microstrip, pad and pixel [11]. In microstrip detectors, a cell is a strip which width is about hundreds of microns and a length of up to tens of centimeters, if several sensors are connected in series to a ruler - a "ladder" [12]. In the pad and pixel detectors, the cell has a comparable length and width. Pixel systems [13] are used under high load conditions, which allows to reduce the frequency of events in one cell. The downside of this is the need to read more channels.

The pixel sensor determines two coordinates at once; in micro-strip detectors, for this purpose, two-sided sensors or two "back-to-back" sensors are installed so that their strips intersect.

1.2.1. Surface-barrier detectors

The simplest SCD is a *p*-*n*-junction made on the basis of *n*-type silicon, and as the *p*-type material used gold, which is an acceptor and simultaneously serves as an electrode. Gold is sprayed with a thin layer (-50 nm or less) to minimize the loss of particles passing through it (the window). In this structure, the depleted layer starts very close to the surface. Standard material for the back electrode SCD is aluminum [14].

Under the action of energy left in the SCD ionizing particles, electrons from the valence band or from the lower filled zones are transferred to the conduction band or to the above-situated filled zones. After interaction with the crystal lattice accompanied by the emission of phonons, in a very short time (-10 psec), all electrons situate at the bottom of the conduction band, and holes are at the top of the valence band. Transmission of a significant fraction of the energy required to form an electron-hole pair, which in silicon is E_0=3,66eV [15].

Thus, the front electrode implements the function of rectifying contact, and the back electrode must be only an ohmic contact. To reduce the resistance of the transition from the *n*-layer to the metal, on the border with it, the content of the electrons are increased - creating a layer of *n*+. Here the sign «+»indicates an increased content of electrons. As a result, the backside of the SCD acquires a structure of the *n*- n^+-type metal.

The most important characteristic of SCD is the it's leakage current I_L consisting of two components-surface (l_s) and volumetric (l_b).The value L_s is determined by the conductivity of the surface between the front and back electrode. To reduce L_s, an oxide layer (SiO_2) is applied to this surface. Which is a dielectric.

Inside the volume of the SCD, which is a diode closed by an external voltage, the reverse current I_b flows. The current I_b depends on the quality of the material and the volume $V_0$of its depleted part [16]:

$$I_b = qnV_0/2\tau_1 \qquad (1.2)$$

where *q*- is the electron charge, *n*- is the bulk density of the charge carriers:

$$\tau_1 \approx (\sigma V_T N_t)^{-1} \quad (1.3)$$

Here σ- is the capture cross section of an electron or hole by a trap, V_T is the thermal velocity of charge carriers in silicon, and N_t is the bulk density of traps, which are the centers of recombination or attachment.From the expressions (1.2) and (1.3) it follows that$I_b \infty nN_t$.

1.2.2. Diffusion Detectors

Another method of manufacturing SCD is based on the diffusion into the surface of semiconductor of the dopant. Thus, in [17] a thin layer with electronic conductivity was obtained on the surface of *p*-type silicon by diffusion of phosphorus from the gas medium at T=1200 ^{0}C. To create a rear, non-injecting, p^+contact, boron diffusion at a temperature of 1000 ^{0}C was used. Better results instead of diffusion gives the implantation of ions with energy in the range of tens of kiloelectronvolts, since there is no need to subject the sample to high temperature heating, which can lead to the formation of defects that increase the current leakage. The implantation of ions in a semiconductor allows the creation of sharp transitions with a thin input layer. Detectors of this type have proven themselves, in general, more attractive devices than surface-barrier detectors.

A combination of thermal diffusion with ion implantation was also used, which was done [18], in which three detectors were made of a circular disc of ultrapure n-type silicon with a diameter of 10 cm and a thickness of 380 μm, each of which consisted of four independent elements with area 1.945 x 1.475 cm^2. The total area of the detector was 1.945 × 5.9 cm^2. The *p*-*n* junction was created by implanting boron ions to the one side of the sample, on the other side, after the thermal diffusion of phosphorus a mutual contact was formed. Of the 4,480 such detectors located in four planes, a matrix of 99×111.2 cm^2 was collected. The matrix is intended to determine the charge composition of cosmic rays with an energy of 10^{10} -10^{13}eV in the range Z = 1-26in balloon experiment ATIC.

1.2.3. Diffusion-drift detectors

Thickness of sensitive area of SCD can be increased by entering into volume of the sample an impurity of opposite conductivity with the help of its diffusion at high temperature and drift in the electric field. Such a standard donor impurity for silicon of *p*-type conductivity is lithium, the ions of which are distinguished by a sufficiently large mobility in an electric field. Lithium is applied to the back of the sample, which is placed in a vacuum or atmosphere of inert gas . To carry out the drift process, an inverse shift voltage is applied to the resulting *n*-*p* junction [19]. The value of V is chosen to be

high enough that the drift flux of lithium ions exceeds the diffusion flux. Under the action of the electric field, the Li ions move to the *p*-region, compensating for the original acceptor impurity, which leads to the formation of a layer-i whose resistance is high and close to the intrinsic resistance of the semiconductor. As a result, the structure of the volume of such lithium-drift detectors looks like *p-i-n* [20].

As an illustration of technological process of manufacturing Si (Li) detector, the manufacturing proceduredescribed in [21] is given below.

It was used *p*-type silicon with ρ = 4 kOhm * cm in the form of discs 5 mm thickness and 83 mm in diameter. The lifetime of electrons in it was more than 500 microseconds, and the oxygen concentration was less than 10^{16} cm^{-3} (it is known that the lithium drift velocity increases with decreasing oxygen concentration). Lithium was deposited on silicon by sputtering in a vacuum chamber at a temperature of 450 ^{0}C for 6 minutes. The lithium ion drift came at 110^{0}C in an electric field of ≥ 10 3 V/cm until the Li + concentration in the silicon volume became equal to the acceptor concentration. Then the temperature and V = 400B of the product was held for about a month (see Fig.1.2.). This regime made it possible to obtain a fairly uniform distribution of Li + in the volume of silicon. The surface of the manufactured product was treated with an abrasive (10 μm Al_2O_3) and polishing dust was washed off with a stream of distilled water [22].

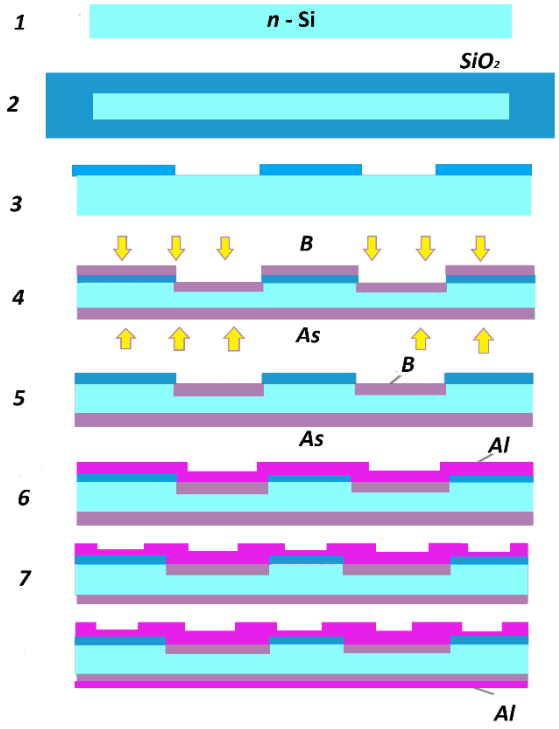

Figure 1.2– The stages (1-8) of the planar technology for manufacturing silicon detectors[25].

From the obtained material in this way, samples with a sensitive region of 5 mm in thickness and from 3 to 38 cm in area were made. Etching of the surface of the material, holding it at room temperature for two days, and then spraying gold (~ 30 nm) onto the front surface and silver (~50nm) onto back surface, lithium was entered with it, were carried out. The leakage current of the samples at the voltage shift of 400 V did not exceed 0.1 μA / cm^2, which made it possible to use in gamma spectroscopy at normal room temperature with a fairly good resolution. In particular, when detector with an area of $3cm^2$ was irradiated with radioactive source practically with a zero pedestal, recorded conversion electrons (E_e about 650 keV) and γ-quantum with an energy of 662 keV with a resolution of 25-30 keV. The efficiency of registration of such photons was 3% [23].

On the basis of a thick (5 mm) silicon detector, short portable gamma and beta spectrometers can be built to work in field conditions, for example, to determine soil contamination with radionuclides [24]. Gamma spectrometers are significantly less efficient in registration compared with standard spectrometers with NaI, but they significantly exceed them in terms of energy resolution.

1.2.4. Pixel Detectors

Pixel detectors (PD), in comparison with microstrip detectors, are much smaller in their coordinates, which makes it possible to work with large loads, better spatial accuracy of measurements and better separation of closely lying tracks. Among the first experiments with the implementation of PD refers the experiments with a fixed target at CERN: WA986 DELPHI and NA60 [26].

Naturally, PD require significantly more channels of recording equipment. For this reason, the track system in many installations is composed of a combination of microstrip and pixel detectors. In addition, the system can also include drift detectors. For example, the internal track system of the ALICE experiment [27], which is depicted in Fig.1.3, is constructed. The system surrounds the interaction region of the collider beams of 24 cm in length. At a distance of 4 and 7.5 cm from the beam axis (Z) two layers of PD are placed, and then two-layer of drift detector layers are located and then two layers of double-sided PD, with an outer radius of 45 cm. The pixel dimensions are 300 μm along the Z axis and 50 μm in the perpendicular direction. PD in the amount of 256 ×256 cells are made on a single substrate with a length of 81, a width of 13.3 and a thickness of 0.15 mm. Each of the cells is connected to its channel of the electronic reader in 16 chips.

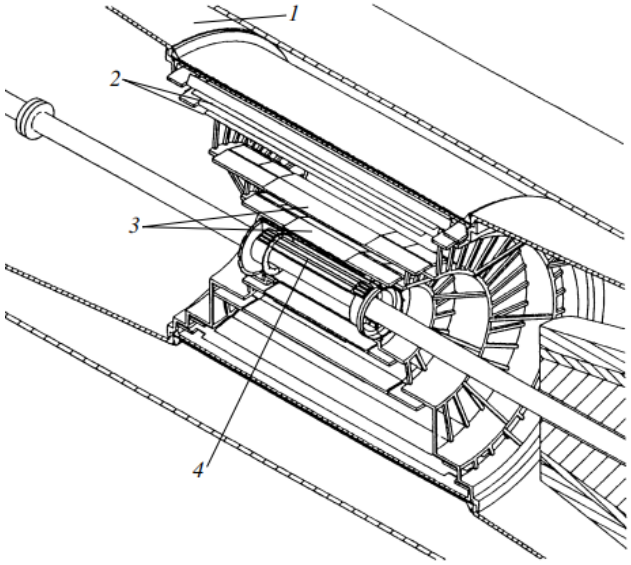

Figure 1.3 – System of inner coordinate detector ALICE [27]. 1- time projection camber, 2- double sided silicon strip detectors, 3- silicon drift detectors, 4- silicon pixel detectors.

Communication is carried out through conducting tubercles, the distance between which corresponds to the step between the pixels.

Modern technology allows you to place chips in direct contact with pixels. The output from each pixel articulates with its field effect transistor, which is the input element in the chip. The typical noise of a field-effect transistor is ~ 250 electrons, and the power consumed by one channel is about 50μW. Such a device is called a hybrid pixel detector [28].

a) 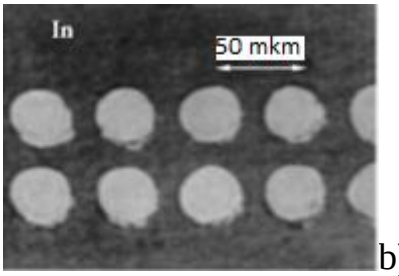

b) 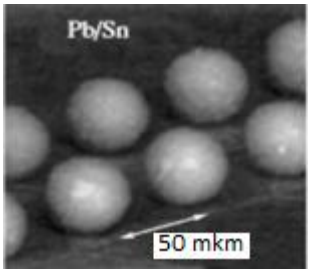

Indium (a) and solder (b)

Figure 1.4 –Indium and solder rows of tubercles in increments of 50 mkm [29]

The typical distance between the tubercles is ~ 50 μm. The articulation is carried out either through indium cylinders or solder from Pb / Sn beads (63% Sn and 37% Pb) with a diameter of 20-30 μm (see Fig. 1.4 [29]). The indium compound is soft enough and flattens to ~ 6 μm, so contacts can be made by simply mechanically compressing two substrates. Another way of forming contacts between two substrates is to heat

indium above its melting point (156 ℃). Lead-tin beads are grown galvanically on a chip waffle, and their contacts with the registrating microcells are obtained by heating the solder above the melting point (183 ℃) [29-31].

It is noted that the maximum area of a pixel, modern technology still capable to provide (0.25-μm structural dimensions) is ~ 50x50 μm^2. In particular, approximately in such dimensions were made PD on a single substrate in the amount of 256x256 pcs for radiology [33].

From the modules similar in structure to those discussed above for the ALICE detector, a 16-plan telescope of the NA60 experiment was constructed on the SPS accelerator, CERN [34]. The telescope is located behind the target in a magnetic field of 2.5 T. It was found that the chips produced by 0.25-μm-technology remain fully operable after irradiation with a dose of 12 Mrad.

Analogous modules were also used in two internal layers of the vertex detector of the PHENIX experiment at the relativistic heavy ion collider (RHIC). The detector (40x80 cm) is made up of four coaxial layers and four cone-shaped layers at the ends (see Figure.1.5. [35]).

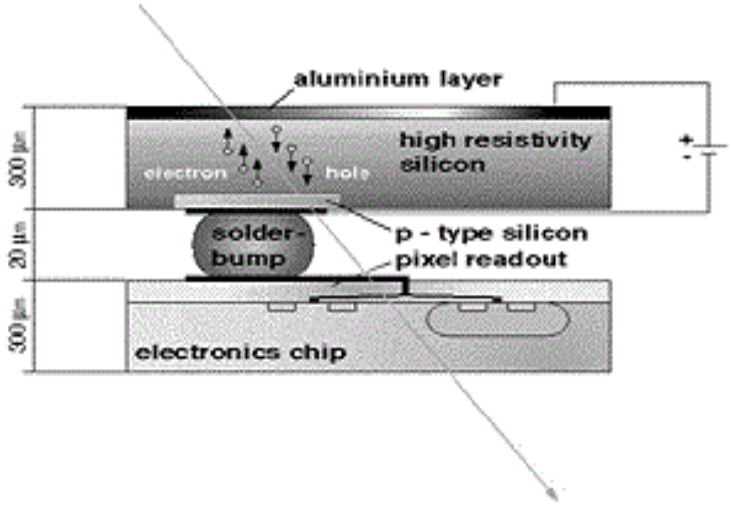

Figure 1.5 – Schematic of Hybrid Pixel detector.

The third and fourth coaxial layers of the "barrel" are exposed to less radiation, and in order to reduce the number of channels of electronic equipment they were made of pixels of another original construction. The electrode of pixel is made in the form of two non-contacting G-shaped strips that fit one into the other. One of these strips is connected to the X-line, and the other to the Y-line. The distance between the strips is chosen to be less than the nspfm. curve describing the diffusion of the released charge, which provides two-coordinate information. Spatial resolution determines the size of the pixels, which in the PHENIX detector were 80x1000 μm. The two-dimensional image in this design is achieved by removing information from only one side of the detector, which provides better characteristics than in standard two-way microstrip detectors.

The end layers of the PHENIX detector contain micro-strips 50 μm wide and 2.2-13 mm long, which are connected to fast-acting chips. Barrel-shaped multilayer structure is typical for most silicon track detectors, the largest of which are detectors in ATLAS [36] and CMS installation [37] (both for LHS), LHCb [38], BTeV in Fermilab [39]. So, the sensitive area of ATLAS should be 70 m^2, and in CMS-210m^2. Detectors in ATLAS and CMS contain pixels with typical dimensions of 50x400 and 150x150 μm, respectively.

ATLAS pixel detector has $1.1x10^8$ digital registering channels and is made in the form of a three-layered barrel with internal and external diameters of ~ 10 and ~ 24 cm, respectively, and disks at both ends [40]. Dimensions of the construction-38x185 cm^2. Sensitive area of the ~ 1.7 m^2.

The device of a separate pixel cell is shown in Fig. 1.6 [41]. Its main volume is depleted n-type material, into which thin layers of n + p + are implanted [42]. One section of n + (left) serves to output the signal, and the second - creates a guard grid around the pixel output. The layer p covers narrow gaps (5 μm) between these sections in order to isolate them from each other and, as shown by measurements, increases the radiation resistance of the detector [43].

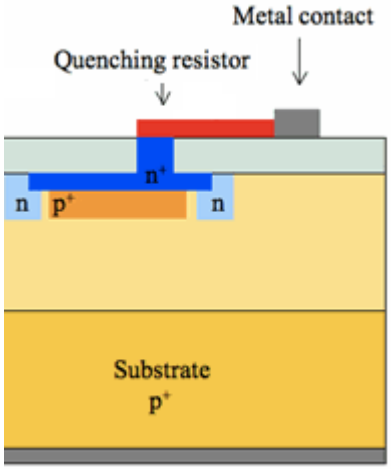

Figure 1.6 – Silicon Pixel Detector structure [41].

When a LHC beam collides, there will be about 20 primary interactions and several thousand ionizing particles passing through the detector at a frequency of 40 MHz. Oxidized silicon was used to make the detector, which is distinguished by increased radiation resistance. The detector was irradiated with a dose of 1.1×10^{15} $n*cm^{-2}$ [44]. After that, the thickness of the depleted layer in it decreased from 300 to 200 μm at V = 600 V, but the spatial resolution did not change, and the registration efficiency was 97%.

In order to reduce the leakage current, especially after training, the pixel detectors in ATLAS operate at a temperature of -6 °C. The temperature on the components of the chips can vary within + 25 °C.

The track detector Fermilab, at a temperature of -5 °C, must operate for 10 years, made up of 23 million pixels measuring 50x400 microns with a total area of 0.5 m^2. The

mechanical and electrical (noise, thresholds) characteristics of the PD depending from temperature were investigated [39]. In the range from +70°C to -5°C, the changes in all characteristics of the detectors remained quite acceptable. Only in individual indium joints was a somewhat larger deformation at low temperatures than in Pb / Sn beads.

1.2.5. Coordinate-sensitive detectors

For the experiments on accelerators of high-energy particles and especially with colliding beams (colliders) in the early 80s of the last century, large sized detectors of bulb type began to be created, allowing to register and identify simultaneously a large number of particles, measure their energies, trajectories and the place of formation. Hence, such requirements as compactness, high spatial resolution, weak sensitivity to the magnetic field, and acceptable radiation resistance followed for this vertex detector. In contrast, the inaccessibility to the vertex detector would greatly complicate, for example, the replacement of broken wires in the chambers. The above mentioned characteristics of the vertex detector would cause difficulties, for example, in the replacement of broken wires in the chambers. A significant growth of the reliability of the operation of such microstrip detectors (MSD) and a reduction in the current leakage (≤10Na) was provided by planar technology.

The first silicon MSD for measuring the coordinates of the detected high-energy particles were intended for experiments at the CERN SPS accelerator [45, 46] Production of MSD steel is intensively used on various accelerators of the world [47]. The microstrip silicon detectors were introduced into the central part of most collider installations [48-52].

Fig.1.7. [53] shows the mechanism(installation) of the first silicon vertex detector, which was used in the Mark experiment at the SLAC collider. In the tube 1, beams of positrons and electrons collide. In the place of their collision around the tube, three layers of MSD are coaxially located.

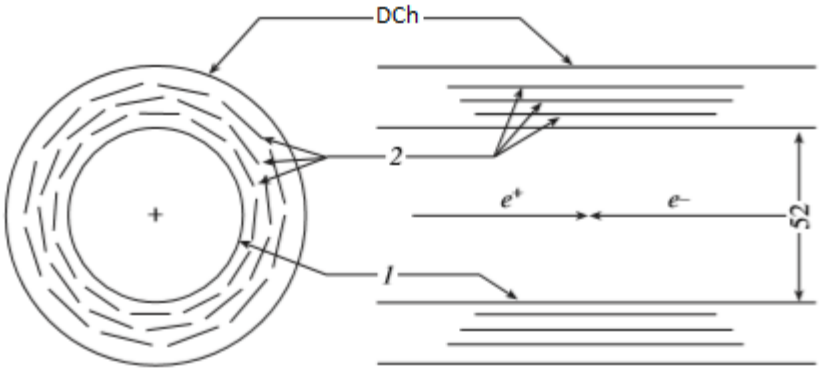

Figure 1.7 – Structure of vertex detector Mark II. 1- tube for opposite beam of electron and positron, 2 – detector layer, DCh – drift chamber [53].

Close to the above mentioned is the mechanical structure of the silicon vertex detectors of the Belle experiment on the $e^+ e^-$KEKW collider (Japan), which currently has a maximum luminosity of $1.06 \cdot 10^{34}$ $cm^2 \cdot s^{-1}$. In that, the MSD occupy four layers (see figure. 1.8.). Signals from the detectors are taken from the opposite ends of each adder and transmitted to electronic recording devices. All electronic equipment are made up of multichannel chips, manufactured by CMP-technology allowing to get the structural dimensions of the product less than 1 mkm.

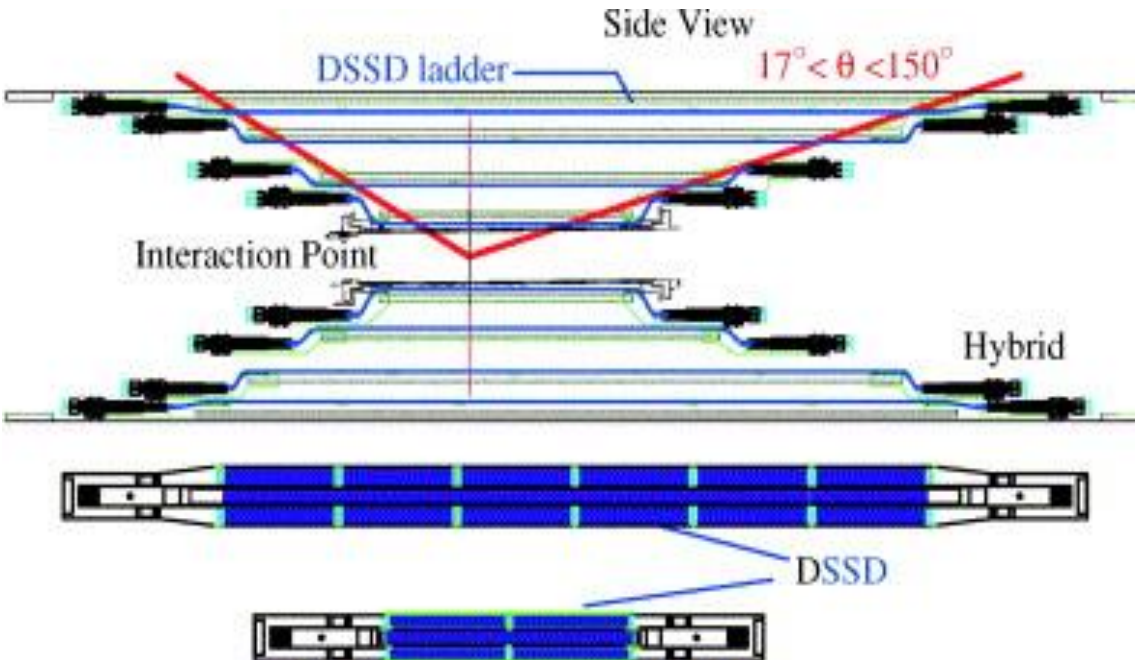

Figure 1.8 – Microstrip detector structure.

The spatial resolution along the beam was 12 μm, and along the azimuthally angle it was 22 μm.

In the used commercial chips , the distance between the channels decreased during the time, and as it turned out, this led to an increase in their radiation resistance. If at 1-2 μm technology the performance of the chips was limited to 200 krad, then at 0.8 μm technology - 2 Mrad, 0.35-μm of technology 20 Mrad.

When irradiating chips made with 0.25-μm technology, by $5x10^{13} n*cm^{-2}$ particle flow an inversion of the silicon type was occurred, but the chips were still operational.

The location of the modules on the "stairs" is also used in other detectors, for example, the BaBar and STAR RHIC experiments. The first of them consists of five layers. The radius of the lower layer is 3.3 cm and the upper layer is 14.6 cm. MSD are made on the basis of silicon with specific resistance from 6 to 30 kOhm×cm, and in it are made from two sides by microstrips with a step from 50 to 210 microns. A particle with a minimum ionization releases in a separate MSD about 24000 electrons, and the ENC is consisted of 700 to 1500 electrons.

The STAR MSD is a complement to the vertex pixel detector located in the zone with lower radiation, along ribbon cables 60 cm long. Cooling devices are mounted in that place. This concentration allowed to obtain a minimum amount of substance in the path of detecting particles. The signal to noise was~10 (with a formation time of 3 μs).

Construction of device made from MSD of another type is shown in figure.1.9.where one of 12 layers of the internal station of the track detector is shown for the LHCb experiment at CERN. The station consists of four individual boxes. All MSD in each box have a height of 11 and a width of 7.8 cm and contains microstrips with a step of about 200 μm. The thickness of the samples is 320 μm in the upper and lower boxes and 410 μm - in the side, which are chosen thicker, because in them microstrips in vertically adjacent samples are connected together. Signals for registration are taken from one end of each box (they are shaded in the figure) and are fed to the recording devices via a 40-cm-long kapton cable. Another 143,000 channels are connected to a track system of similar construction, 130 cm height and 160 cm wide that is remote from the opposing beams. Also, in order to reduce the cost of installation, the microstrips are articulated to a length of 38 cm.

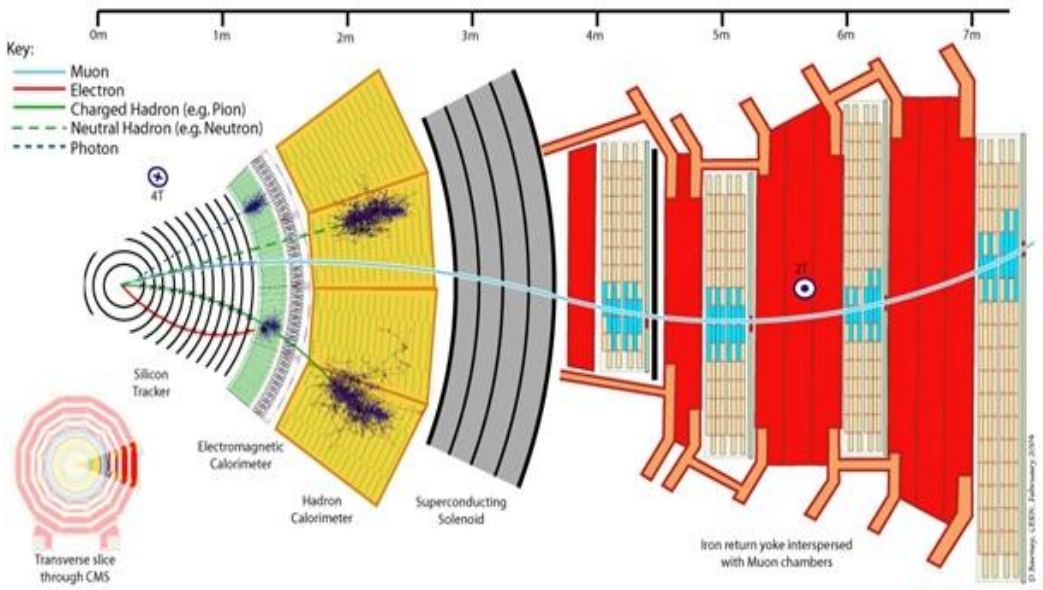

Figure1.9 – Structure of the detector for an experiment LHCb.

To each microstrip of this detector its own channel of an analog electronic device is connected, consisting of 128 multichannel integrated circuits. The chips are made on the basis of the special technology, providing 0.25-μm structure of the elements. The short formation time of 25 mks is used in amplifiers . The signal-to-noise ratio during the detection of relativistic particles was~10.

The microstrip detectors of the vertex detector for LHCb cover a total of 12.2 m^2.Compactness, vibration resistance, weak sensitivity to the magnetic field and other valuable properties of MSD made them attractive for use as track instruments in space

research. So, on board of the Russian satellite Resurs DK, a silicon coordinate detector PAMELA was installed, intended for studying the spectra of particles and antiparticles in cosmic rays [54].

The silicon track detector is the heart of the larger telescope-rays (GLAST) installed on the satellite [55]. The detector has an area of 80 m2 and about 1 million channels. The telescope can examine the sky in search for gamma rays, in the energy range from 20 MeV to 300 GeV.

For astronomy of gamma rays of medium and lower energies from 0.4 to 50 MeV, the MEGA telescope was designed [56].

The detector considered in [57] is designed in the form of a stack about 1 m height, consisting of a series of layers disposed one above the other in 1 cm steps. Each layer consists of 3 X 3 samples with a thickness of 500 μm and an area of 6×6 cm^2. Samples have 128 microstrips on each side. Microstrips on both sides are mutually perpendicular, which provides two-coordinate measurements, and the third coordinate is determined by the number of the layer in which the information originated. In addition to the coordinates, the energy of electrons / positrons with a resolution of 15-20 keV is also measured.

Silicon detectors are also attractive for detecting X-rays with energies up to ~ 20 keV. In X-ray diffract meters, usually X-ray tubes with copper anodes are used, in which radiation with energy ~ 8 keV is formed. Silicon detectors 300 μm thick register such rays with an efficiency of about 100%. SD can also be useful for various studies in solid state physics, the science of materials and biological research using synchrotron radiation. In most of such applications, two-coordinate MSD are used. The spatial resolution of the detector, in principle, improves with a decrease in the width of the microstrips. The restriction on their width is imposed by the intrinsic spatial resolution of the detector, which arises from Compton scattering of X-rays. The ratio of the cross sections of Compton scattering and photo-absorption in silicon belonging to light materials is quite large [58].To increase the efficiency of X-ray absorption with relatively high energy and to reduce the effect of their scattering on the spatial resolution, it was suggested to direct photons from the edge of the detector along the microstrips. In this case, usually a mechanical scanning system is used. The disadvantage of such a device is a small recording space [59].

The signal from X-rays with E = 8 keV is obtained by an order less than the signal from detector thickness of 300 μm, it is therefore extremely important to have, if possible, a minimum noise level. So, in work on a detector with 128 microstrips 1 cm long and 100 μm in steps, ENC amounted to 150 electrons, which made it possible to reliably detect x-rays at room temperature, starting at 6.4 keV. Information was captured by 64-channel chips containing preamps, drivers and discriminators [60].

Spectroscopy with X-ray absorption is carried out by the main layer, in the energy range from 200 eV to 35 keV [58]. The most typical for studying the spatial distribution of low-energy x-ray radiation is the use of a proportional counter as well as mechanical

scanning. The advantage of the silicon microstrip detector is a significant reduction in the time measurement, which was demonstrated, in particular, on MSD with 1024 microstrips with dimension 4000 X 15 μm, separated by an interval of 25 μm. The detector had a thickness of 500 μm. Information from the detector was obtained through chips, each of which contained 128 preamplifiers. The detection rate of synchrotron radiation with an energy of 5-25 keV on this detector was 100 times higher than on a proportional counter.

One of limitations of silicon detectors is the speed [61]. The speed of silicon detectors will start to become an issue if event rates will continue to rise. The speed depends on the drift field and thus on the bias voltage, but_ at normal operational parameters, electrons take about 3ns to traverse 100 μs while holes need about 8ns for the same distance. Thus, 25ns is the minimum time needed when the p-side is read out, and the full signal is required for a detector is that is 100 μm thick. In cases of very low occupancy, several events can be read out together. Hits from different events are then separated through additional information. This option has rarely been used, but it should be looked into more often. Second limitation is size of silicon detectors. Many applications call for very large areas of silicon. Square-meters of silicon are planned for LHC, and this trend will continue. Very often the segmentation into small individual wafers causes problems. Basically, all detectors today are manufactured from 10 cm wafers. However, 15 cm wafers have been used to produce detectors, and there is no physical law preventing 25 inch wafers. However, the over-all properties of a detector can be ruined by a single defect. The probability for a defect is at least proportional to the area of the device. It will be very difficult to have a good yield for very large detectors, and that will most likely result in forbidding costs per cm^2. Third limitation is Resolution and Material Budget. As far as resolution is concerned, the limit is about 1μm.That has beenachieved for strip detectors and could be done with pixels. The corresponding structures on the silicon are of the order 10 μm and pose no real problem to good manufacturers. However, the actual resolution of a silicon system is usually not limited by the intrinsic resolution of the detectors. The main limitation of vertex detectors come from the material needed for the beam pipe and the detector itself. This is why Roman pot systems become increasingly popular, and some experiments try to use thinner silicon detectors [62]. Extremely important is the amount of material track has to traverse before its first hit can be recorded.

1.3 Readout electronics of X- ray system

Electronics are a key component of all modern detector systems. Although experiments and their associated electronics can take very different forms, the same basic principles of the electronic readout and optimization of signal-to-noise ratio are applied to all. This chapter provides a summary of front-end electronics components and discusses signal processing with an emphasis on electronic noise. Due to the limitations

of chapter, the electronics are only briefly reviewed. A more detailed discussion of electronics with emphasis on semiconductor detectors is given in [63].

The purpose of front-end electronics and signal processing systems is to:

1. Acquire an electrical signal from the sensor. Typically this is a short current pulse.

2. Define the time response of the system to optimize

– the minimum detectable signal (detect hit/no hit);
– energy measurement;
– event rate;
– time of arrival (timing measurement);
– insensitivity to sensor pulse shape;
– or some combination of the above.

3. Digitize the signal and store for subsequent analysis.

Position-sensitive detectors utilize the presence of a hit, amplitude measurement or timing, so these detectors pose the same set of requirements [64].

Generally, these properties cannot be optimized simultaneously, so compromises are necessary. In addition to these primary functions of an electronic readout system, other considerations can be equally or even more important. Examples are radiation resistance, low power (portable systems, large detector arrays, satellite systems), robustness, and – last, but not least – cost.

Figure 1.10 illustrates the components and functions of a radiation detector system. The energy deposited by a particle (or photon) is converted by sensor to an electrical signal. This can be obtained in a variety of ways. In direct detection – semiconductor detectors, wire chambers, or other types of ionization chambers – energy is deposited in an absorber and converted into charge pairs, whose number is proportional to the absorbed energy [65]. The signal charge can be quite small, in semiconductor sensors about 50 aC ($5 \cdot 10^{-17}$ C) for 1 keV x-rays and 4 fC ($4 \cdot 10^{-15}$ C) in a typical high-energy tracking detector, so the sensor signal must be amplified. The magnitude of the sensor signal is subject to statistical fluctuations and electronic noise further “smears” the signal. These fluctuations will be discussed below, but at this point we note that in order to minimize electronic noise the sensor and preamplifier must be designed carefully [66]. A critical parameter is the total capacitance in parallel with the input, i.e. the sensor capacitance and input capacitance of the amplifier [67]. The signal-to-noise ratio increases with decreasing capacitance. The contribution of electronic noise also depends critically on the next stage, the pulse shaper, which determines the bandwidth of the system and hence the overall electronic noise contribution. The duration of the pulse also limited by the shaper, which sets the maximum signal rate that can be accommodated. An analog-to-digital converter (ADC) is fed by the sharper, which converts the magnitude of the analog signal into a bit-pattern suitable for subsequent digital storage and processing [68].

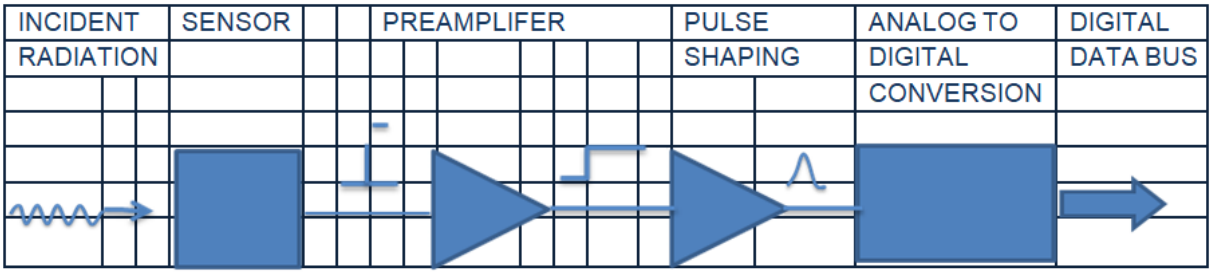

Figure 1.10 – Basic detector functions: Radiation is absorbed in the sensor and converted into an electrical signal. This low-level signal is integrated in a preamplifier, fed to a pulse shaper, and then digitized for subsequent storage and analysis.

A scintillation detector (Figure.1.11) utilizes indirect detection, where the absorbed energy is first converted into visible light. The absorbed energy is proportional to the number of photons. The photomultiplier (PMT) consists of a photocathode and an electron multiplier, and it detects scintillation light. Photons absorbed in the photocathode release electrons, whose number is proportional to the number of incident scintillation photons[69]. At this point energy absorbed in the scintillator has been converted into an electrical signal whose charge is proportional to energy. The signal at the PMT output is a current pulse which is increased in magnitude by the electron multiplier. Integrated over time this pulse contains the signal charge, which is proportional to the absorbed energy. Figure 2 shows the PMT output pulse fed directly to a threshold discriminator, which fires when the signal exceeds a predetermined threshold, as in a counting or timing measurement. There is no necessity for preamplifier, because the electron multiplier can provide sufficient gain. This is a common arrangement used with fast plastic scintillators[70]. In an energy measurement, for example using a NaI(Tl) scintillator, the signal would feed a pulse shaper and ADC, as shown in Figure 1.10.

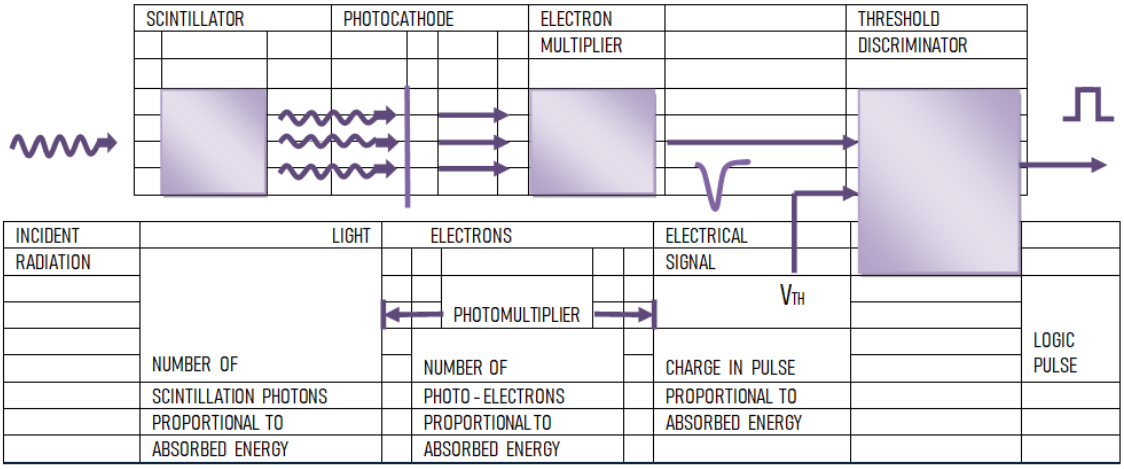

Figure 1.11 – In a scintillation detector absorbed energy is converted into visible light. The scintillation photons are commonly detected by a photomultiplier, which can provide sufficient gain to directly drive a threshold discriminator.

If the pulse shape does not change with signal charge, the peak amplitude – the pulse height – is a measure of the signal charge, so this measurement is called pulse height analysis [71]. The multiple functions can be served by pulse shaper, these functions are discussed below. One is to tailor the pulse shape to the ADC. Since the finite time is required by the ADC to acquire the signal, the input pulse may not be too short and it should have a gradually rounded peak. In scintillation detector systems the shaper is frequently an integrator and implemented as the first stage of the ADC, so it is invisible to the casual observer. Since the PMT output is plugged directly into a charge-sensing ADC the system appears very simple.

A detector array combines the sensor and the analog signal processing circuitry together with a readout system [72]. The electronic circuitry is often monolithically integrated. The circuit blocks in a representative read-out integrated circuit (IC) is shown in Figure 1.12 [73]. Individual sensor electrodes connect to parallel channels of analog signal processing circuitry. Data are stored in an analog pipeline pending a readout command. Variable write and read pointers are used to allow simultaneous read and write.

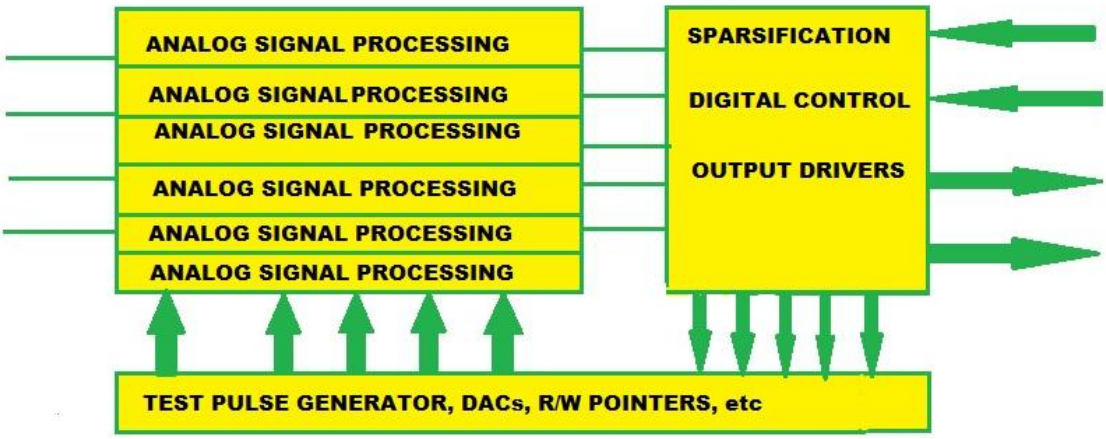

Figure 1.12 – Circuit blocks in a representative readout IC. The analog processing chain is shown at the top. Control is passed from chip to chip by token passing.

The signal in the time slot of interest is digitized, compared with a digital threshold, and read out. Circuitry is included to generate test pulses that are injected into the input to simulate a detector signal. This is a very useful feature in setting up the system and is also a key function in chip testing prior to assembly. Analog control levels are set by digital-to-analog converters (DACs). Multiple ICs are connected to a common control and data output bus, as shown in Figure.1.13. Each IC is assigned a unique address, which is used in issuing control commands for setup and *in situ* testing. Token passing controls the sequential readout. IC1 is the master, whose readout is initiated by a command (trigger) on the control bus. When it has finished writing data it passes the token to IC2, which in turn passes the token to IC3. When the last chip has completed its readout the token is returned to the master IC, which is then ready for the next cycle. The readout bit stream begins with a header, which uniquely identifies a new frame. Data from individual ICs are labeled with a chip identifier and channel identifiers. Many variations on this scheme are possible. As shown, the readout is event oriented, *i.e.* all hits occurring within an externally set exposure time (*e.g.* time slice in the analog buffer in Figure 3) are read out together. For a concise discussion of data acquisition systems [74].

In colliding beam experiments only a small fraction of beam crossings yields interesting events. The time required to assess whether an event is potentially interesting is typically of order microseconds, so hits from multiple beam crossings must be stored on-chip, identified by beam crossing or time-stamp. Upon receipt of a trigger the interesting data are digitized and read out. This allows use of a digitizer that is slower than the collision rate.

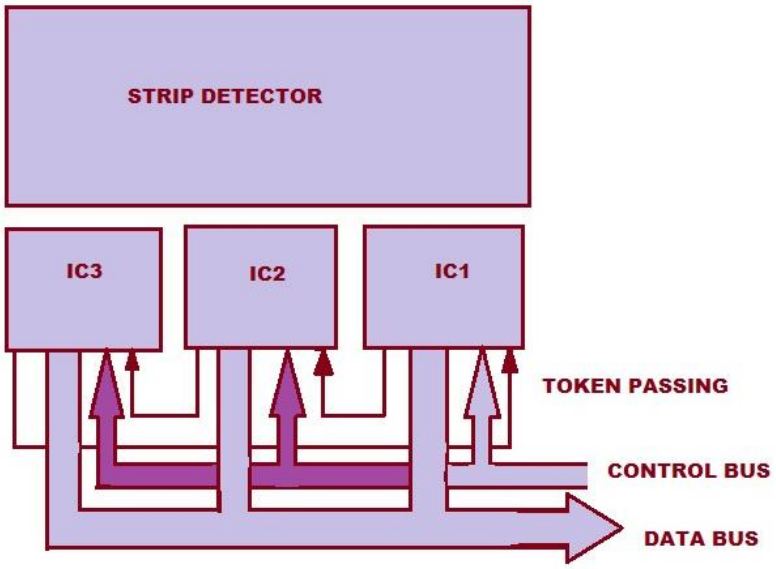

Figure 1.13 – Multiple ICs are ganged to read out a silicon strip detector. The right-most chip IC1 is the master. A command on the control bus initiates the readout. When IC1 has written all of its data it passes the token to IC2. When IC2 has finished it passes the token to IC3, which in turn returns the token to the master IC1. [74]

It is also possible to read out analog signals and digitize them externally. Then the output stream is a sequence of digital headers and analog pulses. An alternative scheme only records the presence of hit. The output of a threshold comparator signifies the presence of a signal and is recorded in a digital pipeline that retains the crossing number.

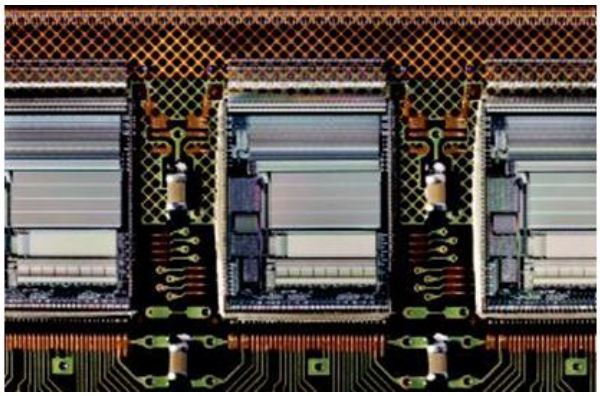

Figure 1.14 – Close up of ICs mounted on a hybrid utilizing a flexible polyimide substrate. The high-density wire bonds at the upper edges connect via pitch adapters to the 80 µm pitch of the silicon strip detector. The ground plane is patterned as a diamond grid to reduce material. (Photograph courtesy of A. Ciocio.)

Figure.1.14. shows a close up of ICs mounted on a hybrid using a flexible polyimide substrate [74]. The wire bonds connecting the IC to the hybrid are clearly visible. Channels on the IC are laid out on a ~ 50 μm pitch and pitch adapters fan out to

match the 80 μm pitch of the silicon strip detector. The space between chips accommodates bypass capacitors and connections for control busses carrying signals from chip to chip.

1.4 Detection limits and resolution

Fluctuations limit the minimum detectable signal and the precision of the amplitude measurement. The signal formed in the sensor fluctuates, even for a fixed energy absorption. In addition, electronic noise introduces baseline fluctuations, which are superimposed on the signal and alter the peak amplitude. Figure.1.15. (left) shows a typical noise waveform. Both the amplitude and time distributions are randomly chosen. When superimposed on a signal, the noise alters both the amplitude and time dependence, as shown in Figure 6 (right). As can be seen, the noise level determines the minimum signal whose presence can be discerned [76].

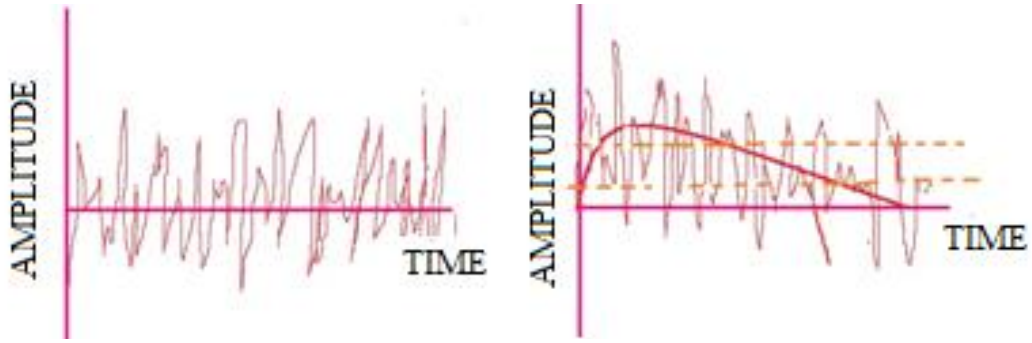

Figure 1.15 – Waveforms of random noise (left) and signal + noise (right), where the peak signal is equal to the rms noise level (S/N = 1). The noiseless signal is shown for comparison.

In an optimized system, the time scale of the fluctuations is comparable to that of the signal, so the peak amplitude fluctuates randomly above and below the average value. This can be seen in Figure.1.16., which shows the same signal viewed at four different times.

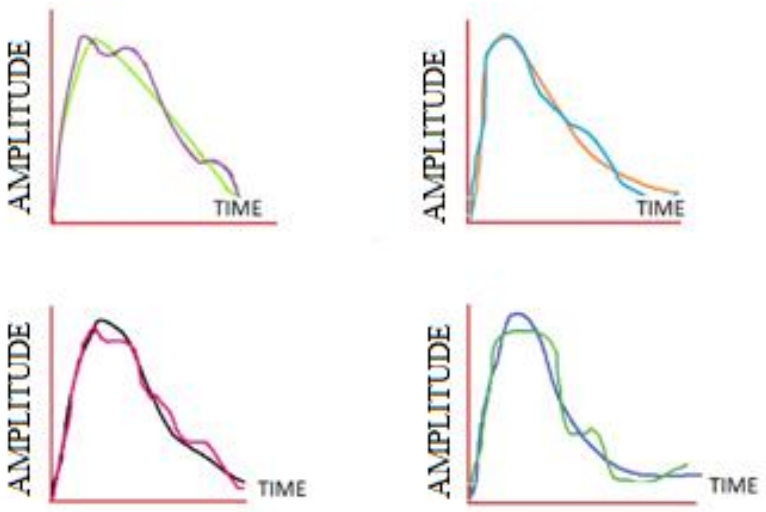

Figure. 1.16. Signal plus noise at four different times, shown for a signal-to-noise ratio of about 20. The noiseless signal is superimposed for comparison.

The fluctuations in peak amplitude are obvious, but the effect of noise on timing measurements can also be seen. If the timing signal is derived from a threshold discriminator, where the output fires when the signal crosses a fixed threshold, amplitude fluctuations in the leading edge translate into time shifts. If one derives the time of arrival from a centroid analysis, the timing signal also shifts (compare the top and bottom right figures). From this one sees that signal-to-noise ratio is important for all measurements – sensing the presence of a signal or the measurement of energy, timing, or position.

1.5 Charge-sensitive amplifiers

When a semiconductor detector such as Si is used for the measurement of soft X-rays and low to high-energy gamma rays, the output signal is a weak charge pulse which have a pulse width of several tens of nanoseconds [77]. Since the detector element itself is a capacitive device, it has very high impedance. Therefore, when amplifying this output signal the performance of the preamplifier to be connected must be taken into consideration [78]. In such applications, operational amplifier mode integrators using feedback capacitance are commonly used. As the preamplifiers have high input impedance, they integrate weak charge pulses and convert them into voltage pulses for amplification then provide a low-impedance output. Due to this operation, this type of amplifier is called a “charge amplifier”. The first stage of a charge amplifier is usually a low-noise FET and its open-loop gain is set sufficiently high so that the amplification is not influenced by the detector capacitance. The output stage is a low impedance buffer so as to drive an external stage which is connected using a long cable [79].

The preceding discussion assumed that the amplifiers are infinitely fast, so they respond instantaneously to the applied signal. In reality this is not the case; charge-sensitive amplifiers often respond much more slowly than the time duration of the

current pulse from the sensor. However, as shown in Figure. 1.17, this does not obviate the basic principle. Initially, signal charge is integrated on the sensor capacitance, as indicated by the left hand current loop. Subsequently, as the amplifier responds the signal charge is transferred to the amplifier.

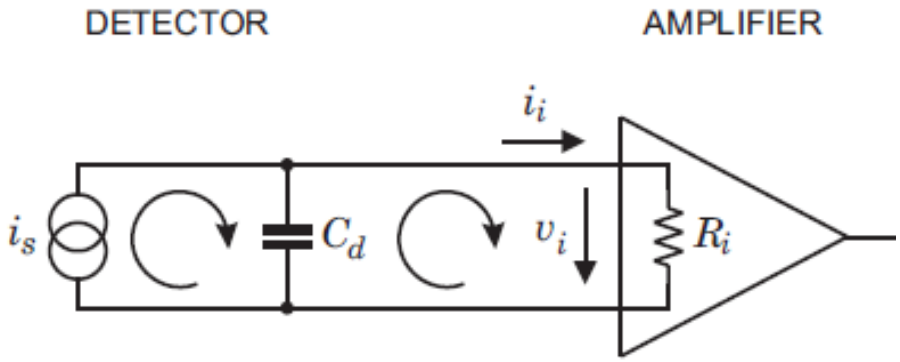

Figure 1.17 – Charge integration in a realistic charge-sensitive amplifier. First, charge is integrated on the sensor capacitance and subsequently transferred to the charge-sensitive loop, as it becomes active.

Nevertheless, the time response of the amplifier does affect the measured pulse shape. Simple consideration is a simple amplifier as shown in Figure.1.18.Sensitivity is expressed in the output voltage (mV) per one MeV of particle energy irradiated onto a detector. The amplitude of the signal charge obtained with a semiconductor detector is determined by the input particle energy such as soft X-rays and gamma rays and also by the material of the semiconductor.

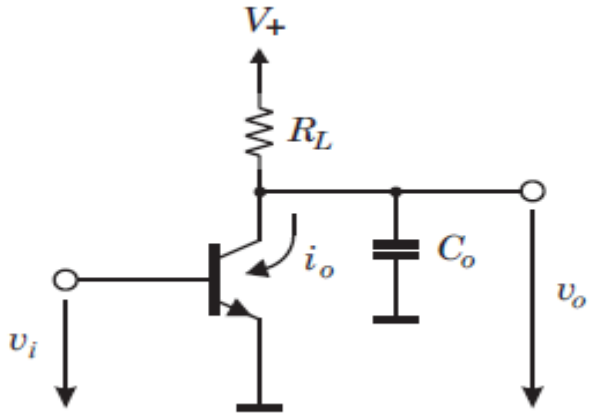

Figure 1.18 – A simple amplifier demonstrating the general features of any single-stage gain stage, whether it uses a bipolar transistor (shown) or an FET.

There are various semiconductor detectors used for the detection of soft X-rays and gamma rays[2,10]. Even among Si detectors for example, a variety of types are used to match the application, which have different active areas and depletion layer thicknesses.

Furthermore, detectors also differ in regards to capacitance. However, when the same Si detector is used for the detection of soft X-rays and gamma rays, the amount of generated charge must be the same if the particle energy of the soft X-rays and gamma rays is equivalent. Therefore, charge amplifier must provide a constant gain regardless of the capacitance value.

In [80] a compact and low noise charge sensitive spectroscopy amplifier which can be integrated into position sensitive micro-channel plate (MCP) detectors has been constructed. The amplifier was optimized by using a wave form generator and tested by a chevron shape MCP detector. The output noise of 4 mV rms was achieved while the gain is 10(12) V/C and the shaping time is 700 ns. A readout electronics system for silicon detectors to measure the space cosmic-ray charges are presented in this work. It shows that the readout system has features of low noise (less than 0.1fC when silicon the detector connects), low power dissipation (about 0.3mW/channel), high dynamic range (200fC) and high integration (64 channels in one chip).

The noise performance of the amplification stage (preamplifier) determines the overall system noise. A folded cascade architecture is commonly used in the implementation of the preamplifier, mainly because of its low input capacitance [81-89].

In general, the following characteristics are required of charge amplifier used for the detection of soft X-rays and low to high energy gamma rays.

- High gain
- Low level of noise
- Good integration linearity
- High-speed rise time
- High temperature stability, etc.

1.6 Pulse shaper

In semiconductor detector systems the primary function of the pulse shaper is to improve the signal-to-noise ratio[66]. Although we are considering signal pulses, i.e. time-varying signals, the signal power is also distributed in frequency space, quantified by the pulse's Fourier transform[90]. The frequency spectra of the signal and the noise differ, so one can improve the signal-to-noise ratio by applying a filter that tailors the frequency response to favor the signal, while attenuating the noise. Changing the frequency response also changes the time response, the pulse shape, so this function is called pulse shaping. As will be shown below, improving the signal-to-noise ratio commonly implies reducing the bandwidth, which increases the duration of the pulse (Figure.1.18.). Usually, it is not interested in measuring just one pulse, but many pulses in succession and often at a very high rate. Too large a pulse width will lead to pile-up of successive pulses, as shown in Figure. 1.19. (left). A system that measures the peak amplitude will give an erroneous result for the second pulse. Pile-up can be ameliorated by reducing the pulse width, as shown in the second panel of Figure. 1.19. Figure. 1.20. shows how the pulse transformation shown in Figure 1.18.can be accomplished.

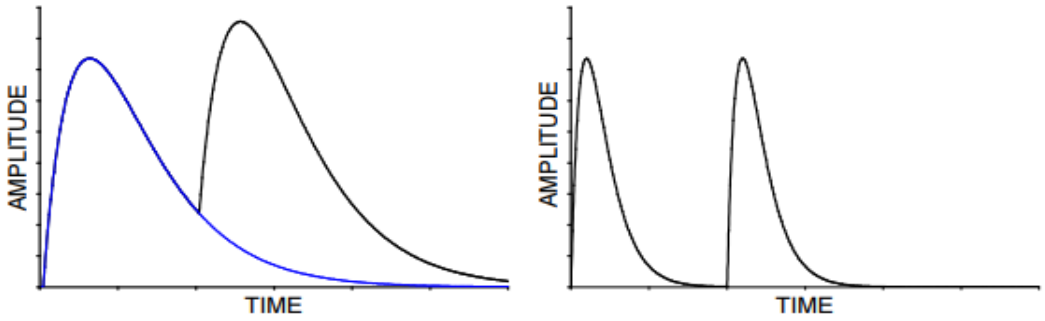

Figure 1.19 – Amplitude pile-up occurs when two pulses overlap (left). Reducing the shaping time allows the first pulse to return to the baseline before the second pulse arrives.

The preamplifier is configured as an integrator, which converts the narrow current pulse from the sensor into a step impulse with a long decay time. A subsequent CR high-pass filter introduces the desired decay time and an RC low-pass filter limits the bandwidth and sets the rise time[91]. Shapers can be much more complex, using multiple integrators to improve pulse symmetry, for example. However, common to all shapers are operations that constrain the upper frequency bound, which sets the rise time, and the lower frequency bound, which determines the pulse duration. When designing a system it is necessary to find a balance between the conflicting requirements of reducing noise and increasing speed. Sometimes minimum noise is crucial, sometimes rate capability is paramount, but usually a compromise between the two must be found[66]. Although the primary measure of the signal energy is the charge, when the pulse shape is the same for all signal magnitudes, the pulse amplitude or "pulse height" is equivalent (hence the frequently used term "pulse height analysis"). The pulse height spectrum is the energy spectrum.

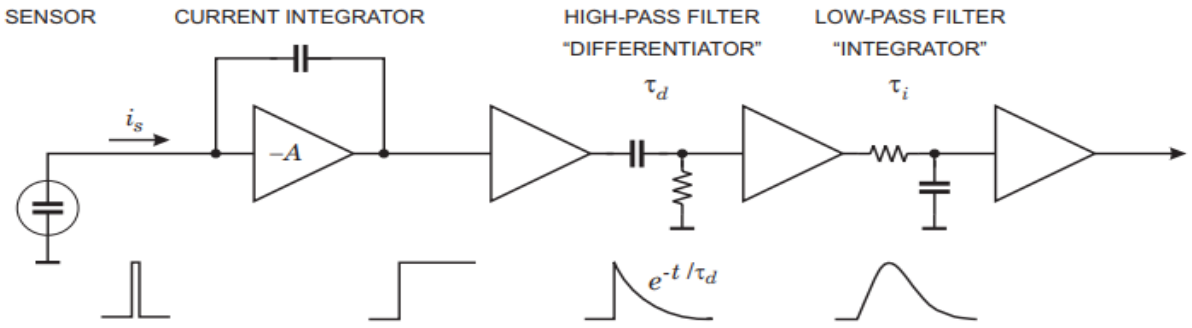

Figure 1.20 – Components of a pulse shaping system. The signal current from the sensor is integrated to form a step impulse with a long decay. A subsequent high-pass filter ("differentiator") limits the pulse width and the low-pass filter ("integrator") increases the rise-time to form a pulse with a smooth cusp.

This is convenient, since analog-to-digital converters (ADCs) measure voltage or current amplitude[92]. However, this imposes an additional requirement on the pulse shaper; the pulse shape should be compatible with the digitizer. Since the digitizer has a finite response time, the maximum signal amplitude should be maintained for a commensurate time, so the shaper output should have a smooth maximum. This is worth remembering, since the filter that theoretically "optimizes" signal-to-noise ratio for many detectors is a cusp, where the peak amplitude is attained for only an infinitesimally short time, as shown in Figure.1.21.

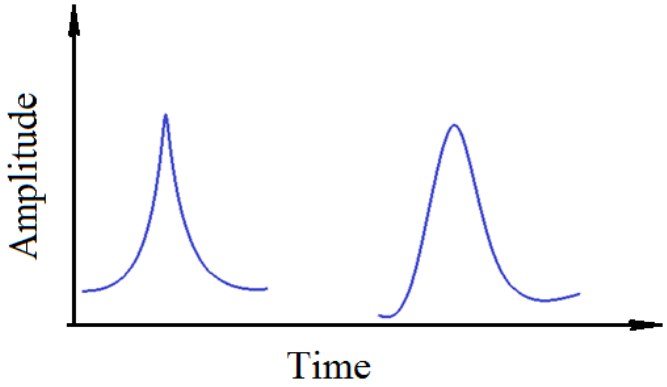

Figure 1.21 – The theoretical "optimum" shaper output (left) and a practical pulse (right), which attains its maximum for a measurable time.

Clearly, determining the amplitude of this pulse in a realistic system is fraught with uncertainties. Sometimes the shaper is hidden; "charge sensing" ADCs are often used to digitize short pulses from photomultiplier tubes. Internally, the input stage integrates the input pulse and translates the signal charge to a voltage level, which is held for the duration of the digitization. This is also a form of pulse shaping. Very sophisticated shapers have been developed to optimize noise and rate capability, and also to reduce sensitivity to variations in sensor pulse shape. However, in many applications, shapers can be quite simple. Since all amplifiers have a limited bandwidth, every amplifier is a pulse shaper. Frequently, rather sophisticated pulse shaping can be implemented by tailoring the bandwidths of the amplifiers needed anyway to increase the signal level.

1.7 Analog-to-digital converters (ADCs)

For data storage and subsequent analysis the analog signal at the shaper output must be digitized. Important parameters for analog-to-digital converters (ADCs or A/Ds) used in detector systems are[93]

- Resolution: The "granularity" of the digitized output.
- Differential non-linearity: How uniform are the digitization increments?
- Integral non-linearity: Is the digital output proportional to the analog input?

- Conversion time: How much time is required to convert an analog signal to a digital output?
- Count-rate performance: How quickly can a new conversion commence after completion of a prior one without introducing deleterious artifacts?
- Stability: Do the conversion parameters change with time?

Instrumentation ADCs used in industrial data acquisition and control systems share most of these requirements[94]. However, detector systems place greater emphasis on differential non-linearity and count-rate performance. The latter is important, as detector signals often occur randomly, in contrast to systems where signals are sampled at regular intervals. As in amplifiers, if the DC gain is not precisely equal to the high-frequency gain, the baseline will shift.

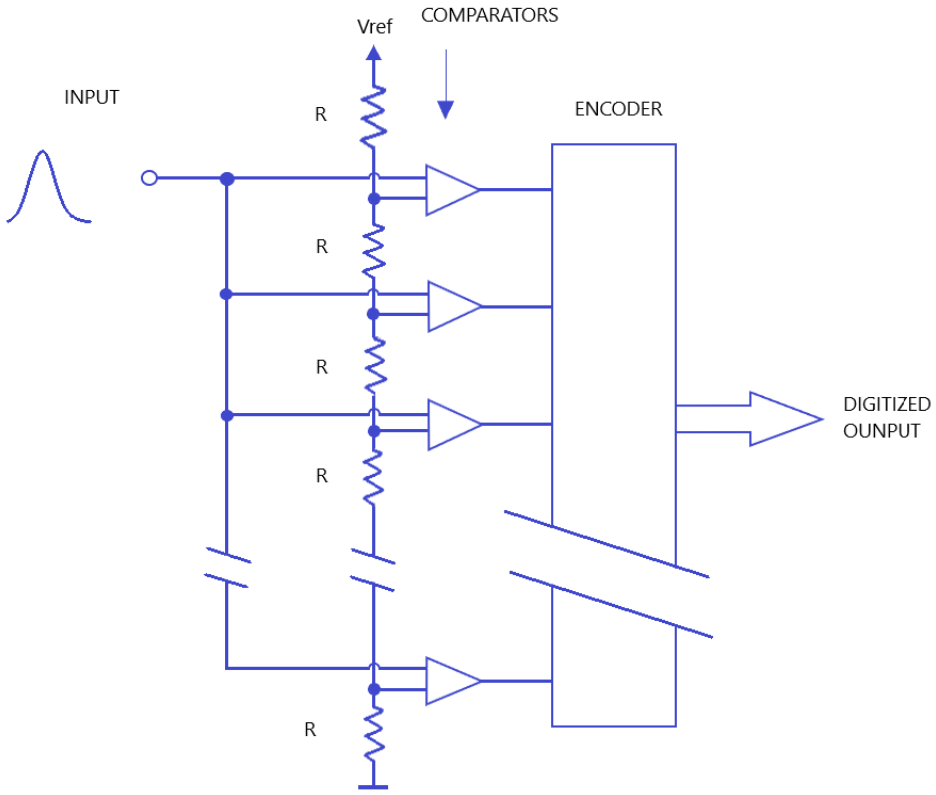

Figure 1.22 – Block diagram of a flash ADC.

Furthermore, following each pulse it takes some time for the baseline to return to its quiescent level. For periodic signals of roughly equal amplitude these baseline deviations will be the same for each pulse, but for a random sequence of pulse with varying amplitudes, the instantaneous baseline level will be different for each pulse and affect the peak amplitude.

Conceptually, the simplest technique is flash conversion, illustrated in Figure.1.22. The signal is fed in parallel to a bank of threshold comparators. The individual threshold levels are set by a resistive divider. The comparator outputs are encoded such that the output of the highest level comparator that fires yields the correct bit pattern. The threshold levels can be set to provide a linear conversion characteristic where each bit corresponds to the same analog increment, or a non-linear characteristic, to provide increments proportional to the absolute level, which provides constant relative resolution over the range.

The big advantage of this scheme is speed; conversion proceeds in one step and conversion times < 10 ns are readily achievable. The drawbacks are component count and power consumption, as one comparator is required per conversion bin. For example, an 8-bit converter requires 256 comparators. The conversion is always monotonic and differential non-linearity is determined by the matching of the resistors in the threshold divider. Only relative matching is required, so this topology is a good match for monolithic integrated circuits. Flash ADC's are available with conversion rates > 500 MS/s (megasamples per second) at 8-bit resolution and a power dissipation of about 5 W.

The most commonly used technique is the successive approximation ADC, shown in Figure.1.23. The input pulse is sent to a pulse stretcher, which follows the signal until it reaches its cusp and then holds the peak value. The stretcher output feeds a comparator, whose reference is provided by a digital-to-analog converter (DAC). The DAC is cycled beginning with the most significant bits. The corresponding bit is set when the comparator fires, *i.e.* the DAC output becomes less than the pulse height. Then the DAC cycles through the less significant bits, always setting the corresponding bit when the comparator fires. Thus, *n*-bit resolution requires *n* steps and yields 2^n bins. This technique makes efficient use of circuitry and is fairly fast. High-resolution devices (16 – 20 bits) with conversion times of order μs are readily available. Currently a 16-bit ADC with a conversion time of 1 μs (1 MS/s) requires about 100 mW [95].

A common limitation is differential non-linearity, since the resistors that set the DAC levels must be extremely accurate. For DNL < 1% the resistor determining the 2^{12}-level in a 13-bit ADC must be accurate to $< 2.4 \cdot 10^{-6}$. As a consequence, differential non-linearity in high-resolution successive approximation converters is typically 10 – 20% and often exceeds the 0.5 LSB (least significant bit) required to ensure monotonic response.

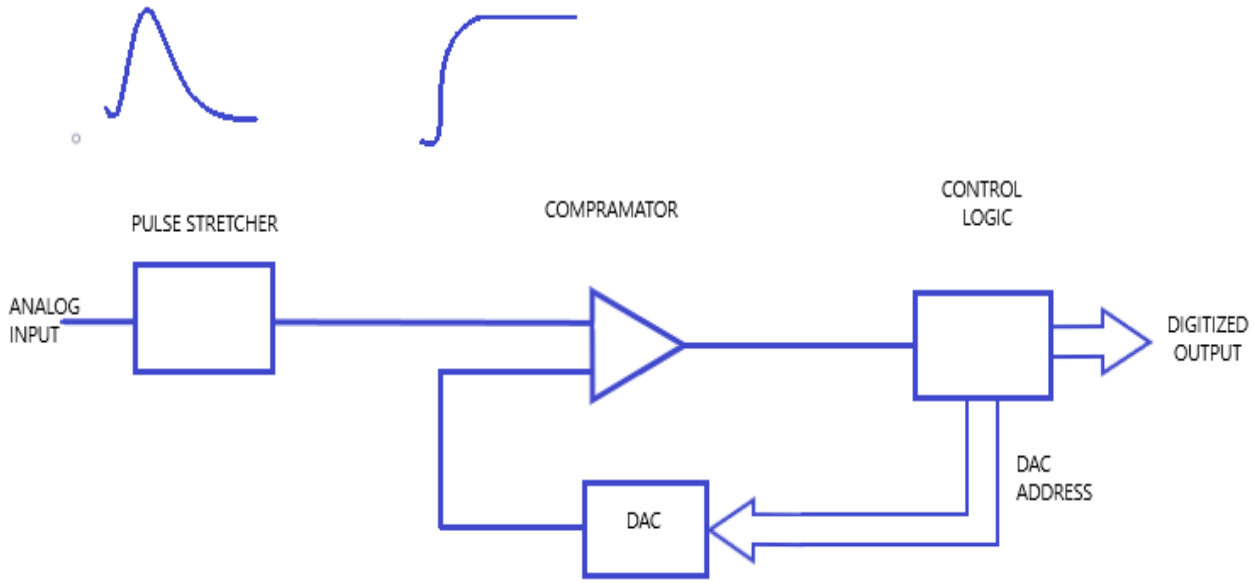

Figure 1.23 – Principle of a successive approximation ADC. The DAC is controlled to sequentially add levels proportional to 2^n, 2^{n-1}, . . . 2^0. The corresponding bit is set if the comparator output is high (DAC output < pulse height).

The Wilkinson ADC [96] has traditionally been the mainstay of precision pulse digitization. The principle is shown in Figure. 1.24. The peak signal amplitude is acquired by a combined peak detector/pulse stretcher and transferred to a memory capacitor. The output of the peak detector initiates the conversion process:

- The memory capacitor is disconnected from the stretcher,
- a current source is switched on to linearly discharge the capacitor with current I_R, and simultaneously
- a counter is enabled to determine the number of clock pulses until the voltage on the capacitor reaches the baseline level V_{BL}.

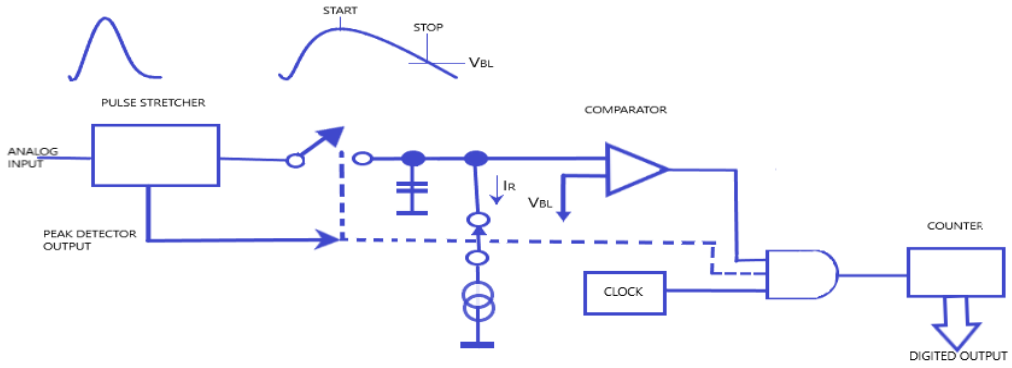

Figure 1.24 – Principle of a Wilkinson ADC. After the peak amplitude has been acquired, the output of the peak detector initiates the conversion process. The memory

capacitor is discharged by a constant current while counting the clock pulses. When the capacitor is discharged to the baseline level V_{BL} the comparator output goes low and the conversion is complete.

The time required to discharge the capacitor is a linear function of pulse height, so the counter content provides the digitized pulse height. The clock pulses are provided by a crystal oscillator, so the time between pulses is extremely uniform and this circuit inherently provides excellent differential linearity. The drawback is the relatively long conversion time T_C, which for a given resolution is proportional to the pulse height, $T_C = n \times T_{clk}$, where n is the channel number corresponding to the pulse height. For example, a clock frequency of 100 MHz provides a clock period T_{clk} = 10 ns and a maximum conversion time T_C= 82 μs for 13 bits (n = 8192). Clock frequencies of 100 MHz are typical, but > 400 MHz have been implemented with excellent performance (DNL < 10^{-3}). This scheme makes efficient use of circuitry and allows low power dissipation. Wilkinson ADCs have been implemented in 128-channel readout ICs for silicon strip detectors [13]. Each ADC added only 100 μm to the length of a channel and a power of 300 μW per channel.

1.8 Criteria for selecting a digitizer waveform.

The essence of digital processing is that the physical signal (voltage, current, etc.) is converted into a sequence of numbers, which is then subjected to mathematical transformations in the computing device. A transformed digital signal (sequence of numbers) can be converted back to voltage or current if necessary.

The source signal from the radiation detector is a continuous function of time. Such signals, defined at all times, are called analog. The sequence of numbers representing a signal in digital processing is a discrete series and may not fully match the analog signal. The numbers that make up the sequence are the signal values at individual (discrete) points in time and are called signal counts (samples). As a rule, samples are taken at regular intervals of time T, called the sampling period (or interval, sampling interval - sample time). The reciprocal of the sampling period is called the sample frequency.

A signal that is discrete in time but not quantized by level is called a discrete signal. A signal that is discrete in time and quantized by level is called a digital signal (sample).

When processing a signal in computing devices, its samples are represented as binary numbers having a limited number of digits. As a result, counts can take only a finite set of values and, therefore, when a signal is presented, it inevitably rounds. The process of converting the signal samples to numbers is called quantization by level, and the rounding errors that occur in this process are called quantization errors (or noise). We note the important fact that, from a formal point of view, an object widely used in nuclear physics, the frequency spectrum of events, falls under the definition of digital signals. Indeed, the energy, mass, angular distributions are usually represented on a discrete scale of the measured quantity (X-axis, channels), and each channel can contain

an integer corresponding to the number of events with a given value of the measured parameter. A set of algorithms based mainly on the least squares method was developed for processing spectra in nuclear physics. Classic DSP applications are almost entirely based on methods derived from Fourier transforms. The historical difference in the approaches to digital signal processing has objective reasons. Indeed, the shape of the spectra, which are realized in nuclear-physical measurements, can vary widely. Continuous, ruled, and mixed types of spectra are known. All of them, as a rule, are not of a periodic nature. In addition, many classic DSP applications require real-time processing, while this limitation is rarely encountered when processing spectra. This determined the specifics in the methods used to process the spectra. However, the same requirements also apply to signals coming from a nuclear radiation detector. In the present work, an attempt was made to use a number of well-developed spectral processing methods applied to signals coming from nuclear radiation detectors. Let us consider in more detail the effects that occur when quantizing an analog signal. The value of the input signal obtained during quantization may have a maximum error equal to the price of the channel of the amplitude-digital converter, which in turn depends on the bit width of the ADC.

Figure 1.25. shows the quantization error (c), which is equal to the difference between the original analog signal (a) and the received discrete signal (b). An important feature of the conversion from analog to digital is that the quantization error behaves like random noise that was added to the main signal. A feature of the work of many ADCs is that in the process of converting the amplitude to a number, they also introduce a digital signal and a systematic bias in addition to random noise. Depending on the type of converting ADC, a systematic decrease or increase in values relative to the level of the input signal occurs (rounding to the nearest whole number, and always in one direction). However, the simple procedure of adding each sample in a digital signal with a random number varying within the price of the ADC channel allows leveling the constant offset and making the quantization noise random. In most cases, quantization only leads to an increase in the contribution of random noise with respect to the desired signal. This additive noise is evenly distributed in amplitude within the channel of the transforming ADC.

The representation of effects introduced by discretization as random noise, which is added to any noise already present in an analog signal, is extremely useful. Imagine an analog signal with a maximum amplitude of 1.0 V, on which random noise with an amplitude of 1.0 mV is superimposed. When digitizing this signal with an 8-bit ADC, the sampling noise can be ~ 4 mV. Thus, the total noise in the digital signal will increase by 4 times. If you do the same procedure, but with the help of a 12-bit ADC, the sampling noise will be ~ 0.25 mV, which is negligible compared to the already existing analog noise. This example clearly shows how important it is to correctly select the digitizer at the design stage of the spectrometer.

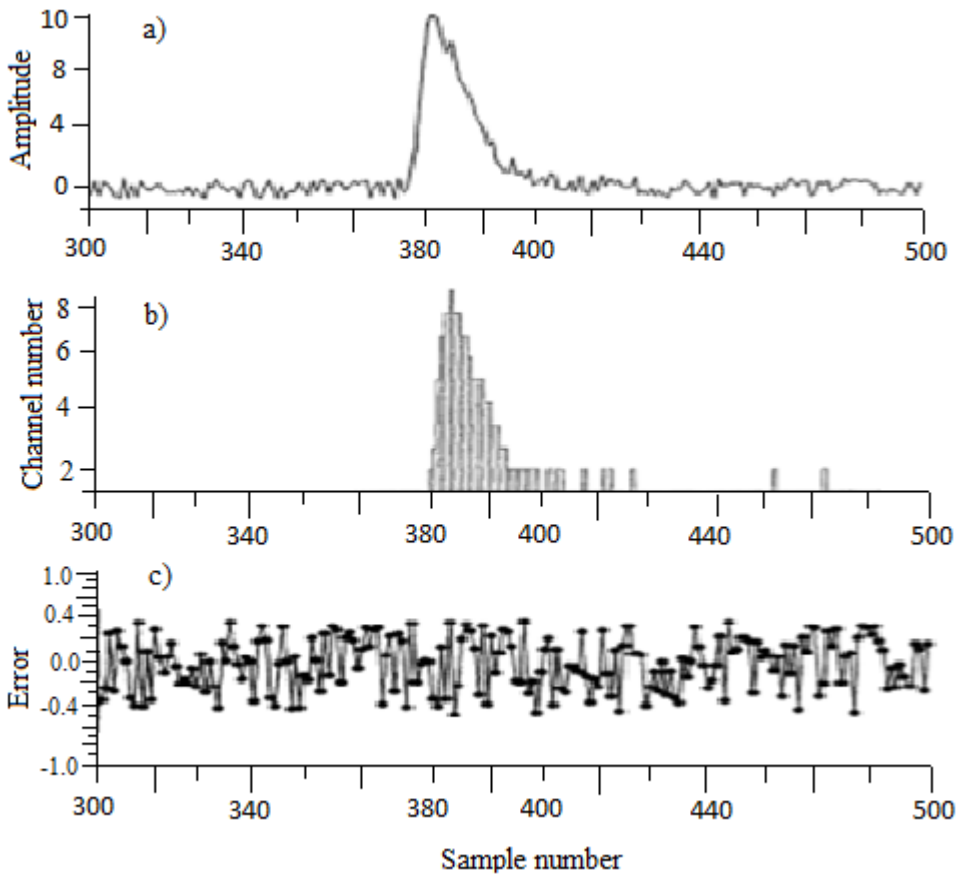

Figure 1.25 – The error occurring when converting an analog signal to digital, a) Analog signal; b) Digital signal; c) sampling error.

Every time when choosing the digitizer we need to find the answer to three basic questions 1) how much noise is there already in the analog signal ?; 2) how much noise is permissible to have in a digital signal ?; 3) What is the dynamic range of the amplitudes of the pulses to work?

Another major problem is the correct choice of sampling rate. It is clear that, in the general case, the representation of a signal by a set of discrete samples leads to a loss of information, since we know nothing about the behavior of the signal in the intervals between samples.

We will assume that the signal was digitized correctly if the original analog signal can be accurately reconstructed from the received digital signal. When choosing the sampling frequency, the discretization theorem, often also called the Kotelnikov theorem (in foreign sources, this theorem is called the Nyquist theorem), and the concept of the Nyquist frequency play a key role. According to this theorem, any harmonic signal can be adequately represented by discrete samples if its frequency is less than half the

sampling frequency (this frequency is called the Nyquist frequency). The origin of these constraints is illustrated in Figure 1.26.

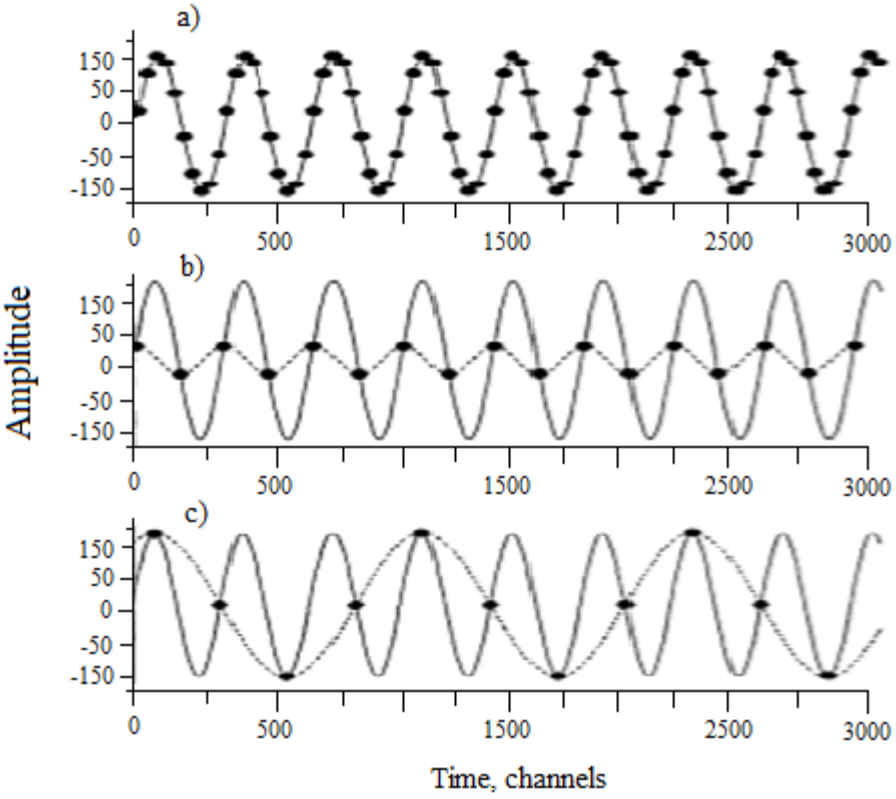

Figure 1.26 – Illustration of the origin of the distortion that may occur when digitizing an analog signal, a) The digitization frequency is greater than twice the frequency of the harmonic signal; b) The digitization frequency is equal to twice the frequency of the harmonic signal; c) The digitization frequency is less than twice the frequency of the harmonic signal.

This effect is called the appearance of false frequencies (aliasing). False frequencies can distort information in both high and low frequencies.

To prevent the appearance of the effect of spurious frequencies, a necessary element of any system based on digital signal processing is an analog high-pass filter. The task of this filter is to suppress all frequencies above the limit established by the sampling theorem in the input analog signal [82]. When digitizing signals from nuclear radiation detectors, it is necessary to keep in mind that each component used to receive and pre-process a signal (for example, the detector itself, a preamplifier, a photomultiplier, and even the cable over which the signal is transmitted) has its limited bandwidth. Often this minimal integration is enough to satisfy the condition set by the sampling theorem, and no additional filtering is required.

To select the optimal frequency of the digitizer, the following factors should be taken into account: 1) The temporal properties of the detector. As a rule, the most informative is the transition process in the detector, during which the charge is collected in the detector. This time can vary from a few nanoseconds to tens of microseconds, depending on the type of detector; 2) Processes in the detector leading to the integration of useful information (carrier diffusion, integrating components in the detector itself and in the electronic circuits used); 3) The nature and structure of the noise characteristic of this installation is important.

The correct choice of digitization and frequency digitizer allows you to save in a digital signal all the useful information that was contained in the analog signal. In this case, only that part of the signal that is associated with high-frequency noise having a small amplitude will be distorted [90].

There is another important parameter that must be taken into account when choosing a digitizer - this is the length of the sample. Modern digitizers allow you to receive digital signals presented from several points to many millions. Unfortunately, it is difficult to propose a universal algorithm for determining the required sample length, since this value depends entirely on the experimental conditions. We confine ourselves to some private examples.

In the simplest case, it is necessary to determine some parameters of the pulses arriving at the input of the digitizer at a random time, and the time of appearance of the pulse and the temporal correlations with other pulses are not the subject of research. In conditions when noise can be neglected, it is enough to choose the interval during which the registration process takes place (transient process in the detector). In the event that there are noise and extraneous harmonic pickups in the signal, to correctly select the digitization interval, their frequency and amplitude spectra must be taken into account. We will estimate the error in determining the amplitude of a pulse after a charge-sensitive preamplifier (A_p) in the event that a sinusoid with a period T and amplitude As is superimposed on it.

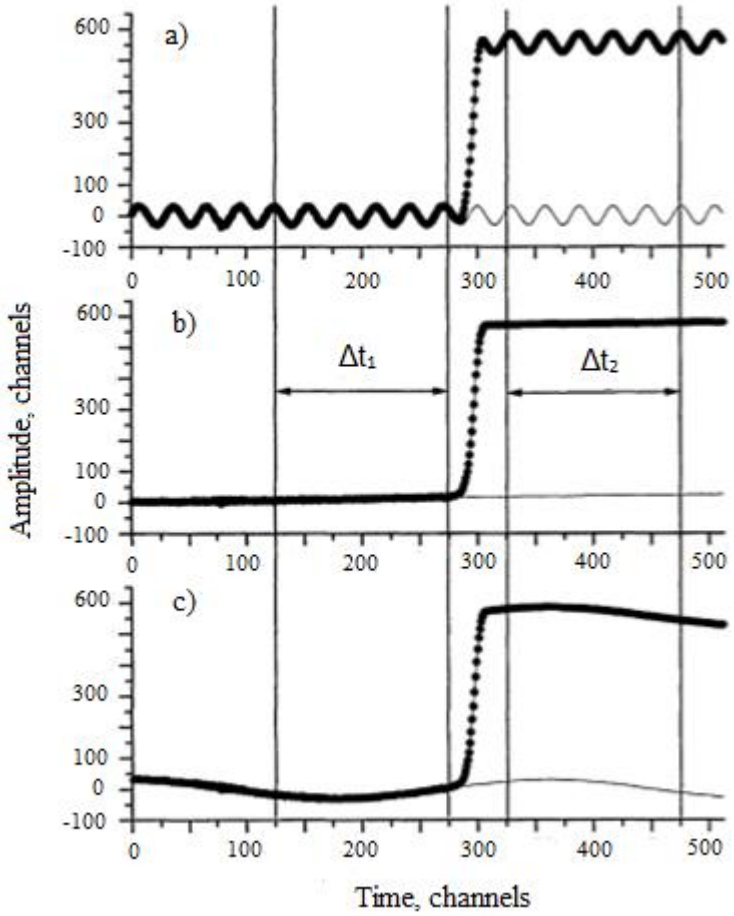

Figure 1.27. – Illustration of the effect of periodic interferences of different frequencies on the signal after the charge sensitive preamplifier. a) high frequency guidance; b) low frequency guidance; c) aiming, the frequency of which is comparable with the digitization interval.

As an estimate of the pulse amplitude, we take the difference of average values in the region where the signal reached the maximum value and the zero line (see Figure 1.27). For simplicity, we choose the same integration intervals for both cases (At). Obviously, if the period of the sinusoid is less than At, then the average values of the signal in selected areas may differ from the true values within ± As * T depending on the phase of the sinusoid (Figure. 1.26, a). In this case, an increase in the integration interval leads to a decrease in the distortion factor of the pickup.

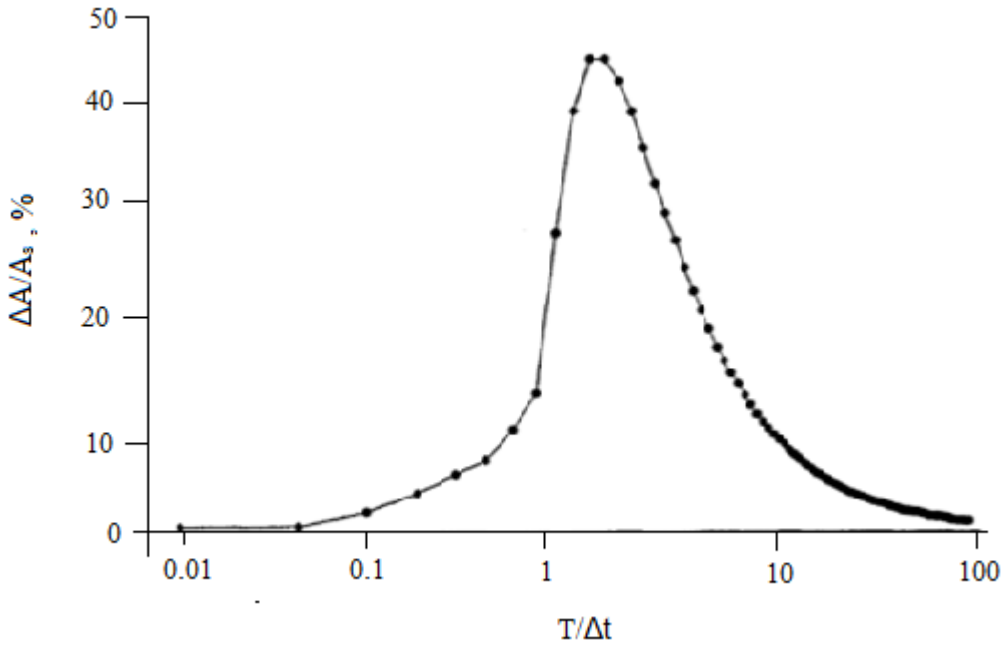

Figure 1.28. – The calculated dependence of the amplitude resolution as a function of the ratio of the pickup period to the digitization interval.

In that case, if the period of the sinusoid is significantly longer than At, the maximum amplitude distortion can be estimated as ~As*At/T (Figure. 1.26., b). Thus, the energy resolution of the spectrometer weakly depends on the contribution of low frequencies.

The main conclusion that can be drawn from the above qualitative assessments is that those parasitic frequencies, the period of which is close to half the digitization interval, have the most destructive influence on the energy resolution (Figure. 1.26., c). In the event that the dominant frequency is present in the noise spectrum (for example, from an external source of electromagnetic or acoustic interference or the natural frequency of the preamplifier), the digitization interval should be chosen so that it differs markedly from the period of this pickup. Figure 5 shows the calculation results, in which a harmonic oscillation of a fixed amplitude and frequency was added to the original signal from the detector (see Figure. 1.26.). The phase of harmonic oscillation was played out randomly. Amplitude resolution related to amplitude of harmonic oscillation is plotted on the vertical axis. The horizontal axis shows the ratio of the period of the harmonic oscillation to the digitization interval.

As another example, let us consider a time-of-flight experiment, in which it is important not only to determine the parameters determining the pulse shape, but also the time of its appearance. As is known, the time of appearance of a pulse from a detector is uniquely related to the energies of the incident particles. In this case, the digitization interval will be determined by the energy interval of the incident particles, which are of

interest in this experiment, and the time required for high-quality detection of the pulse from the type of detector used.

2. FEATURES OF TECHNOLOGY OF FORMATION OF DETECTOR STRUCTURES OF BIG VOLUMES

In the second chapter it considers the manufacturing technology of large-size silicon detectors (surface diameter more than 110 mm) with a thickness about 4 mm, which have Si (Li) p-i-n structure. As initial material the dislocation free monocrystalline cylindrical silicon crystal of the p-type, obtained by the float-zone method (with diameter 110 mm, thickness 8-10 mm, resistivity $\rho = 1000 \div 10000$ Ohm * cm and with life time $\tau \geq 500$ μs) and silicon crystal of the p-type (with a diameter of 110 mm, with a resistivity $\rho = 10 \div 12$Ohm*cm, lifetime $\tau \geq 50$ μs, grown in an argon atmosphere) obtained by the Czochralski method were used. Here, a new method for obtaining a Si (Li) p-i-n structure was proposed. Correspondingly, the technological route for obtaining these structures is described in detail. Also, the technological processes of mechanical and chemical processing of semiconductor wafers based on silicon of a large area have been improved. Furthermore, the optimal modes of diffusion of lithium atoms in p-Si of large diameter and the optimum drift mode of lithium ions into a large area silicon is developed. The last part of this chapter, deals with the development of technology of the electronic part of the detecting system.

Currently, in world practice, detection systems based on relatively small detectors are well developed. At the same time, there is an urgent need to develop semiconductor detection systems operating with the use of large-sized detectors. However, the creation such systems have their own not only physical, but also technical, technological features and difficulties. They are mainly associated with the development of large-size detectors [97]. In particular, this is due to the provision of high-quality detector structures of p-n- or p-i-n type on large-sized crystals. Hence, the need for a deep understanding of the physical processes caused by the effects of large sizes of a semiconductor crystal, that is, the ability to purposefully control them in complex processes, in particular, chemical and mechanical treatments, diffusion, drift, ensure sharp p-n, p-i, i-n transitions across the entire area of the crystal, obtaining thin high-performance current-collecting contacts, etc. [98].

It is known that the stability and efficiency of the parameters of the SCD are primarily determined by the degree of perfection of the surface and the surface of the region of the crystal plates. Therefore, it is necessary to pay special attention to the issues of their pretreatment and surface preparation (especially of large sizes), including the processes of mechanical and chemical processing, so that the initial platinum of the crystal has optimal surface properties, as well as the uniform thickness over the entire area.

2.1. Machining of silicon wafers of large sizes

The technical problems include mechanical and chemical processing of silicon wafers of large diameters. To form the required p-n or p-i-n structures on large-diameter plates, ensuring a high plane-parallelism of their surfaces requires the solution of a number of technical problems on mechanical and chemical treatments. In this regard, this chapter discusses the physical and technological methods for obtaining Si (Li) p-i-n structures based on a large area of silicon. In particular, the use of chemical etching for the preparation of clean surfaces, the detection of pn junctions, for the removal of controlled material by dissolution, and for carrying out chemical polishing of a surface of silicon detector over a large area was considered.

Mechanical processing. Received after cutting the ingot, silicon wafers have a number of violations, which include: the presence of a mechanically disturbed layer, flatness and non-flatness of the sides, bending and a large variation in thickness. Therefore, after carrying out the cutting process, grinding is a mandatory technological operation.

In order to obtain good grinding results, the following requirements must be fulfilled: the work must be carried out in clean, dust-free rooms and under protective covers with excessive air pressure; all installations for carrying out grinding processes should be divided according to the type of processing and the type of abrasive used; All materials must be carefully sorted and stored in separate sealed space suits.

The following abrasives were used as an abrasive material for processing semiconductor wafers: boron carbide B4C and silicon carbide SiC.

The microhardness of the powders was 10^{-9} values on the Moss scale, the range of grit was in the range of M – 5 to M – 14 [99,100]. Grinding was carried out by successive changes in the granularity of the powders, from large grains to fine. In Figure. 2.1 presents single-crystal high-resistance silicon of a large area, grinding with a free abrasive is performed on machines, one-sided and two-sided processing of silicon wafers, using various suspensions and pastes. In the process of processing the abrasive grains are in a free state, i.e. not tightly connected to each other. The abrasive slurry creates a thin layer between the grinder and the silicon wafer to be processed, in which the abrasive grains roll freely.

Grinding with a bonded abrasive differs significantly from grinding with a free abrasive, both in terms of the physical principle of semiconductor material removal during processing and in the kinematics of the process. Grinding with a bonded abrasive is performed on machines with rigid axes, a feature of which is the immutability of the position of the axes of rotation of the grinder and the plates to be machined. The main feature of this process is the design of the grinding wheel, which is a metal disc with a diamond layer deposited on its surface. Diamond grains are firmly connected to the surface of the grinding disc with a special lashing ligament.

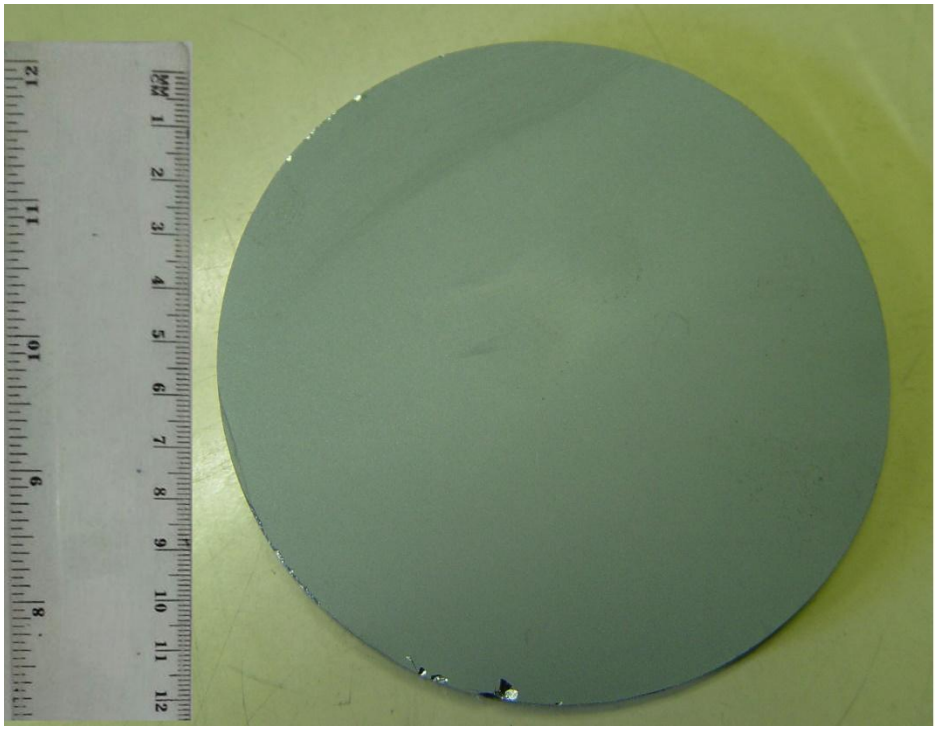

Figure 2.1. Monocrystalline silicon of p- type.

All this causes the emergence of recombination centers, which significantly reduce the carrier lifetime. Therefore, the plates must be ground on both sides to a depth of 50 μm with M14-M5 micropowders on both sides with the successive use of smaller powders, and after each powder number the plates are washed in running distilled water using ultrasonic mixing.

In general, the machining of silicon wafers of various large diameters (diameter> 50 mm) and thicknesses should be ensured with an accuracy of flatness of no more than 1 ÷ 1.5%.

2.2 Chemical treatment of large silicon wafers

The process of chemical processing of semiconductor plates consists in dissolving their surface layer under the action of acid or alkaline etchants. This process is heterogeneous, since the interaction of a semiconductor material with an etchant occurs at the interface between two different media: solid and liquid. Another feature of the chemical interaction of the substrate with the etchant is that the etching process of the substrate is not an equilibrium - the volume of the removed semiconductor material is less than the etchant. Excess etchant and fixing its temperature allow the process of chemical treatment at a constant speed, and thus, accurately calculate the thickness of the layer being removed evenly over the entire surface area of the semiconductor material.

However, it is necessary to take into account the fact that the etching rate of the layer disturbed by machining and the original undisturbed material is not the same. The etching rate of the mechanically disturbed layer is much higher. This is explained by the presence in the mechanically disturbed layer of a large number of structural defects, which increase the effective area of interaction of the semiconductor material with the etchant, which leads to an increase in the etching rate.

Before chemical polishing, the surface should be cleaned. Dust and particles are usually removed by immersing the sample in distilled water, with vigorous stirring.

Before diffusion, a thorough processing of the plates is carried out, consisting of successive processes: treatment in water using soap, thorough drying and treatment in toluene or trichlorethylene, carbon tetrachloride to remove organic impurities. In order to remove inorganic contaminants, as well as atoms or ions in heavy metals, nitric acid HNO_3 is used [99,100].

The crystals in special fluoroplastic cassettes are placed in HNO_3, which is brought to a boil and boiled for 5-7 minutes, then, without removing from the acid, the plates are neutralized with a stream of high-purity deionized water with a specific resistance of> 10 mΩ. Washing under water lasts at least 5 minutes. It should be noted that a longer boiling is ineffective because the nitric acid is also provided by the boiling process as a result of the removal of volatile vapor from the reactive component HNO3 — nitric oxide N0.

To preserve and ensure optimum flatness of silicon wafers during chemical processing, it is necessary to ensure in these processes a uniform etching rate at the same time over the entire surface of their large area. To ensure such conditions, we have developed the optimal compositions of chemical reagents, and also developed a dynamic process of chemical etching. The essence of this process lies in the fact that the plates of silicon crystals were at a certain angle (60 ÷ 650) and rotated also with a specially selected speed. These modes of chemical processing processes were selected in accordance mainly with respect to the diameters of the initial silicon crystal plates.

2.3 Technology of double sided diffusion of lithium silicon structures of large sizes

The development of semiconductor instrumentation, microelectronics is based on the introduction (doping) into the volume of a semiconductor crystal of impurity atoms to a predetermined depth and the necessary concentration. The widespread method of introducing (doping) an impurity atom into the bulk of a crystal is based on the diffusion process. On the surface of a semiconductor crystal, it is necessary to create a “reservoir” of the doped impurity atom, and subsequently diffusion and drift at certain high temperatures.

Lithium diffusion. In order to inject lithium into the p-Si wafer volume, the reservoir is created in the near-surface region of the plates by diffusion of lithium atoms in the necessary area to compensate for the acceptor impurity. The depth of diffusion

and the concentration of lithium ions in the tank depends on how much p-Si needs to be compensated. The question of creating a diffusion region with the required distribution profile of the concentration of introduced impurity atoms in a semiconductor has been studied quite well. In particular, the technology of diffusion for silicon wafers of not large diameters <40 ÷ 50 mm [101,102] is well known. For diffusion processes for obtaining large-size PPDs (> 50 mm and W> 2 mm), we have optimized the technological conditions and modes of the temperature diffusion process. It should be noted that these conditions and modes were determined taking into account the type of SCD relative to their dimensions of the surface of the sensitive area and their length (thickness). For these purposes, a corresponding installation was designed and specially manufactured.

Lithium diffusion is carried out in a vacuum. Caused by thermal evaporation, preheated to a predetermined temperature, lithium diffuses to a predetermined depth. The temperature and diffusion time are determined by the diffusion equation and an infinite source in a bounded body [103,104,105] on both sides of the crystal plate. Lithium sputtering onto silicon platinum heated to 300–500 °C is carried out in a vacuum chamber at a pressure of 10^{-5} torr.

At the first moment of sputtering, organic compounds and oxide burn out from the lithium surface, which are formed as a result of its storage in petroleum jelly and rinsing in toluene before diffusion process occurs. From the ingress of these substances, the surface of the silicon wafers can be protected with a magnetic gate controlled from the outside. The diffusion time is selected depending on the type of radiation detector obtained from the calculation of the required diffusion depth.

After diffusion, the heater is rapidly cooled by blowing compressed air through its cavity. However, the cooling time of the substrate for the first 1000 may take longer than the diffusion time, and due to the instability of some parameters of the technological process during diffusion, the cooling modes of the substrate may vary from process to process.

This in turn can lead to a lack of repeatability of the diffusion depth and distribution of lithium in the n - layer. Therefore, for accurate diffusion depth, it is possible to use mechanisms that eject plates immediately after diffusion from a heated substrate onto a substrate cooled by running water. This ensures reproducibility of the cooling mode and, therefore, the depth of diffusion.

The diffusion temperature is chosen depending on the resistance of the source material, provided that the surface concentration of lithium should be much higher than the concentration of the initial acceptors in silicon N_A, i.e. $N_{Li} >> N_A$ (two orders of magnitude or more), since the surface concentration is determined by the limiting solubility, depending on temperature.

The permissible temperature variation during diffusion is –200 °C, if the criterion is that the permissible variation thickness of the diffusion layer is no more than 5%. The

practically admissible temperature variation is due to the experimental choice of the zone on the substrate when using the middle zone of the substrate.

When choosing diffusion modes, it is taken into account which diffusion parameters (diffusion depth d, surface concentration Ns) must be obtained. Higher temperature is required to obtain significant surface concentration. Given the high diffusion rate of lithium ions at $d \leq 100$ μm, it is very difficult to ensure the reproducibility of the diffusion process at high temperatures. Therefore, the diffusion mode is selected for each type of SCD device. However, it should be remembered that when high silicon is heated to a temperature above 400 °C, the carrier lifetime decreases [106]. In order to evaluate the effect of reducing the lifetime on the electrical and spectrometric characteristics of the detector, it is possible to calculate the lifetime from ~ 1000 to ~ 10 μs on the density of the diffusion current and the current generated by the space charge.

It is known that lithium behaves as a donor in silicon, but, unlike other elements (phosphorus, arsenic, etc.), due to its small ionic radius, it is located not in the lattice sites, but in its internodes [102,103]. Therefore, the mobility, therefore, and the diffusion coefficient of lithium in silicon *D* are obtained abnormally large, i.e. 10^7 times higher than that of ordinary elements giving donor levels in silicon. However, the diffusion coefficient of lithium depends on the oxygen concentration in silicon, since diffusing in the crystal lattice, lithium forms a compound with oxygen in the form of a complex of LiO_2 and can easily move on only after thermal decomposition of the compound [106]. This makes it difficult to drift, since the oxygen content in silicon reaches 10^{18} cm^3. Therefore, for the manufacture of semiconductor detectors, silicon is usually used with a minimum concentration of oxygen (10^{15}-10^{16} cm^{-3}).

However, we have shown [107] the possibility of carrying out the process of the drift of lithium ions at various values of the oxygen concentration. In this case, it is necessary to take into account in these cases the concentrations in the bulk of the crystal of free lithium ions and in the LiO complex.

2.4 Technology of double sided drift of lithium ions

The drift of lithium ions was carried out on a specially designed and manufactured drift installation. Voltage was applied to each crystal independently, and was monitored directly during the drift. The temperature mode of lithium drift (essential for obtaining detectors with a given value of the "output window"), which allows you to calculate the "blurring" of the concentration profile of lithium in silicon during the drift and choose the optimum temperature mode at which the blurring of the profile and accordingly increase the thickness of the "output window" minimally. In this regard, the drift mode

was chosen as follows: temperature T_{dr} = 70÷80 ° C, bias voltage 100÷400 V, depending on the magnitude of leakage currents on each specific chip.

An important parameter to be controlled during the drift is the depth of the compensated area W. If we assume that W> W0, where W0 is the initial thickness of the pn junction after diffusion, and temperature T and voltage V_{dr} drift applied to the sample are unchanged, then Compensation the flux of lithium ions transferred per unit of time is $\rho\mu E_x$. It creates compensation, so the speed of movement of lithium ions $\rho\mu E_x$ will determine the change in the transition thickness [108].

2.5 Features of the technology for producing p-i-n structures for large-sized detector

When forming detector structures on crystals of large diameter and thickness, features of physical processes of diffusion, drift, contact phenomena, etc. arise, which need to be studied and found for them optimal physical, technical, design and technological solutions.

There is a known technology for producing the p – n junction in semiconductors by the melting of metals, for example, indium, tin, gold, or their alloying [102].

However, it has several significant drawbacks: the non-uniform depth of the melting front due to the presence of unbiased areas; the occurrence of mechanical stresses and the resulting formation of cracks in the semiconductor.

The production technology is also known [108], including cleaning, sputtering and diffusion of lithium. This technology is the most efficient compared to other technologies for creating high-quality p-n junctions of large and small areas. Silicon produced by floating zone method is used to fabricate semiconductor detectors [104], in it, the oxygen content is significantly less (10^{15}-10^{16} cm^{-3}). Lithium is applied to the surface of silicon, sprayed in vacuum from lithium metal. In this method, it is possible to strictly control the location of the p-n junction in terms of area and depth, concentration and gradient of the concentration of impurities, which allows you to create semiconductor detectors with highly reproducible characteristics.

The process of manufacturing p-i-n structures consists of the following steps:

1) To remove the layer damaged during cutting, double-sided grinding is used on a grinding machine using M-14, M-5 micropowders with a consistent decrease in the diameter of the abrasive. In this case, a layer with a thickness of at least 50 μm is removed from each side. After grinding, flush the plates with deionized water with alkaline soap.

2) Obtaining the initial structure occurs due to diffusion of lithium. The diffusion of lithium was carried out in a vacuum p ~ 10-5mm.rt.st. at a depth of 300μm over the entire surface of the plate for t = 3 min at a temperature of 450ºC.

3) Etching in a polishing etchant - a mixture of acids HF: HNO_3: CH_2COOH_2 with a ratio of 1: 3: 1 and in aniline etchant.

4) The drift of lithium ions in the electric field of the p-n junction should be carried out at a temperature of 70-80^{0}C and a reverse bias voltage of 100 ÷ 400 V in 10 ÷ 10 days. Depending on the thickness of the sensitive area Figure. 2.2.

5) After the end of the drift, in order to detect the i-region, the two sides of the n^+ -region of the n^+ -i – p structures are ground on a glass disk with silicon carbide micropowder. The thickness of the layer to be removed, taking into account the diffusion of the diffusion profile.

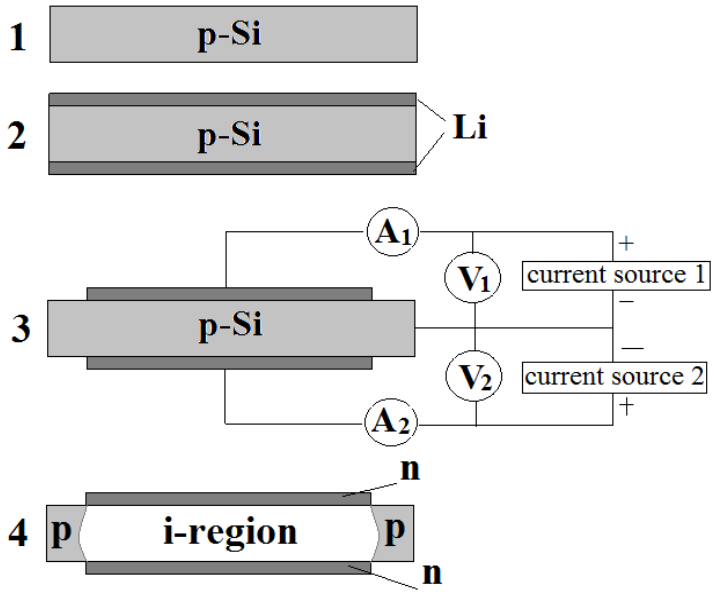

Figure 2.2. Schematic of drift process of Li ions into monocrystalline silicon.

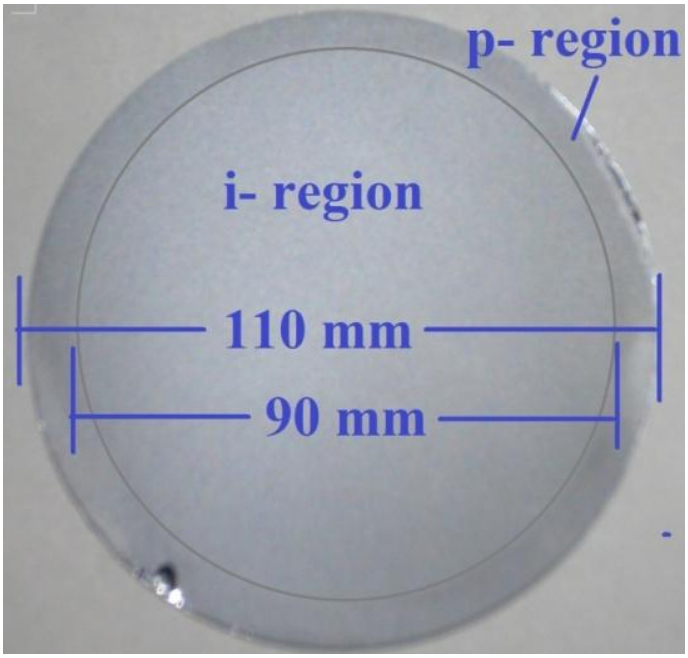

Figure 2.3 – Pictorial representation of the experimentally obtained i-region, after the drift process.

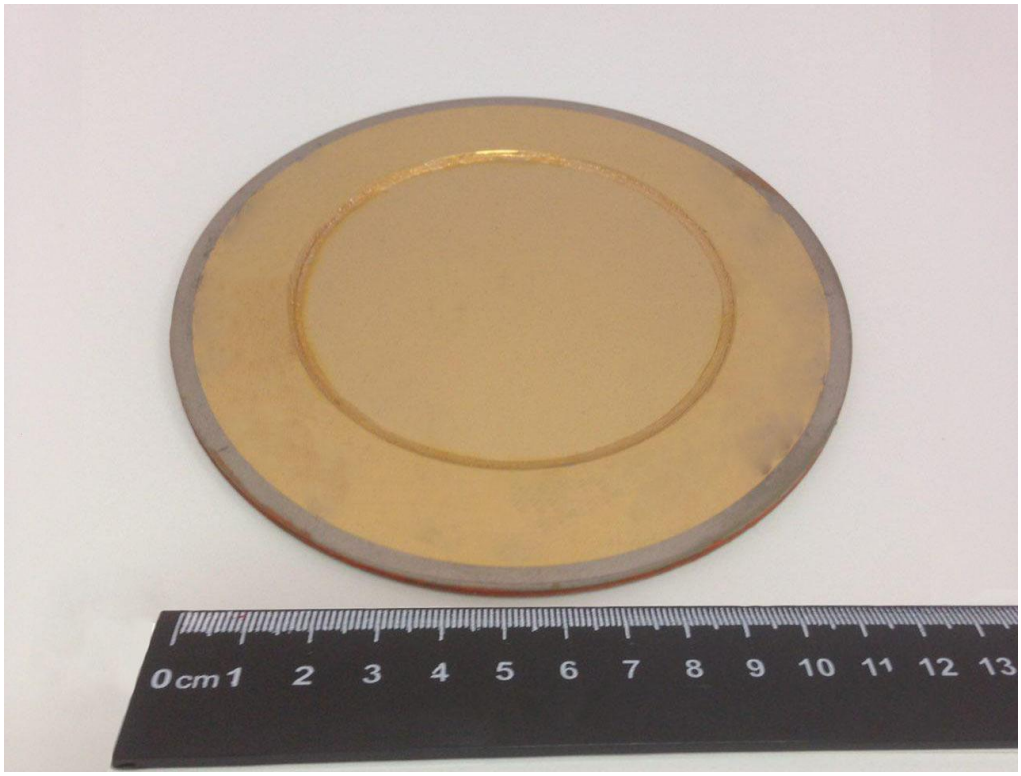

Figure 2.4 – Image of double sided Si(Li) p-i-n detector

The thickness of the polished layer is usually 50 ÷ 400 microns. Removal of the i-region is performed using the decorating etchant HNO_3: HF = 1: 1000. An i-region is considered to be completely deduced when its contours are close to a circle with a diameter equal to the diameter of the diffusion region.

On Figure 2.3. it is shown prepared Si(Li) p-i-n structure after drift process. Figure 2.4. picture of Si(Li) p-i-n detector with metal contact.

2.6 Technology of manufacturing of printed circuit board

This is the initial stage and consists in preparing the surface of the future printed circuit board for applying a protective coating on it. In general, over a long period of time, the surface cleaning technology has not undergone any significant changes. The whole process is reduced to the removal of oxides and dirt from the surface of the board using various abrasives and subsequent degreasing[109].

For the removal of deep dirt the following material can be used: the fine-grained sandpaper, fine abrasive powder or any other tool that does not leave deep scratches on the surface of the board.

In case only a thick oxide film is present on the printed circuit board, it can be easily removed by treating the printed circuit board for 3-5 seconds with a solution of ferric chloride, followed by washing in cold running water. However, it should be noted that it is desirable to either perform this operation immediately before applying a protective coating, or after the treating the work piece should be immediately kept in a dark place, since copper is rapidly oxidized in the light.

The final stage of surface preparation is degreasing. To do this, a piece of soft tissue that does not leave fibers, moistened with alcohol, gasoline or acetone can be used. After degreasing, the board should be washed in running cold water. The quality of cleaning can be monitored by observing the degree of wetting of the copper surface with water. A surface completely wetted with water, without the formation of drops or tears of a film of water on it, is an indicator of the normal level of cleaning. Violations in this water film indicate that the surface is not sufficiently cleaned.

2.6.1 Application of the protective coating for printed circuit board

Applying a protective coating is the most important step in the process of manufacturing printed circuit boards, and this determines the quality of the manufactured board by 90% [110].

For the application of a protective board the "technology of the laser printer and iron" is used. The technology is based on the transfer of toner (powder used for printing in laser printers) from a substrate to a printed circuit board. In this case, two options are possible: either the substrate used is separated from the board before etching, or, if aluminum foil is used as the substrate, it is etched together with copper. The first stage of using this technology is to print a mirror image of a printed circuit board pattern on a

substrate. The print parameters of the printer should be set to the maximum print quality (since in this case a layer of toner of the greatest thickness is applied). As a substrate, a thin coated paper (covers from various magazines),a paper for faxes, aluminum foil, a film for laser printers, a base from Oracal self-adhesive film or any other materials can be used. In case of applying the too thin paper or foil, they need to be glued around the perimeter on a sheet of thick paper. In the ideal case, the printer should have a path for the paper to pass without kinking, which prevents crushing of a similar sandwich inside the printer. This is of great importance when printing on foil or on the basis of Oracal film, because the toner on them is kept very weak, and if the paper is bent inside the printer, there is a high probability that you will have to spend several unpleasant minutes to clean the printer's stove from adhered toner residues. In addition to the printer, also a copy machine can be used, the application of which sometimes gives even better results than printers by applying a thick layer of toner. The main requirement for the substrate is the ease of its separation from the toner. In addition, when using paper, it should not leave lint in the toner. In this case, two options are possible: either the substrate after transferring the toner to the board is simply removed (in the case of a film for laser printers or the basis from Oracal), or soaked beforehand in water and then gradually separated (coated paper). Transferring the toner to the board consists in applying the substrate with the toner to the previously cleaned board, followed by heating to a temperature slightly above the melting point of the toner. Perhaps there are a huge number of options to do this, but the simplest is to press the substrate to the board with a hot iron. At the same time, in order to evenly distribute the pressure of the iron on the substrate, it is recommended to lay several layers of thick paper between them. The temperature of the iron and the exposure time has a very big importance. These parameters vary in each specific case and in order to get qualitative results, the experiment may be run more than once. There is only one criterion: the toner should have time to melt enough to stick to the surface of the board, and at the same time should not reach a semi-liquid state, so that the edges of the tracks do not become flat. After the “welding” of the toner to the board, it is necessary to separate the substrate (except when using aluminum foil as a substrate: it should not be separated, since it dissolves in almost all pickling solutions) [111]. The film for laser printers and the base from Oracal are simply gently removed, while plain paper requires pre-soaking in hot water. It should be noted that due to the peculiarities of printing laser printers, the toner layer in the middle of large solid polygons is small enough, so the usage of such areas on the board should be avoided as much as possible, or after removing the substrate, the board needs to be retouched manually. In general, the use of this technology after some training allows to achieve the width of the tracks and the gaps between them up to 0.3 mm.

2.6.2 Etching of printed circuit board

There are many compositions for chemical etching of copper. All of them differ in the speed of the reaction, the composition of the substances released as a result of the reaction, as well as the availability of chemical reagents necessary for preparing the solution. Below the information on the most popular etching solutions is given [111].

Chloric iron (FeCl3) - perhaps the most famous and popular reagent. Dry ferric chloride is dissolved in water until a saturated solution of golden-yellow color is obtained (this will require about two tablespoons per cup of water). The etching process in this solution can take from 10 to 60 minutes. The time depends on the concentration of the solution, temperature and mixing. Stirring significantly speeds up the reaction. For these purposes, it is convenient to use a compressor for aquariums, which provides mixing of the solution with air bubbles. Also, the reaction is accelerated by warming the solution. At the end of etching, the board must be washed with plenty of water, preferably with soap (to neutralize the acid residues). The disadvantages of this solution includes the formation of waste during the reaction process, which settle on the board and prevent the etching process from proceeding normally, as well as the relatively low reaction speed.

Ammonium persulphate ($(NH4)_2S_2O_8$) [112] is a light crystalline substance, soluble in water based on the ratio of 35 g of substance to 65 g of water. The etching process in this solution takes about 10 minutes and depends on the area of the copper coating being etched. To ensure optimal conditions for the reaction, the solution should have a temperature of about 40 ^oC and constantly stir. After etching, the board must be rinsed in running water. The disadvantages of this solution include the need to maintain the desired temperature and mixing.

A solution of hydrochloric acid (HCl) and hydrogen peroxide (H_2O_2). To prepare this solution, it is necessary to add 200 ml of 35% hydrochloric acid and 30 ml of 30% hydrogen peroxide to 770 ml of water. The finished solution should be stored in a dark bottle, not closed hermetically, since the decomposition of hydrogen peroxide produces gas. Attention: when using this solution it is necessary to observe all precautions when working with caustic chemicals. All work must be done only in the open air or under the hood. If the solution gets onto the skin, it should be immediately washed with plenty of water. The etching time depends strongly on the mixing and temperature of the solution and is about 5–10 minutes for a well-stirred fresh solution at room temperature. Do not heat the solution above 50 ^oC. After etching, the board must be rinsed with running water. This solution after etching can be restored by the addition of H_2O_2. Estimation of the required amount of hydrogen peroxide is carried out visually: the copper plate immersed in the solution must be repainted from red to dark brown. The formation of bubbles in the solution indicates an excess of hydrogen peroxide, which leads to a slower pickling reaction. The disadvantage of this solution is the need for strict compliance with all precautions when working with it [113].

2.6.3 Billet cleaning, drilling, fluxing, tinning

After etching and rinsing of the board, it is necessary to clean the surface of the protective coating. This can be done with any organic solvent, for example, acetone.

Next, all the holes should be drilled. This should be done with a sharply sharpened drill at maximum revolutions of the electric motor. If during the application of a protective coating in the centers of the contact pads the empty space is not left, it is necessary to pre-mark the holes (this can be done, for example, with an awl). The clamping force in the drilling process should not be too big so that no hillocks form around the holes on the back side of the board. Conventional electric drills are practically not suitable for drilling boards, because, firstly, they have low revolutions, and secondly, they have a sufficiently large mass, which makes it difficult to control the downforce. The most convenient way to drill boards is to use electric motors of the type DPM-35N and resembling to them motors with a small collet chuck mounted on their shaft. After drilling, the holes must be treated: all the notches and burrs should be removed. This can be done with sandpaper.

The next step is to cover the board with flux followed by tinning. The special industrial-grade fluxes (best washed with water or not at all requiring rinsing) can be used, or the board can be covered simply with a weak solution of rosin in alcohol. Tinning can be done in two ways: by immersion in the melt of solder or by using a soldering iron and a metal braid soaked in solder. In the first case, it is necessary to make an iron bath and fill it with a small amount of Rose or Wood alloy. The melt must be completely covered on top with a layer of glycerin in order to avoid oxidation of the solder. To heat the bath, you can use an inverted iron or electric stove. The board is immersed in the melt, and then removed with the simultaneous removal of excess solder with a squeegee from hard rubber.

In the next stage, on the made board, elements of digital electronics are installed.

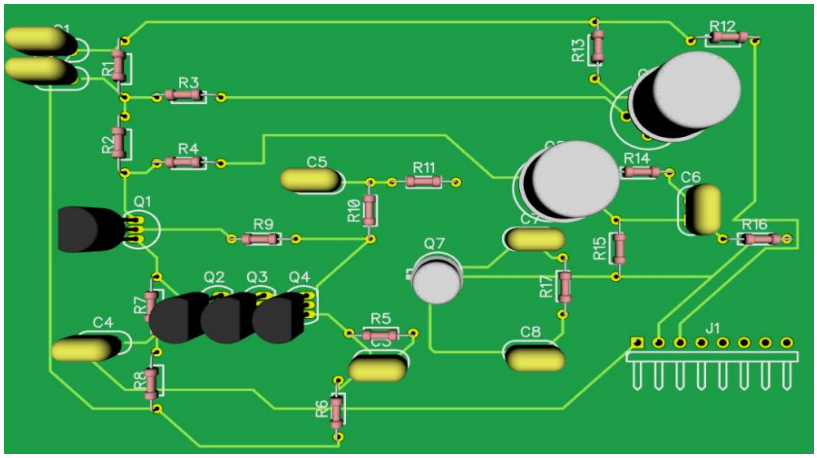

Figure 2.5. The schematic diagram of Charge sensitive preamplifier.

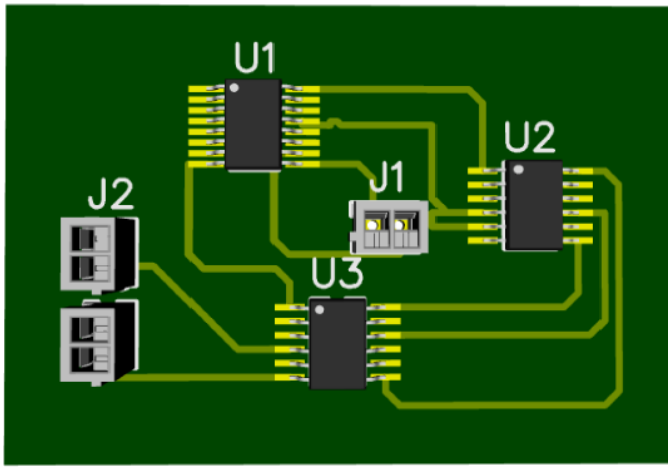

Figure 2.6. The schematic diagram of Counter Converter.

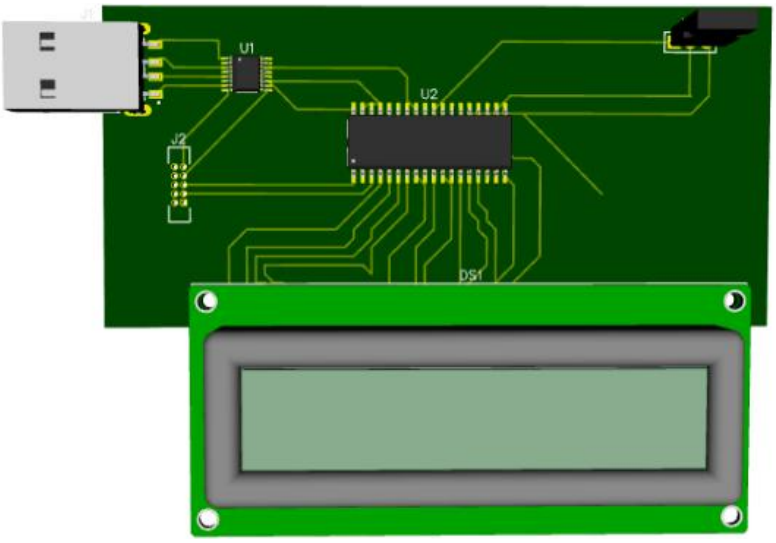

Figure 2.7. The schematic diagram AVR micro scheme with LCD.

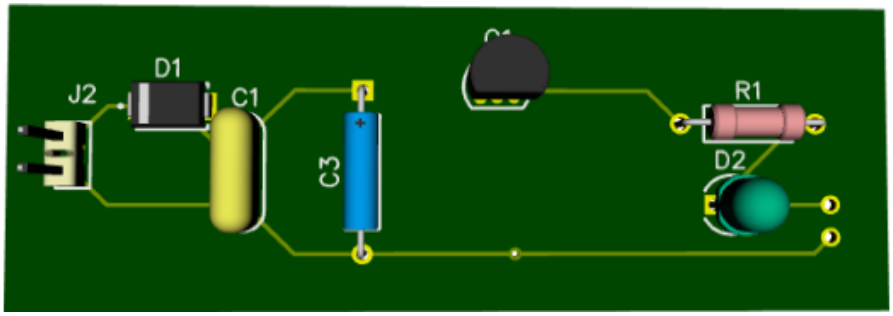

Figure 2.8. The schematic diagram of Current source

To clear view of detector electronic part, it was modeled each block of detector electronics in Dip Trace software. On Figure 2.5, Figure 2.6, Figure 2.7 and Figure 2.8 it was shown schematic diagram of each electronic part of detecting system.

Figure 2.8 Electronic part of detector, assembled in plastic housing

Figure 2.9 Personal computer

Figure 2.8 illustrates pictorial representation of detector electronics. Housing for electronic part was prepared by 3D printer after determination of sizes of detector frontend electronics. On Figure 2.9 it was used personal computer for monitoring and Labview software for analyzing spectrum of charged particles. Detailed description of each part of the electronics is given in Chapter-4.

3. PHYSICAL FEATURES OF THE FORMATION OF THE Si (Li) P-I-N DETECTOR STRUCTURES

In the third chapter, the theoretical aspects of the double-sided diffusion of lithium atoms and the double-sided drift of lithium ions into mono-crystal silicon are considered. Here it was proposed a new method for double sided diffusion of lithium atoms into a mono- crystalline silicon wafer for the further fabrication of Si (Li) p-i-n nuclear radiation. The theoretical assumptions and experimental characteristics of double sided diffusion are considered. To obtain the structure, dislocation-free p-type mono-crystal silicon grown by the Czochralski method and crystal silicon obtained by float-zone method was taken as the initial material. A theory is proposed for an analytical description of the profile of double sided diffusion by the example of a flat silicon wafer with diffusion from an infinite source from two surface planes. Furthermore, it was developed a theoretical model for the double-sided drift of lithium ions in the dislocation free monocrystalline silicon of the p-type, obtained by the float-zone method. It is proposed optimal and temperature regime of drift process for formation of the Si (Li) p-i-n structure.

After diffusion process, a new optimized method for conducting the double-sided drift process of lithium ions into silicon and it's physical and technological peculiarities were considered. The proposed method will help to reduce the drift time and contribute to a uniform distribution of lithium ions over the entire volume of the crystal. As initial material the dislocation free monocrystalline cylindrical silicon crystal of the p-type, obtained by the float-zone method (with diameter 110 mm, thickness 8-10 mm, resistivity $\rho = 1000 \div 10000$ Ohm * cm and with life time $\tau \geq 500$ μs) and silicon crystal of the p-type (with a diameter of 110 mm, with a resistivity $\rho = 10 \div 12$Ohm*cm, lifetime $\tau \geq 50$ μs, grown in an argon atmosphere) obtained by the Czochralski method were used. After manufactoring, the electro-physical characteristics of the detectors obtained by two types of silicon were compared.

3.1 Physical features of double seded lithium diffusion into a silicon wafer

In the last half century, various types of semiconductor detectors [114-115] and modern methods of their manufacture [116-118] which are widely used in various fields of electronic engineering have been created. Nowadays, both elementary (silicon, germanium) and complex semiconductor compounds are used to fabricate silicon detectors[119-121]. However, the use of nuclear radiation detectors based on mono-crystal silicon significantly influenced the development of nuclear physics[9]. They have the following advantages: speed, linearity of signal in a wide range of energy for charged particles of various types [122], high energy resolution, insensitivity to magnetic fields and small dimensions.

One of the long and energy-intensive processes in the technology of manufacturing Si (Li) p-i-n nuclear radiation detectors is the formation of the i-region by diffusion and drift of lithium ions[123]. So, to create a sensitive area of the detector with a thickness

of more than 4 mm, months of painstaking work are required. In addition, providing a large sensitive surface of semiconductor detectors in combination with high energy resolution is still a rather difficult task. This is primarily due to a special requirement for the technology of growing semiconductor materials for semiconductor detectors. The most developed industrial detector materials of silicon of large diameters contain significant inhomogeneities in the distribution of electro-physical parameters over the volume of the crystal[124]. The local and impurity bands present in the sensitive volume of semiconductor detectors significantly impair its radiometric characteristics. Consequently, the requirements of a large sensitive surface and high energy expansion are mutually exclusive.

To shorten manufacturing time and avoid inhomogeneities in the fabrication of Si (Li) p-i-n nuclear radiation detectors, we propose a double sided diffusion method for lithium ions, which precedes a further double sided drift, which is the next stage after double sided diffusion in the development of the detector. The fabrication of the Si (Li) p-i-n structure by means of double sided technology helps to shorten the manufacturing time of the detector and optimizes the physical parameters of the detector. The double sided technology of manufacturing p-i-n structure has a number of advantages, this - with the double sided formation of the p-i-n structure, the manufacturing time is reduced by several times, the structure becomes more homogeneous and etc. Because while penetration of lithium ions in silicon, lithium ions are distributed from the surface side of the crystal into the depth, while the deeper the distribution, the greater the non-uniformity appear in the crystal. Accordingly, with the double sided technology, the ion penetration length is halved [125] and this noticeably reduces the manifestations of the non-uniform distribution of lithium ions in mono-crystalline silicon.

Next we will consider the theory of diffusion. It is known that the diffusion of lithium atoms in silicon serves as an example of diffusion through internodes, since diffusing atoms are small, and the lattice is rather loose. The diffusion coefficients of helium atoms are determined from the rate of penetration of lithium atoms in silicon. One of the most important problems in the study of diffusion is the determination of the concentration profile of diffusing particles. To solve such problems, there are a lot of numerical and analytical methods [126, 127]. Here we consider an analytical method for solving the problem of finding the profile of the concentration of double sided diffusion on a rectangular plate of mono-crystalline silicon. These methods include the method of separation of variables, the method of integral transformations, the variation method, etc.

The diffusion flow J caused by the presence of a concentration gradient is described by the following differential equation:

$$J = -DgradC, \tag{3.1.1}$$

where$D = \frac{\lambda^2}{t}$, λ is the distance between adjacent equilibrium positions, or in the case of one-dimensional diffusion by the equation

$$J_x = -D\frac{\partial C}{\partial x}. \quad (3.1.2)$$

Here *C* is the concentration of diffusible particles, D is the diffusion coefficient. The minus sign indicates that diffusion occurs in the direction of decreasing concentration.

To find solutions, it is used ordinary diffusion equation [128,129] with corresponding initial and boundary conditions.

$$\frac{\partial \mathrm{C}}{\partial \mathrm{t}} = D\frac{\partial^2 \mathrm{C}}{\partial \mathrm{x}^2} \quad (3.1.3)$$

For a given diffusion coefficient, this equation describes the nature of the distribution of the concentration of diffusing particles at various points in the medium as a function of time.

The diffusion coefficient is a material constant characterizing the diffusion rate. With an increase in temperature in solids, the diffusion coefficient usually increases sharply, changing according to the exponential law of the form

$$D(T) = D_0 \exp\left(-\frac{Q}{RT}\right). \quad (3.1.4)$$

Here R is the gas constant, T is the absolute temperature, and D_0 and Q are the main diffusion parameters. The value of Q is called the activation energy, and D_0 is often called the frequency factor. These values are associated with the physicochemical properties of the substance in which diffusion occurs, as well as with the physicochemical properties of diffusing particles.

The exponential nature of the change in the diffusion coefficient can be determined by theoretical and empirical methods.

In some cases, the diffusion coefficient also depends on the concentration of diffusible particles.

Diffusion in semiconductors, as in other solids, is closely related to the presence of structural defects and various imperfections in real crystals.

The initial condition consists in setting the concentration values c(x, t) at the initial time t_0, then the function takes the form c(x, t_0). The boundary conditions describe the behavior of the concentration at the ends of the range of values of *x*: for example, the nature of the change in the concentration or flux of particles.

To solve the equation of double sided diffusion of lithium ions in single-crystal silicon, it is necessary to determine the boundary conditions, proceeding from the fact that the acceptor concentrations in silicon are $5*10^{15}$ cm^{-1}, the concentration of the traps is of the same order. The temperature of introduction of lithium ions corresponds to an

interval from $200\,^0$C to $450\,^0$C. Suppose that the concentration at both boundaries is the same:

$$c(0,t) = c(L,t) = c_s \tag{3.1.5}$$

Applying the method of separation of variables (the Fourier method) [130] we will seek a particular solution of the diffusion equation (3.1.3) as a product of two functions, one of which depends only on the coordinate *X (x)*, and the other only on the time, *T(t):*

$$c(x,t) = X(x) * T(t) \tag{3.1.6}$$

Substituting this expression in the diffusion equation (3.1.3) and separating the variables, we obtain:

$$\frac{1}{D}\frac{1}{T}\frac{dT}{dt} = \frac{1}{X}\frac{d^2X}{dx^2}. \tag{3.1.7}$$

The left-hand side of this equation does not depend on *x*, and the right-hand side on *t*. This, obviously, can only take place when both these parts are identically equal to a certain constant negative value $-\lambda^2$. It is clear that this function is negative, in the case of a positive value, the function $\exp(\lambda^2 Dt)$, which is a solution of the equation $\frac{\partial T}{\partial t} = \lambda^2 DT$, would increase without limit with time, and thus the concentration of diffusing particles would increase indefinitely; λ is a real number. From these considerations one can write:

$$\frac{\partial T}{\partial t} + \lambda^2 DT = 0, \quad \frac{d^2X}{dx^2} + \lambda^2 X = 0. \tag{3.1.8}$$

By integrating these equations, it is easy to find:

$$T(t) = \gamma \exp(-\lambda^2 Dt), \quad X(x) = \alpha cos\lambda x + \beta sin\lambda x,$$

here α, β and γ are arbitrary integration constants. Thus, a particular solution of the diffusion equation has the form

$$\begin{aligned} c(x,t) &= \gamma \exp(-\lambda^2 Dt)\,(\alpha cos\lambda x + \beta sin\lambda x) = \\ &= \exp(-\lambda^2 Dt)\,(A cos\lambda x + B sin\lambda x), \end{aligned} \tag{3.1.9}$$

here $A = \gamma\alpha$, $B = \gamma\beta$. Moreover, the constants A and B can be arbitrary functions of λ.

The general solution of the linear diffusion equation (3.1.3) can be represented as a superposition of particular solutions of equation (3.1.8) [131]:

$$c(x,t) = \sum_{m=o}^{\infty} \exp(-\lambda_m^2 Dt)[A(\lambda_m)\cos\lambda_m x + B(\lambda_m)\sin\lambda_m x]. \qquad (3.1.10)$$

Now we will try to bring the resulting solution to our problem. Let's consider the following case from the beginning - both boundaries of the body, *x=0* and *x=l*, absorb lithium particles, i.e. the concentration of particles on these boundaries at any time moment $t > 0$ is zero:

$$c(0,t) = c(l,t) = 0, t > 0. \qquad (3.1.11)$$

From (3.1.9) and (3.1.10) with *x=0* we find:

$$\sum_{m=0}^{\infty} A(\lambda_m)\exp(-\lambda_m^2 Dt) = 0.$$

Since this equality is observed for all values of t, then, from this we can say:

$$A(\lambda_m) = 0. \qquad (3.1.12)$$

At the same time, for *x=l* from (3.1.9) and (3.1.10) we have:

$$\sum_{m=0}^{\infty} B(\lambda_m)\exp(-\lambda_m^2 Dt) sin\lambda_m l = 0.$$

But since B (λ_m) ≠ 0 - otherwise c (x, t) = 0, then $sin\lambda_m l = 0$, $\lambda_m l = m\pi$ and

$$\lambda_m = \frac{m\pi}{l}, \qquad (3.1.13)$$

where m is an integer. Thus, using the boundary conditions (3.1.5), we found the values of two parameters of the three $A(\lambda_m)$ and λ_m. The third parameter is found by referring to the initial condition: $c(x,t)|_{t=0} = c(x,0)$. Taking into account (3.1.9), (3.1.10) and (3.1.11) we get:

$$c(x,0) = \sum_{m=1}^{\infty} B(\frac{m\pi}{l}) sinm\pi \frac{x}{l}, \qquad 0 \le x \le l.$$

Multiply both sides of this equality by $\sin n\pi \frac{x}{l}$, where *n* is an integer, and integrate *x* from *0* to *l*:

$$\int_0^l c(x,0) \sin n\pi \frac{x}{l} dx = \sum_{m=1}^{\infty} B(\frac{m\pi}{l}) \int_0^l sinm\pi \frac{x}{l} sinn\pi \frac{x}{l} dx = \frac{1}{2} \{\int_0^l \cos\left[(m - n\pi x l dx - 0l \cos m + n\pi x l dx\right\}.$$

The second of these integrals, as is easily seen, is zero. The first integral for $m \neq n$ also vanishes. If $m = n$, then

$$\int_0^l \cos\left[(m-n)\pi\frac{x}{l}\right]dx=l.$$

Thus,

$$\int_0^l c(x,0)\sin n\,\pi\frac{x}{l}\,dx = B(\frac{n\pi}{l})\frac{l}{2},$$

it follows that

$$B(\frac{n\pi}{l}) = \frac{2}{l}\int_0^l c(x,0)\sin n\,\pi\frac{x}{l}\,dx. \qquad (3.1.14)$$

Taking into account (3.1.9) - (3.1.10), from (3.1.11) we obtain the formula for the distribution of concentration in a body of finite size with absorbing boundaries:

$$c(x,t) = \frac{2}{l}\sum_{m=1}^{\infty}\exp\left[-(m\pi)^2\frac{Dt}{l^2}\right]sinm\pi\frac{x}{l}\int_0^l c(x,0)\sin m\,\pi\frac{x}{l}\,dx \qquad (3.1.15)$$

After obtaining the original equation, we consider the case where constant and, in general, unequal concentrations of particles are maintained at the body boundaries:

$$c(0,t) = c_1, \quad c(l,t) = c_2, \quad t > 0.$$

Suppose that the initial distribution of particles in the body can be expressed by the function *c(x, 0).* This problem can be considered as diffusion in the body with absorbing boundaries by introducing the function

$$\tilde{c}(x,t) = c(x,t) + (c_1 - c_2), \quad t > 0. \qquad (3.1.16)$$

This function, as is easy to see, satisfies the diffusion equation, and on the boundaries of the body it vanishes. Therefore, for it you can write a general solution of the form:

$$\tilde{c}(x,t) = \frac{2}{l}\sum_{m=1}^{\infty}\exp\left[-(m\pi)^2\frac{Dt}{l^2}\right]sinm\pi\frac{x}{l}\int_0^l \tilde{c}(\xi,0)\sin m\,\pi\frac{\xi}{l}\,d\xi. \qquad (3.1.17)$$

The initial condition for the function $\tilde{c}(x,t)$ can be taken in this way:

$$\tilde{c}(\xi,0) = c(\xi,0) + (c_1 - c_2)\frac{\xi}{l} - c_1. \qquad (3.1.18)$$

Substituting (3.1.18) into (3.1.17) and integrating, we find an expression for $\tilde{c}(x,t)$, from which, using equality (3.3.16), we get:

$$c(x,t) = c_1 + (c_2 - c_1)\frac{x}{l} + \frac{2}{\pi}\sum_{m=0}^{\infty}\frac{(-1)^m c_2 - c_1}{m} * \exp\left[-(m\pi)^2\frac{Dt}{l^2}\right] sinm\pi\frac{x}{l} + \frac{2}{l}\sum_{m=1}^{\infty}\exp\left[-(m\pi)^2\frac{Dt}{l^2}\right] sinm\pi\frac{x}{l}\int_0^l c(x,0)\sin m\pi\frac{x}{l}dx. \quad (3.1.19)$$

Formula (3.1.19) describes the distribution of the concentration of diffusing particles in a finite body, at the boundaries of which constant concentrations of particles are maintained.

The first two terms of formula (3.1.19) describe the stationary distribution established in the body at $t = \infty$:

$$c(x) = c_1 + \frac{c_2 - c_1}{l}x. \quad (3.1.20)$$

The graph of the function (3.1.20) is a straight line with a slope determined by the ratio between c_1, c_2 and l.

Suppose that the concentrations at both boundaries are the same: $c(0,t) = c(l,t) = c_s$. Taking into account the boundary conditions (3.1.11), assume that particles are absent at the initial instant of time: $c(x,0) = 0$. Then the last formula can be written in the form:

$$c(x,t) = c_s\{1 - \frac{4}{\pi}\sum_{m=0}^{\infty}\frac{1}{2k+1}\exp[-(2k+1)^2\pi^2\frac{Dt}{L^2}]\sin(2k+1)^2\pi\frac{x}{L}\}. \quad (3.1.21)$$

here L - is the thickness of a bulk crystal. For $t = \infty$, the sum vanishes and $c(x,t) = c_s$. Thus, after a sufficiently long time in the body, a constant concentration c_s is established.

The number of particles *N(t)*, penetrated into the body at time t, is expressed by the relation

$$C(t) = \int_0^L c(x,t)dx = c_s L\{1 - \frac{8}{\pi^2}\sum_{m=0}^{\infty}\frac{1}{2k+1}\exp[-(2k+1)^2\pi^2\frac{Dt}{L^2}]\} \quad (3.1.22)$$

The equation shows that for $t = \infty$ $C(t) = c_s L$. At the same time, for $t = 0$, the sum in (8) takes the value $\pi^2/8$, so that $N(0) = 0$, as expected. At $t = 0.05L^2/D$, one can restrict oneself to the first term of the sum. If the concentration of particles at the boundaries of the body is the same $c(0,t) = c(L,t) = c_s$, but in the initial state the

particle concentration in the body is different from zero and everywhere has a constant value: $c(x,0) = \text{const} = c_0$. Then, from the general formula (3.1.21), after a simple transformation, we obtain:

$$\frac{c(x,t) - c_0}{c_s - c_0} = 1 - \frac{4}{\pi}\sum_{m=0}^{\infty}\frac{1}{2k+1}\exp[-(2k+1)^2\pi^2\frac{Dt}{L^2}]\sin(2k+1)^2\pi\frac{x}{L}. \quad (3.1.23)$$

Taking into account the above-proposed formula (3.1.23) for general double sided diffusion from an infinite source in a bounded body, we can write down the diffusion equation for an ionized impurity in a mono-crystal semiconductor with concentration-dependent diffusion.

To determine the temperature-time regimes of the diffusion of diffusion profiles to be processed, the diffusion equation must be solved, taking into account the large concentration of the Li- O complex. The solution of the diffusion equation can be presented in the form:

$$\frac{c(x,t)}{c_s} = erfc\{\frac{x}{\sqrt{\frac{D_0 t_0}{1+K(T_0)N_{O_2}} + A\int_{t_0}^{t}\frac{\exp(-B/T(t))}{1+K(T_0)N_{O_2}}dt}} + \frac{L-x}{\sqrt{\frac{D_0 t_0}{1+K(T_0)N_{O_2}} + A\int_{t_0}^{t}\frac{\exp(-B/T(t))}{1+K(T_0)N_{O_2}}dt}}\}. \quad (3.1.24)$$

here $D_0 = A\exp(-B/T_0)$, $K(T) = K[T(t)]$ is the equilibrium constant for a given temperature *T* at time *t*. A and B are respectively the pre-exponential factor and the activation energy of the diffusion. For diffusion of lithium in silicon $A = 23*10^{-4} cm^2/\sec$, $B = 15200 calories/\deg$.

3.2 Diffusion profiles of silicon wafers after diffusion

Mono- crystalline silicon are characterized by a pronounced defectiveness of the crystal structure due to the large content of oxygen and other impurities [131]. For the fabrication of Si (Li) p-i-n structures of large areas with silicon, we often encounter with problems that need to be addressed through an integrated approach. Often this is due to the intense complexity of Li- O, the generation of thermal donors in the bulk of the crystal, and the formation of dipole structures in the places of accumulation of the acceptor impurity. However, the presence of oxygen and associated Li- O complexes largely determines the stability of the p-i-n structures.

Figure 3.1. shows the diffusion profiles in silicon samples, after the double sided diffusion of Li ions grown by the Czochralski method and the floating zone method.

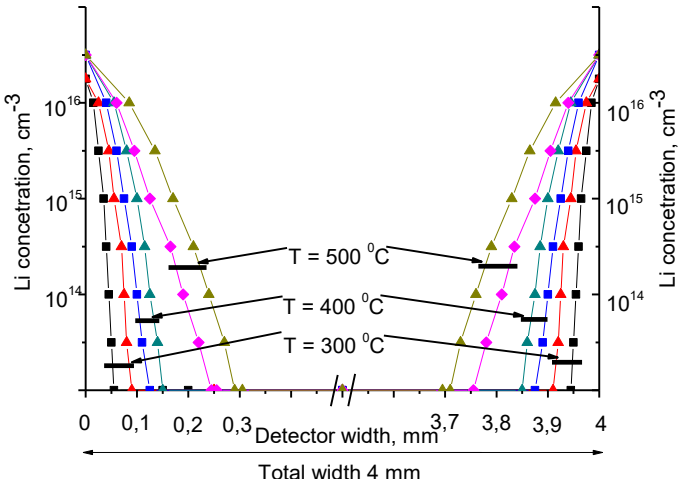

Figure 3.1 – Experimental diffusion profiles of lithium ions in mono-crystalline silicon for different temperature regimes, -■- grown by the Czochralski method and -Δ- by the floating zone method.

The diffusion profiles of two samples obtained by different methods differ significantly. This is due to a decrease in the effective diffusion coefficient due to the complex formation of Li- O in oxygen-containing silicon [132]. As seen from the graph, a mono crystal of silicon grown by the Czochralski method has a large complex formation of Li- O. The Li- O complex reduces the concentration of electric active lithium, but at the same time increases the solubility of lithium in low-ohmic silicon due to the high boron concentration (Rice's Theory). As a result, there is a practical full compensation of most of the diffusion crystal by lithium ions, and incomplete compensation in the p-n junction region leads to a positive effect, that is, the boundary turns out to be sharper than in conventional silicon detector.

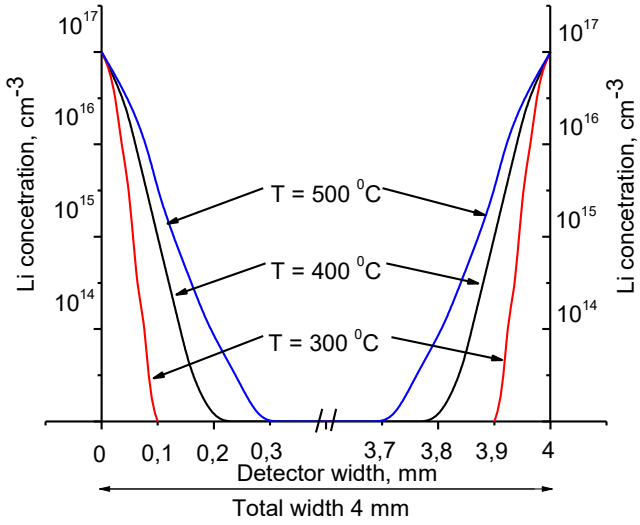

Figure 3.2 – Theoretical diffusion profiles of lithium ions in mono-crystalline silicon for different temperature regimes.

Figure 3.2. shows the theoretical calculation of the diffusion profile of lithium ions in mono-crystalline silicon. The solution of the differential equation (1) was carried out taking into account the boundary conditions (2). The resulting profile in Figure 3.2. shows the general solution of the differential equation of double sided diffusion in the form of expression (10). As can be seen from the figures, theoretical calculations are in complete agreement with the experimental data. The obtained graph of the theoretical distribution of lithium ions in silicon indicates a symmetrical concentration distribution with respect to the middle of the crystal. The sequence in expression (9) converges well for large Dt/L^2 and the better, the larger this value. For small values of Dt/L^2, in order to improve the convergence, it is expedient to use expression (10), taking into account the temperature-time characteristics, which is a sequences in the functions *erfc*.

3.3 Physical features of Double Sided Drift of Lithium Ions in Silicon

The method of lithium ion drift originally proposed by E. Pell [133]. This method found wide application in the production of semiconductor nuclear radiation detectors. Pell proved that if the reverse bias voltage is applied to the p-n-junction with sufficient temperature to excite the donor or acceptor ions, then the ions will drift in the electric field to create intrinsic regions between the p-n junctions. Immediately after the pioneering work of E. Pell, Lechrer and H. Reis's [134] work was published on the investigation of the motion of lithium ions in the region of the p-n junction under reverse bias. Lechrer and H. Reis derived an equations which describe the distribution of lithium ions in the inner part of the crystal depending on time. Then in Pell's theory [135] was considered by Gibbon and Iredal, with more precise assumption to real detecting systems. Here, they considered the accuracy of compensation for acceptor impurities in semiconductors. It was also shown that lithium ions drift technology depends on the distribution of acceptors in initial crystal. It is said that exact compensation is achieved only if the supplied drift field is an orthogonal with flux of the acceptor impurity. Later, in 1969 Lauber[136] stated that the high quality of compensation in the inner part of the crystal mainly depends on the thermally generated electron-hole pairs that were separated by the reverse bias voltage applied during the drift.

Despite the fact that lithium drift technology has been the subject of research since such a long time, Si (Li) detectors are still a relevant research object. In previous work [137], a method and hardware implementation of a segmented and nonsegmental lithium drift detector operating at room temperature was developed. More recently, scientists at Lawrence Berkeley National Laboratory [138] have developed novel types of Ge strip detectors, lithium-drifted Si strip detectors and coplanar-grid CdZnTe type detectors. Also, Si (Li) p-i-n detectors were successfully used for the CBERS project in [139].

These detectors have opened up new possibilities in registering gamma and X ray particles.

There are different types [140,141] and manufacturing technologies [142-145] of Si (Li) p-i-n detectors. Despite a number of advantages of semiconductor spectrometry, it's further development is hampered by technological difficulties of obtaining Si (Li) p-i-n structure for detectors with a large sensitive volume remains the method of p-type silicon compensation by lithium ions.

One of the difficult and very long processes in the development of Si (Li) p-i-n nuclear radiation detectors is the formation of the intrinsic region (i- region) by the drift method. So, to create a sensitive area of the detector with a thickness of about 4 mm it takes months. In addition, when the i region is formed in the crystal, an inhomogeneous distribution of lithium ions arises. Lithium ions move in the field of applied reverse bias along the interstices of silicon atoms from the end part into the depth of the crystal, when the electric field weakens, particles encounter different obstacles (different defects, complexes of various impurities in the crystal and etc.), change the direction of distribution. Therefore, when the i region is formed in the crystal, an inhomogeneous distribution of lithium ions is caused. Another basic factor in the formation of the compensated area is the correct choice of the temperature regime during the drift process. To prevent the negative effects associated with the heating of the crystal above the permissible value due to the passage of a large current through the structure, the drift mode is selected taking into account the heat balance conditions, according to which the amount of heat released (according to the Joule-Lenz law) must be balanced with the heat removed.

In the present work, a new optimized method for conducting the double-sided drift process of lithium ions into silicon and it's physical and technological peculiarities was considered. The proposed method will help reduce the drift time and contribute to a uniform distribution of lithium ions over the entire volume of the crystal.

In proposing method, lithium is diffused from both end surfaces to a predetermined depth sufficient for providing the necessary compensation of the initial acceptor impurity in the required volume to pre-prepared samples of silicon. After the diffusion process by applying a reverse bias voltage and a sufficient temperature, a drift from two flat sides to a cylindrical silicon wafer is carried out. Earlier, technological aspects of double-sided diffusion and drift of lithium ions into low-resistance silicon of the p-type were proposed.

Let's make assumption of the physical description of the double-sided compensation of lithium ions in silicon based on Pell's theory of compensation. Accordingly, a layer of lithium was deposited on a flat circular plate, which is a donor with concentration $N_0 = 5 \times 10^{17}$, by diffusion in vacuum at a depth of 300 μm from both sides of the plate for time t = (3 ÷ 4) min at a temperature of T = (380 - 450) ºC until the p-n junction is formed at the positions x = c. The distribution of lithium is symmetric about the center from two flat sides of the crystal. According to the sufficiently large

thickness of the crystal various boundary effects that contribute to the internal interaction of the particles can be neglected and it is possible to consider the particle distribution as a superposition of two independent functions.

The distribution of lithium ions is a function of the coordinate x dependent on the surface of the crystal, which can be described by a function:

$$N(x,t) = N_s erfc\left[\frac{x}{2(D_0 t_0)^{\frac{1}{2}}}\right] + N_s erfc\left[\frac{l-x}{2(D_0 t_0)^{\frac{1}{2}}}\right] \qquad (3.2.1)$$

here D_0 is the diffusion constant, t_0 is the diffusion time, l - is the total width of the detector.

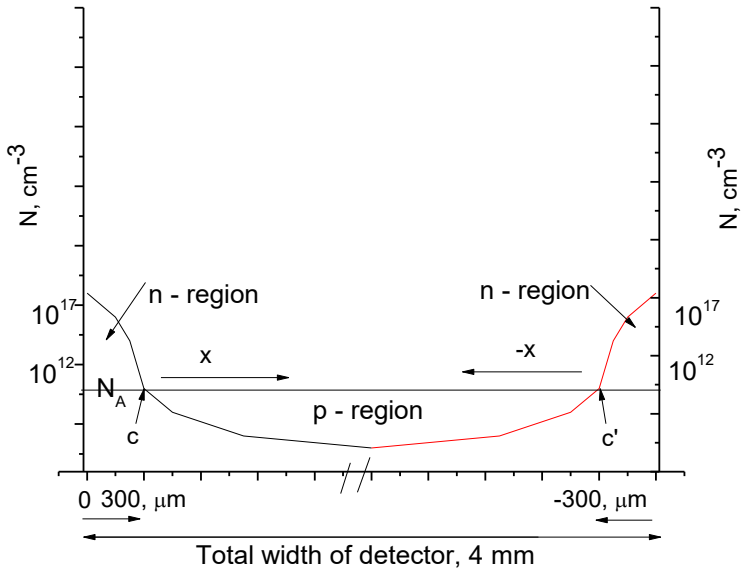

Figure 3.3 – Impurity distribution after preliminary lithium diffusion.

Figure 3.3 shows distribution of lithium ions thought cross section profile of the silicon crystal after the end of double sided diffusion process. To form the drift process, it is useful to consider the region x bordering with x = c and x = c ', with c and c' >> $(D_0 t_0)^{1/2}$.

$$N_D \approx \frac{(2N_0 (D_0 t_0)^{\frac{1}{2}}}{x\sqrt{\pi}} [\exp(-x^2/4 D_0 t_0) + \exp(-(L-x)^2/4 D_0 t_0)]. \qquad (3.2.2.)$$

In the regions x = c and x = c ', the concentration of diffusing ions is equal to the intrinsic concentration of the acceptors of the silicon crystal $N_A \sim 10^{11}$. When drifting, the reverse bias voltage generates an electric field, Figure 3.4.a. The applied external electric field will affect the ions in the inner part of the crystal and will move the

positive Li^+ ions along the electric field into the p- region, thereby compensating for the volumetric charge of the acceptors, which leads to a redistribution of the electric field. And negative ions Li^- will move in the opposite direction starting from the region of p-n junction on both sides from the points x = c and x = c '. As a result, the concentration of lithium and acceptor ions is equal, therefore, the electric field in this region decreases. Since the applied external voltage remains constant, lithium ions continue to penetrate into the n-region. This leads to a complete compensation of the sensitive region of the detector. The shadow area in Figure.3.4.b. shows the formed i -region after double-sided drift of lithium ions.

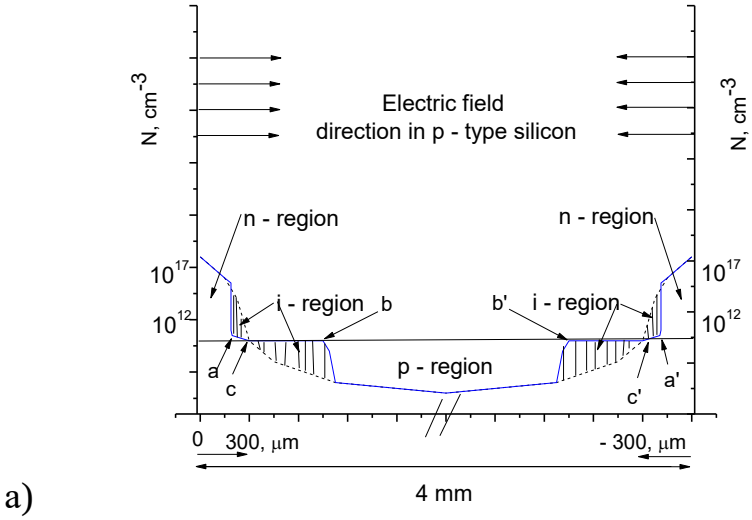

a)

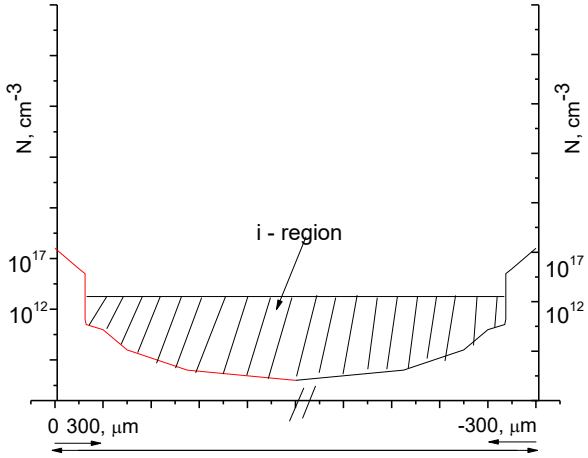

b)

Figure 3.4 – a - impurity distribution during Lithium ion drift, b- formation of i-region over the entire volume of the crystal.

Of course, for the free movement of lithium ions, it is necessary to provide a sufficient temperature taking into account their mobility (μ). The number of mobile ions

around the p-n junction to a square centimeter will propagate along the volume of the crystal from the region where $N_D \approx N_A$. The applied electric field on both sides must be large enough to exceed the diffusion that can occur in the crystal. Only in this case the concentration of lithium ions will decrease in the region c '<x <c and increase in the region c <x <c'. Therefore, the value of donor N_D ions will decrease closer to the region c '<x <c and increase closer to the region c <x <c'.

Now, for these considerations, we can write the following equation describing the drift passage in the shadow region.

$$\int_0^t E\mu N_A dt = (\int_a^c N_D dx) - (c-a)N_A + (\int_{a'}^{c'} N_D dx) - (c'-a')N_A = \\ = (b-c)N_A - (\int_c^b N_D dx) + (b'-c')N_A - (\int_{c'}^{b'} N_D dx) \quad (3.2.3)$$

The solution of this integral can be obtained by an ordinary analytical method,[15]and have the following result:

$$\int E\mu N_A dt = cN_0 erfc\left[\frac{c}{2(D_0t_0)^{\frac{1}{2}}}\right] - aN_0 erfc\left[\frac{a}{2(D_0t_0)^{\frac{1}{2}}}\right] + \\ + \frac{\left[2N_0(D_0t_0)^{\frac{1}{2}}\right]}{\sqrt{\pi}\left[\exp\left(-\frac{a^2}{4(D_0t_0)^{\frac{1}{2}}}\right) - \exp\left(-\frac{c^2}{4(D_0t_0)^{\frac{1}{2}}}\right)\right]} - (c-a)N_A + c'N_0 erfc\left[\frac{c'}{2(D_0t_0)^{\frac{1}{2}}}\right] + \\ + a'N_0 erfc\left[\frac{a'}{2(D_0t_0)^{\frac{1}{2}}}\right] + \frac{\left[2N_0(D_0t_0)^{\frac{1}{2}}\right]}{\sqrt{\pi}\left[\exp\left(-\frac{a'^2}{4(D_0t_0)^{\frac{1}{2}}}\right) - \exp\left(-\frac{c'^2}{4(D_0t_0)^{\frac{1}{2}}}\right)\right]} - (c'-a')N_A \quad (3.2.4)$$

This expression can be written with respect to the b and c regions for explaining the behavior of ions at the initial time:

$$\int_0^t E\mu N_A dt \cong \frac{(c-a)^2}{2L} + \frac{(c-a)^3}{6L^2} + \frac{(c'-a')^2}{2L} + \frac{(c'-a')^3}{6L^2} \approx \frac{(b-c)^2}{2L} + \frac{(b-c)^3}{6L^2} + \frac{(b'-c')^2}{2L} + \\ + \frac{(b'-c')^3}{6L^2} \quad (3.2.5)$$

From this equation, it is possible to calculate the final formula for double sided compensation of Lithium ions in the inner part of the crystal with respect to half the thickness of this crystal W on the one side and half the thickness of the crystal W' on the reverse side.

$$\int E\mu N_A dt \approx \frac{W^2}{8L} + \frac{W'^2}{8L} \quad (3.2.6)$$

Keeping in mind symmetric drift process, we can assume that W≈W', and rewrite (6) as:

$$\int E\mu N_A dt \approx \frac{W^2}{4L} \quad (3.2.7)$$

As shown in equation (3.2.7), the carrier gradient and the electric field are directly proportional to the thickness of the plate. Since, here W - is half the thickness of the entire crystal, it is obvious that the drift path in the crystal volume with double sided technology is reduced by half. To calculate the drift time, we assume the following assumptions.

$$4LE\mu N_A t \approx W^2 \text{and } W \approx \sqrt{4LE\mu N_A t} \quad (3.2.8)$$

For the total thickness of the crystal, we can assume that 2W = d. Then

$$\frac{d}{2} \approx \sqrt{4LE\mu N_A t} \quad (3.2.9)$$

Consequently, expression for the time of compensation in the case of the double sided drift is:

$$\sqrt{\frac{t_1}{t_2}} = 2 \text{ and } t_2 = \frac{1}{4} t_1 \quad (3.2.10)$$

The theoretical result shows, that in the proposed method the compensation time of specified volume of p-Si crystal reduces in 4 times.

Table 1. Temperature and reverse bias voltage regimes.

Regimes	Temperature, ^{0}C	Votage, V	Time, hour
1	55	70	6
2	70	80	16
3	80	90	24
4	110	200	28
5	50	90	10

The degree of compensation in lithium-drift technology of p-i-n structures depends on the temperature-field regimes [16]. By choosing the optimum values of the reverse bias voltage and the drift temperature, it is possible to achieve the maximum degree of compensation, which is characterized by the volume charge in the considered point c and c 'of the compensated i-region. Table 1 shows the experimental data on the mode of reverse bias voltage and temperature, which gradually increase with the expansion of the compensated i-region.

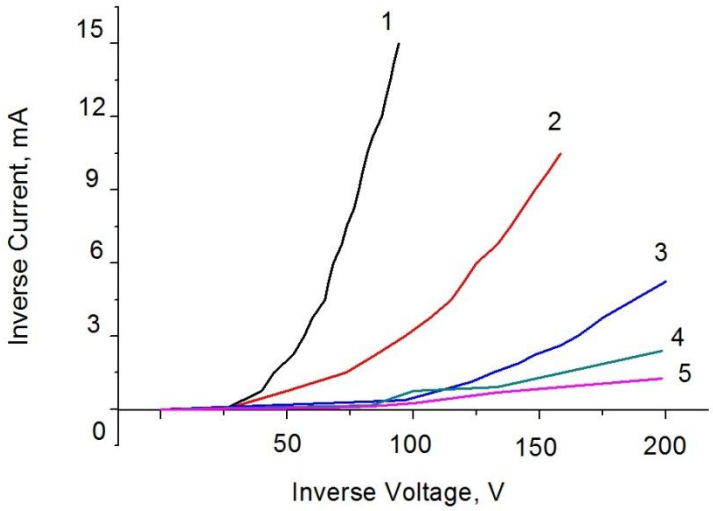

Figure3.5 – Dependence of the reverse current on the reverse voltage, under temperature regimes: T=55°C (1), T=70°C (2), T=80°C (3),T=110°C (4)),T=50°C (5).

Figure 3.5. shows the experimental dependences of the reverse bias voltage and temperature, which gradually increase with the expansion of the compensated i-region. The relative thickness of the high-resistivity layers sharply decreases with increasing temperature in the interval (60-90) °C, and then is fixed at T = 110°C. The drift regime at T = 110°C and a voltage U = (200) V is characterized by a low reverse current, a sufficiently high temperature leads to resorption of precipitates [17], i. e, it can be assumed that the micro-inhomogeneities of the composition is smoothed out.

As can be seen from Table 1, in the proposed method, the drift time is considerably shorter than in the ordinary one-sided drift [21], when months of work are taken to obtain a structure with a thickness $W \geq 4$ mm.

3.4 Electro-physical characteristics of p-i-n detectors

The variation of characteristics of lithium distribution depending on the initial material parameters and basically on dislocation density and specific resistance in Si(Li) p-i-n area have the particular interest. It is widely believed that first, at the process of drift all inhomogeneity of initial material are corrected and the specific resistance of

compensated area is equal to the specific resistance of initial material. Second, electric field distribution in compensated area is almost uniform.

Consequently, during the drift process the intrinsic conduction, corresponding to the drift temperature, is almost achieved. The difference between resistance of compensated area and initial material resistance is the result of influence of drift process of mobile thermal generated carriers. The temperature, necessary to exploit semiconductor detectors, usually is much lower of the drift temperature, consequently, under work condition a quantity of thermal generated vapor is reduced, by that the equilibrium of mobile carriers, donor and acceptor impurities is violated. As a result the basic area of Si(Li) p-i-n structure can be highly overcompensated, with notable excessive impurity gradient. Obviously, this influence will be appeared intensively on low-resistance materials. The effect can be reduced by using additional drift process under lower temperature, wherein the weakening of fixed spatial charge occurs that allows the lithium ions to be redistributed. Under uniform compensation condition, the applied voltage of reversed bias leads to static electric field at every points of the compensated region – it is the ideal state in terms of carrier formation. With increase of specific resistivity of initial silicon the ratio of thermal generated carriers and donor and acceptor impurities varies, also the specific resistivity of compensated region increases.

During the work of semiconductor detectors, the values of current and capacitance play the important role when reverse bias voltage is applied. For the big size semiconductor detectors the flatness of p-n junctions of the entire area of its sensitive surface have great importance. The direct determination of the current- voltage characteristics (CVC) gives useful information. The CVC during application of reverse bias voltage to Si(Li) p-i-n structure were investigated. On Figure. 3.6. the typical CVC of Si (Li) p-i-n structures are shown, made with low-resistance silicon, and grown by Czochralski process (1) and with high- resistance silicon obtained by float- zone method (2). It is obvious from the figure that the low- resistance silicon grown by the Czochralski process (1) have the advantages for manufacturing the lithium drift detectors with big volume, with small reversed current and with high exploitation characteristics. On a par with values of reversed current, the good characteristic of the structure is high breakdown voltage, indicating that the surface of the structure is sufficiently clean.

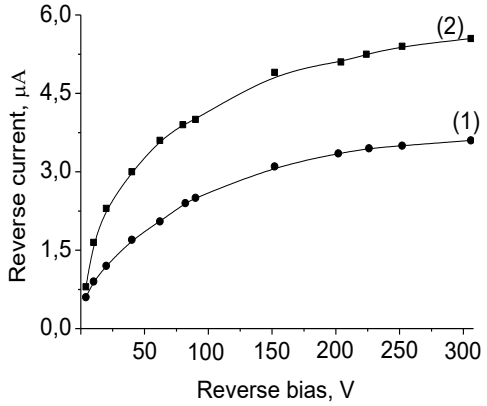

Figure 3.6 –The reverse branch of CVC of Si(Li) p-i-n structure, grown by the Czochralski process (1) and float- zone method (2).

The capacitance of Si(Li) p-i-n structure is directly connected with thickness of the depletion layer and with a specific resistance of initial material. Therefore, by measuring this, it is possible to identify the specific resistance of compensated area of silicon in the prepared structure and predict the values of maximum energy of charged particle, under the conditions of its totally absorption in the depletion layer. The same samples, which were taken to investigate the CVC, were taken to study farad – voltage characteristics (FVC). On the Figure 3.7, the farad-voltage characteristics of Si(Li) p-i-n structure are shown, made with low-resistance silicon, grown by the Czochralski process (1) and with high-resistance silicon obtained by float-zone method (2).

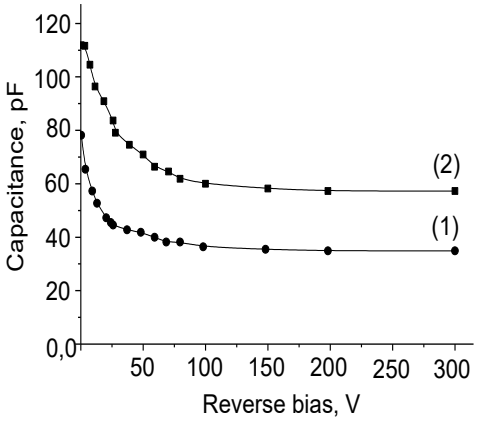

Figure 3.7 – FVC of Si(Li) p-i-n structure, grown by the Czochralski process (1) and float- zone method (2).

One of the main exploitation characteristics of semiconductor detectors of nuclear radiation is the energetic equivalent of noise value. This parameter determines radiometric abilities and efficiency of detection.

On the Figure. 3.8. the curve (1) corresponds to initial crystal, with high resistivity - ρ = 10÷12 Ohm•cm grown by the Czochralski process, and the curve (2) corresponds to the crystal grown by float- zone method with high resistivity ρ = 5000 Ohm•cm.

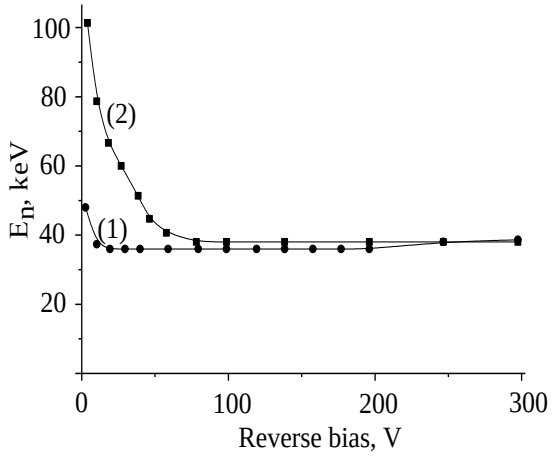

Figure 3.8 – Volt- noise characteristics of Si(Li) p-i-n detectors, made from silicon, grown by the Czochralski process (1) and float- zone method (2).

On the Figure. 3.9., the investigation of amplitude spectra of β-particles from the source of ^{207}Bi is illustrated. The energy resolution of detectors for β-particles from the source of ^{207}Bi is 1 MeV, R_β= 13 keV taken at T = 300 ^{0}C.

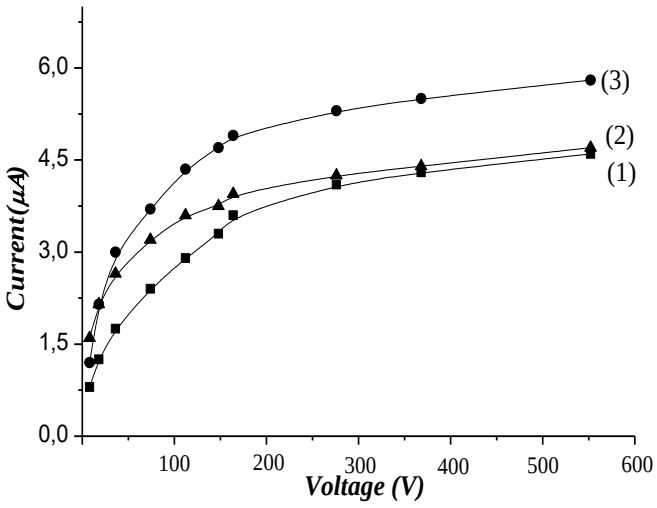

Figure 3.9 –I-V characteristics of Si(Li) p-i-n structures.

On Figure 3.9. and Figure.3.10. it is shown the inverse branches of *I - V* and *C-V*

characteristics of silicon with resistivity 1÷10 kOhm. There curve (1) is for silicon with resistivity 1 kOhm, curve (2) is for 5 kOhm and curve (3) is for 10 kOhm. Leakage current also does not have saturation area and highly dependent on inverse bias value. When inverse bias has value 600 V the leakage current has ≤ 6 μA.

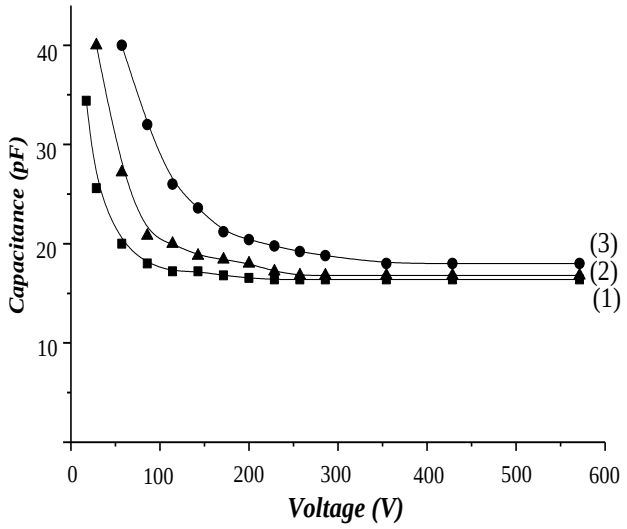

Figure 3.10 –C-V characteristics of Si(Li) p-i-n structures.

One of the basic characteristics of X- ray detectors is its spectrometric characteristics. We used ^{226}Ra for α radiation and ^{207}Bi for β radiation. The energy resolution of detectors for α-particles is R_α = 38 keV (E_α ~ 7.65MeV), and for β-particles is R_β ~ 13 keV (E_β ~ 1 MeV), under temperature T = 300 K.

With the help of ionizing radiation sources the division of the channel was defined. Further by the amplitude distribution diagram the value of noise $E_{ins.noise}$ was defined by this expression:

$$E_{ins.noise} = \sqrt{(\varepsilon_0 N_0)^2 - E_{noise}^2}$$

where $E_{ins.\ noise}$- installation noise (keV), N_0 – number of channel, E_{noise} - noise of detector (keV).

On Figure 3.11. it is shown the dependence of energy resolution on voltage for crystals with various resistivity, the same crystals that was taken above on Figure 3.9. and Figure 3.10. The dependence of energy resolution from voltage of p-i-n structures has a long plateau i.e. wide operating voltage range, where the noise level does not change significantly.

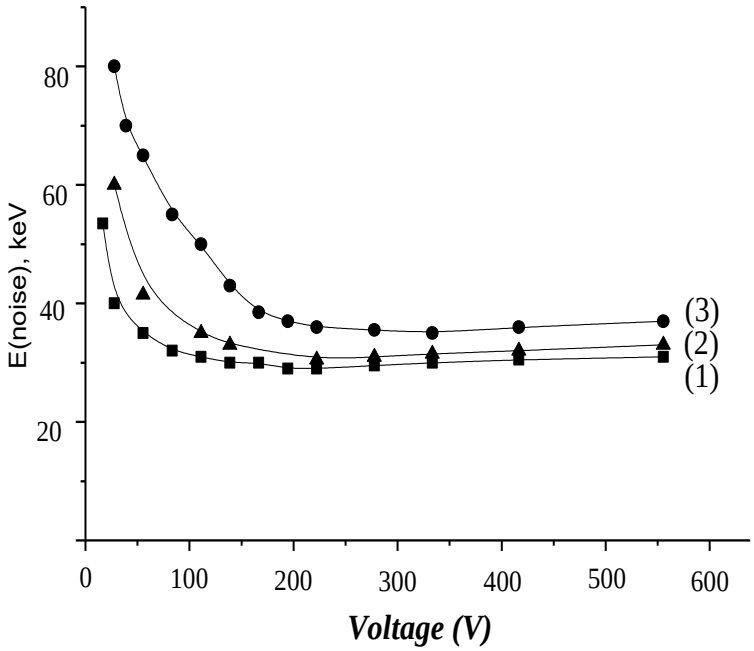

Figure 3.11 –Dependence of energy resolution on voltage Si(Li) p-i-n structures.

Another significant parameter of the semiconductor detectors, such as the energetic resolution, the efficiency of detection, electro-physical characteristics mainly depend on the characteristics, state and stability of junction surface.

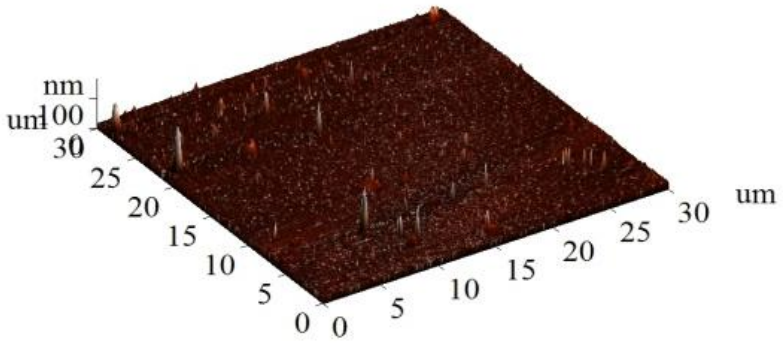

a)

Figure 3.12, p-1. –SPM image of the structure surface of Si(Li) p-i-n structure.

b)

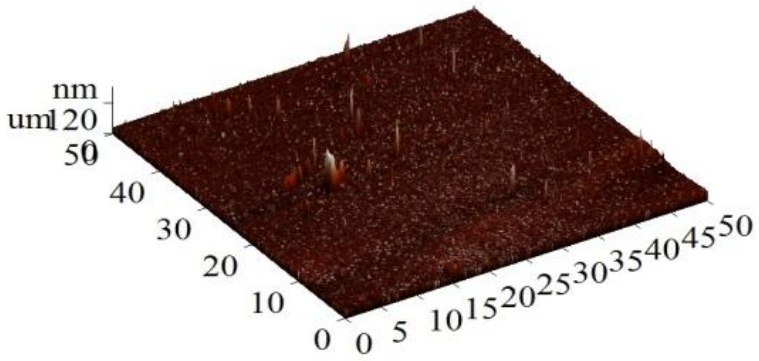

c)

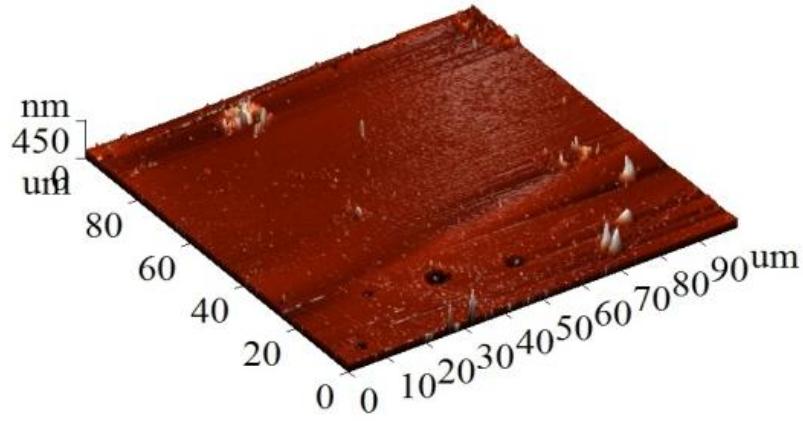

Figure 3.12 . p2. SPM image of the structure surface of Si(Li) p-i-n structure.

So, the investigation of the crystal surface has the specific interest, from the viewpoint of further improvement of the processing and the surface protection.

The Scanning Probe Microscope method (SPM) has been used to study the surface of the samples. On the Figure.3.12, the 3D image of the structure surface (a,b,c) is shown.

4. READOUT ELECTRONICS OF SYSTEM BASED ON Si(Li) P-I-N DETECTORS.

In this chapter, the electronic scheme of a detection system based on a silicon-lithium p-i-n detector is proposed. To extract the signal from the detector, a scheme of a fast current preamplifier, with noise level of the amplifier is 0.43 NV/Hz 1 / 2, for silicon detectors has been developed. The charge sensitive preamplifier is fully compatible with the Si (Li) detector operating in the signal frequency range close to 1-100 MHz. Also, the calculation of the signal frequencies of the detector is proposed, taking into account the size of the detector and stripe contacts. Furthermore, it was considered readout electronics of X – ray detecting system. In the end of the chapter the software part of the readout electronics is described.

4.1 Calculation of detector capacities

Taking into account the above parameters, it is possible to estimate the total capacitance of a detector with a reverse bias of Cr and an inter band capacitance Cs and a volume capacitance Cb [148]. The meaning of the experimental data of Cb is Cb = 300 pF [10]. Cs can be found from this expression:

$$C_s = 2 * (w + L)\left(0.03 + 1.62\frac{w+20}{p}\right)\left[\frac{pF}{cm}\right] = 330 \text{ pF} \qquad (4.2.1)$$

where L is the length, and w is the width of the bands, and p is the step. The total capacitance Cr = Cb + Cs = 330 pF. The resistance of the metal electrodes is R = ρ L / w*t, where ρ = 2.44 μΩ · cm is the resistivity, t is the thickness, for this p-i-n detector R = 0.1 Ω.

4.2 Calculation of frequency of the output signal of the detector

From these calculations it can be said that radiation conditions and detector geometry play a key role for the output signal of the detector, and the total working area of the detector determines the frequency of the detector signals. For example, the current density in the bright detector field can be 0.1 nA / cm2, it gives 160 ns between the events of electrons per cm2 of the working region [18]. In our case, the active working area is 40 mm x 5 mm = 2 cm2, so the electrons will affect on detection contact every 160/2 = 80 ns. From the above calculations, we can say that the electronics of the proposed detector operates at a frequency f ~1/80 ns or 1-10 MHz.

For example, subroutines using the least squares method for signal approximation by various functions, algorithms for Fourier analysis, calculation of convolutions, correlation signals, digital filtering, etc. were included. The third part included general-purpose subroutines used to form one- and two-dimensional spectra, record signals and spectra to disk (both in ASCII and binary files), subroutines for visualizing signals and spectra, search subroutines for signals that meet specified conditions. In all

subprograms, the input and output parameters were coordinated in such a way that the creation of a processing program from them is similar to the assembly of an analog spectrometer.

The texts of many subprograms have a significant amount and cannot be considered in detail in the framework of this thesis. In the following, we confine ourselves to a detailed description of the algorithm.

4.3 Pulse Delay

Pulse delay circuits can be divided into two classes depending on the type of signals that need to be delayed, logical or analog. The delay of logical pulses is due to the need to synchronize in time some control signals. Such delays are often used before the ADC or in one of the time-to-digital converter channels. In analog signal processing, such delay circuits are implemented using a coaxial cable (5 not per 1 m 50 Ohm cable), precision one-shot, or using high-frequency generators and pulse counters. Using DSP, pulse delay can be performed by shifting the signal along the time axis by a specified distance. Note that such a move can be performed not only on an integer number of samples, but using signal interpolation, for any given time interval.

The delay of analog pulses is necessary in order to obtain information that may come later and, depending on it, to process the event that has occurred. The simplest example of such a situation was discussed earlier, when in order to optimally form a pulse, it is necessary to know the time of its rise. It is hypothetically possible to organize a measurement of the pulse front and, depending on the value obtained, change the formative time of the spectrometric amplifier. However, the necessary information will appear no earlier than the passage of the leading edge of the input pulse. So it is necessary to delay the copy of the input signal for the time required to obtain temporary information and only then begin processing it.

Unfortunately, the algorithms associated with the delay of the signal from the detector are not widely used in analog electronics. The reason for this is that the delay of analog signals for more than 100 times does not lead to significant distortions of the waveform and, consequently, to loss of information. Consider the simplest device that delays signals - a long coaxial cable. Due to the effect of the skin effect, the resistance (active) of the cable depends on the frequency.

$$R(f) = 4.17 * 10^{-8}\sqrt{f}\left(\frac{1}{a} + \frac{1}{b}\right) \quad (4.1)$$

where R is the resistance in Ohm 1 meter of cable, f - frequency, a-diameter of the inner core of the cable, b-diameter braid.

It is easy to calculate that, for a standard cable the resistance for a frequency of 100 kHz will be 2.4 10 'Om / m, and for a frequency of 1 GHz - 2.4 Ohm / m. So in the output signal, the high frequency amplitudes will be suppressed more than for the low ones. Often talk about the effect of "leakage" of high frequencies through a dielectric.

The output signal will be integrated by the transmission line. By suppressing high frequencies, you can lose much of the information about the waveform. Another problem that occurs when a signal passes through a long cable is reflections. Defects of the cable, arising during its production and during operation (bending and displacement of the central core relative to the braid), lead to the fact that the characteristic impedance is not constant throughout the line. Each of these defects generates a reflected signal, which will be combined with the main signal.

The presence of effects that distort the transmitted signal does not allow to delay the signals for the required (~ 1 μm) times.

If we understand the time delay between the appearance of a signal in the detector until the next device starts processing it, then we can say that the signals stored on the hard disk of the computer can be stored for an arbitrarily long time without experiencing any distortion. Along the way, the problem of transmitting signals over long distances is being solved. Indeed, it is possible to conduct an experiment in one place and, using the capabilities of a computer connection, transfer them over great distances to where they will be processed. There will be no distortions that appear during data transmission.

4.4 The general scheme of the spectrometric tract with digitizer

The block diagram of the digital spectrometry tract is shown in Figure 1. The circuit includes: 1) detector, 2) Filter, 3) Microcontroller, 4) Personal Computer.

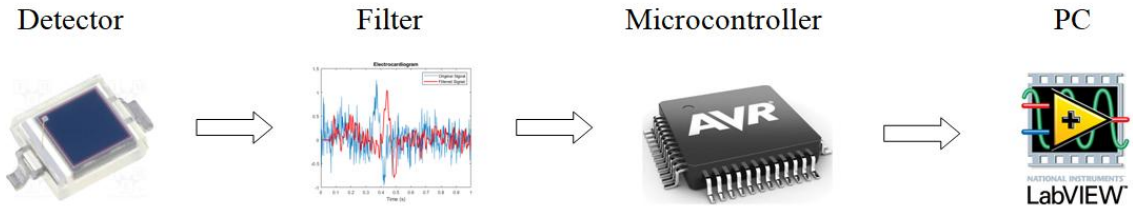

Figure 4.1. General scheme of detecting system.

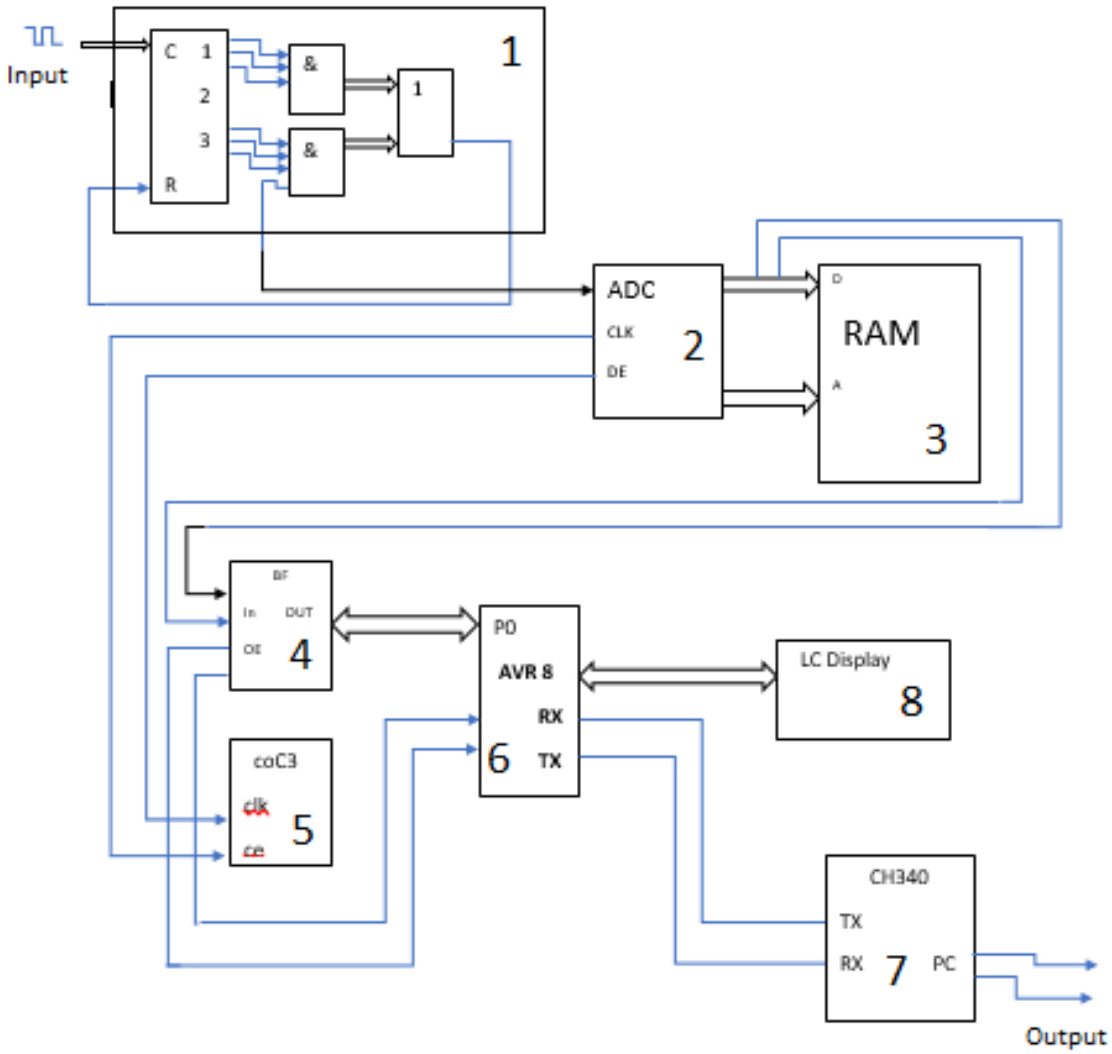

Figure 4.2. – Block diagram of the digital spectrometric tract.

Filter consist of two main part- charge sensitive preamplifier and counter converter. Signal reading tract of filter contains - 1) Counter converter, 2) ADC, 3) RAM, 4) Buffer, 5) Registers, 6) AVR 8, 7) Driver, 8) LCD display, which is shown in Figure. 4.2. Charge sensitive preamplifier locates between detector and counter converter.

4.5 Fast charge sensitive preamplifier

The signals taken from silicon detectors can be used for amplitude analysis and generation of a signal to start the selection system, which, for example, in the [48-49], ensures the start of reading data from the vertex detector. The generation of the trigger signal requires a higher speed than the formation time, i.e. the time to reach the maximum signal in the amplitude channels of the vertex detector, which can have a

value of 400 nsec [60] and less. Traditionally used in silicon detector systems, charge-sensitive amplifiers have a drop significantly longer than the front, and therefore require further additional signal formation. The described pre-amplifier operates in the current mode, its output signal is very close to the current form of the detector when exposed to an ionizing particle and is determined by the time of collection of carriers in the detector, which lies in the region of 15-30 nsec, depending on its thickness. Measurement of the current form is in demand in silicon detector measuring systems as well to determine the quality of the detector [52]. In the problems of complex modeling and testing of a channel with a silicon detector, knowledge of the current form of the detector allows to correctly assess the characteristics of the channel, especially if the detectors are connected in series and long communication lines are used to connect the detector with electronics, for example, in the project [63], where knowledge of the time of occurrence of an event with an accuracy of 2-3 ns is required.

The purpose of developing the current amplifier was the amplifier had a low noise level, low sensitivity to the capacitance of the detector, and the ability to compensate for the impedance of the communication line with the detector and, thus, to reduce capacity is given to the input of the amplifier.

The schematic diagram of the amplifier is shown in Figure. 1. The amplifier has an input complex cascade T_1-T_4, which has local feedback and provides low noise amplifier. Local feedback from collectors of T_2-T_4 to the base of T_1,it improves the linearity of the preamplifier. T_2-T_4 transistors connected in parallel provide noise reduction, thus reducing the equivalent base impedance, which is the main source of noise in a bipolar transistor. The spectral noise density is white noise with a level of 0.43 nV/Hz 1/2.

The second cascade T_5-T_7 is a voltage repeater and provides efficient operation of the common feedback circuit, as well as low output impedance of the preamplifier. General feedback formed by the resistors T_9 and T_{10} (capacity C_5 is a correction),allows to obtain the desired input impedance, which in the case of high steepness of the transistor T_1 is equal to: $R_{вх} \approx R_3$ [R_{10}/(R_9 + R_{10})], and corresponds to $R_{вх} \approx 25$ Ohms. By changing the ratio of resistorsR_3,$R_9$and R_{10}, you can change the input resistance and match it with the impedance of the line connected to the input of the amplifier, for example 50 Ohms. The input current range is 4 mA and the consumption is 50 mW. The capacity of the connected detector can reach more than 1500 pF. The preamplifier allows operation at a load of 50 Ohms.

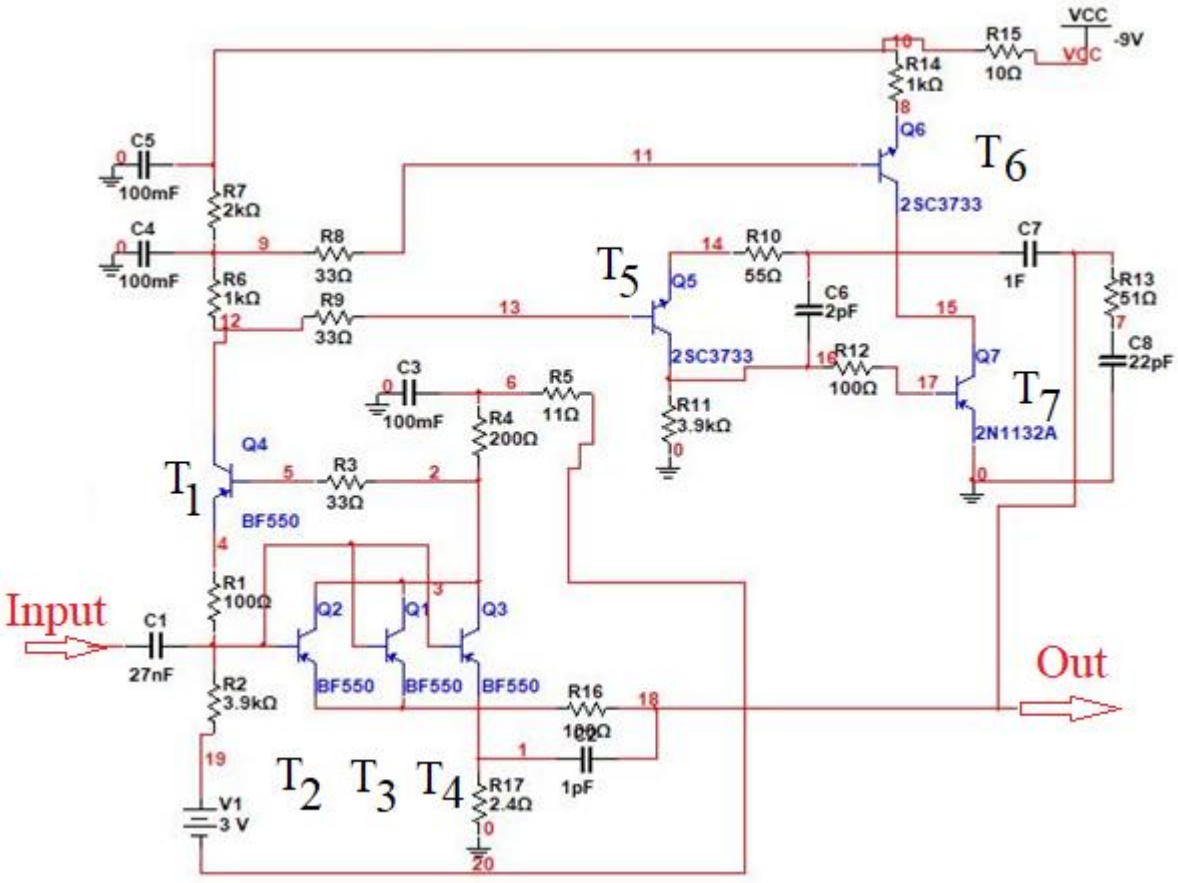

Figure. 4.3. Schematic diagram of the preamplifier. T_1 – T_4 – BF550, T_5, T_6 – 2SC3733, T_7-2N1132A.

A typical preamplifier output in low signal mode is shown in Figure 1. The test action at the input of the amplifier has the form of a short quasi-rectangular pulse with a duration of 8 nsec (channel 1 on the oscillogram). The output signal of the amplifier is reflected on the oscillogram. The rise time of the output signal does not exceed 5 nsec. The output signal of the amplifier in the large signal mode with the same form of test exposure is shown in Figure. 4.4.

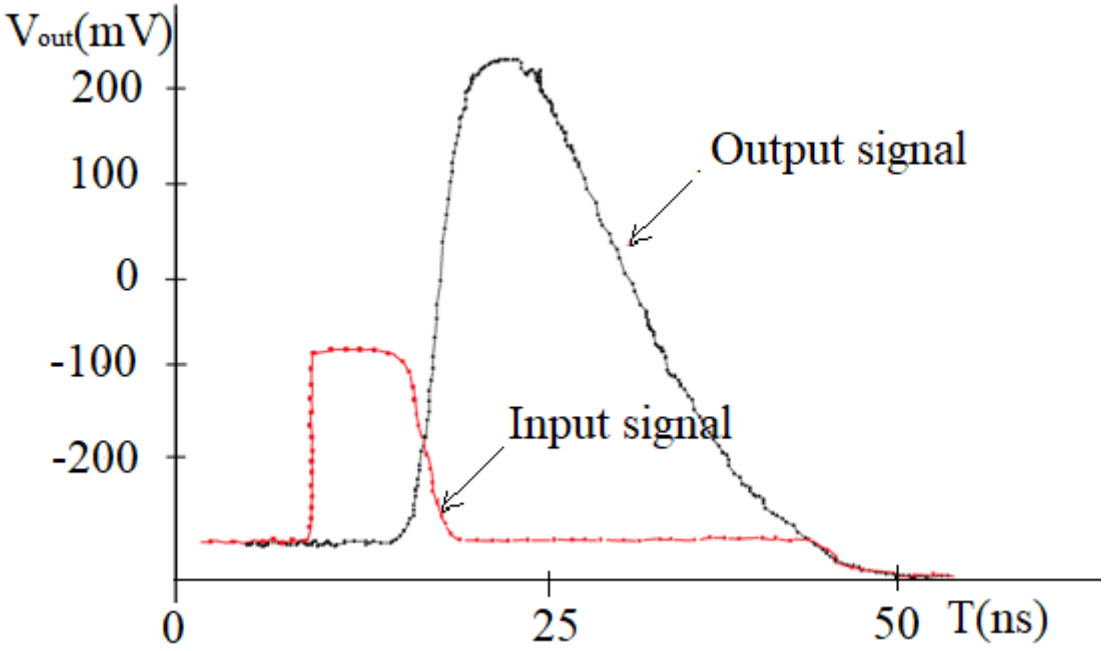

Figure. 4.4. The response of the preamplifier in a small signal on quasi parabolic momentum.

The preamplifier has been tested with real silicon detectors with a capacity of 330 pF. Alpha and Beta particles acted on the detector connected to the input of the amplifier. Responses of the preamplifier for real-signal detector of confirm the possibility of using the preamp for the pickup of signals from silicon detectors for the formation of fast signals, comparable in duration with the collection time of the carriers in the detector.

The amplifier is made by hybrid technology with dimensions of 8 × 45 mm. such small dimensions allow to place several amplifiers on one ceramic substrate. In addition, it is possible to manufacture such an amplifier in a multi-channel version of one of the modern ultra-high frequency submicron or nanotechnology.

4.6 Counter converter

Counter converter transfers the amplitude of the high-frequency input signal to a low-frequency signal without changing the shape characteristics. The counter of the converter, the circuit diagram of which is shown in Figure. 4.5., is designed to work together with a voltage-frequency converter (node U2), the description of which is given above. Specifications:

- The number of characters count – 4
- Input signal (multi-polar) with amplitude, V - ± 1 ... ± 4
- Measuring interval, with - 0.131
- Display time, s - 0.8

- Measurement cycle, s - 1.05
- Mode of operation - periodic

The counter consists of the actual counter, performed on one full decade (D1) and one digit of the highest partial decade (D2 - D3), one frequency dividers on digital integrated circuits D1 and D2, and a device providing periodic operation.

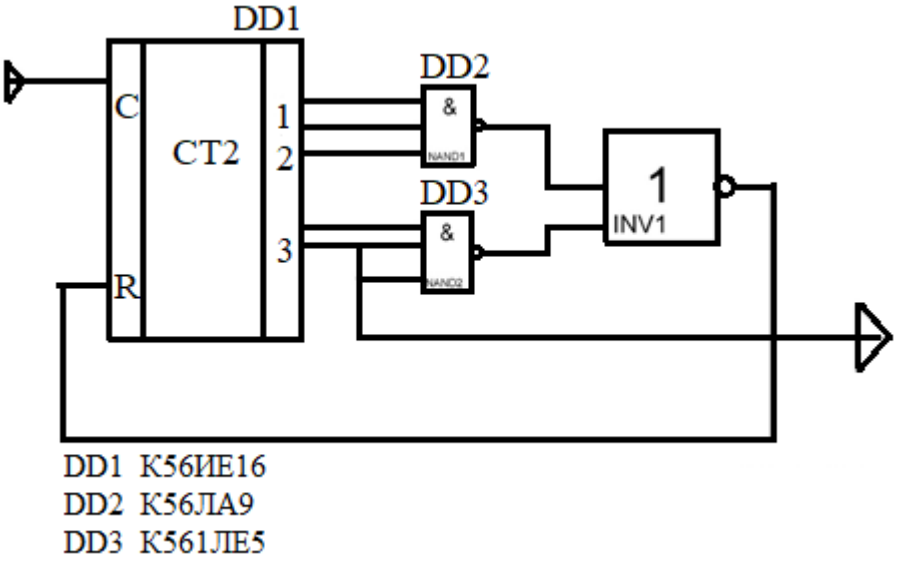

Figure.4.5. – Counter converter

The counter counts the number of pulses of unknown frequency over a reference time interval. The cycle of the counter is divided into three cycles. In the first cycle, the D1 R element (reset) forms a “Reset” pulse, which sets the counter to state 0. During the second cycle (measurement interval), the counter receives the number of pulses proportional to the measured frequency. During the third cycle (indication cycle) the number of pulses recorded in the counter is sent to the ADC. Then the cycle repeats. All three paths are produced by dividing the frequency of the 1 MHz crystal oscillator by a 14-bit binary divider (assembled on the D1 chip in the ultrasonic node) to a frequency of 1.5 MHz. Printed circuit board of the counter, of the converter Timing diagrams explaining the operation of the counter in continuous startup mode are shown in figure. 2. The duration of the reset pulse is equal to the duration of the measuring interval and is 0.131 s.

The reading device provides a visual readout of the measurement result: the digital indication of the measured value using the 16 * 2 sign display. The arrangement of parts and their connection on the board are given in Figure. 3. The efficiency of the meter is checked in conjunction with the converter voltage - frequency (node U2). When adjusting the counter, the KPP converter's voltage-to-frequency ratio is 10 kHz / V. In this case, should be somewhat reduced. Indeed, with the measuring interval t = 0.131 s and the capacity of the counter 2000 is maximum and the frequency that can be fed to the input of this counter is equal to f_{MAX} = 2000 / 0.131 = = 15258.8 Hz, and because of

this frequency should correspond to the input voltage of 2 V, then gain = f_{max} / U_{in} = 15 253.8 / 2 = 7629.4 Hz / V. The counter collected without errors starts to work immediately. Chip K561IE16 works on type T triggers, which is shown in Figure 3.

Chip K561IE16 contains a 14-bit asynchronous counter (pulsation counter), which gives Q0-Q13 16384 binary samples at its outputs. The diagram of the input part of the K561IE16 counter (the driver and the first trigger with the master assistant circuit) are shown in the figure. The output wire QO receives a signal from the buffer inverter. Counter K561IE16 resets the output signals to zero at a high level voltage at the reset input R. The content of the counter increases according to each negative clock pulse difference. The maximum clock frequency reaches 3 MHz, the duration of the reset pulse should exceed 550 ns. The foreign analog of the K561IE16 chip is the CD4020A chip.

4.7 Analog to digital converter for X- ray detecting system based on Si(Li) p-i-n structures

The frequency divider classifies the analog signal at the output to the binary codes of the pulses. 10-bit 1-channel ADC with a sampling rate of 1 MSa/s. Features**:**

1. TSMSCMOP 90nm
2. The bit depth is 10 bits.
3. Sampling rate 1 MSa / s
4. Use of separate power buses 1V for digital and 3.3V for the analog part of the ADC circuit, respectively
5. Low consumption in standby mode (current consumption <230nA)
6. Dissipated power in the range from 0.69 mW to 3.08 mW
7. The real dynamic range with a 24.41 kHz unary output signal is 65 dB
8. Supported technologies: UMC, Global Foundries, SMIC, iHP, Vanguard, SilTerra

The ADC is built on a sequential approximation architecture. The main blocks are: a sampling / storage device, a voltage comparator (comparing the input voltage with the voltage generated by the internal DAC) and a digital module that implements a sequential approximation algorithm. The sequential approximation algorithm consists in sequential comparison of the initial value with the output of the internal DAC. In the first cycle, the value is compared with half of the reference scale of the DAC and the result is written to the register. If the input voltage is higher than half the scale, then the next time it is activated by the output of the DAC, the half of the scale is plus a quarter of the scale; if below, only a quarter of the scale is generated, the result of the comparison is written to the register. In the subsequent cycle, voltages are added, respectively, equal to the eighth part of the scale, the sixteenth, etc. This procedure is repeated 10 cycles, receiving at the output a 10-bit approximation of the input voltage in a digital code. The ADC consists of an input multiplexer, a core, output logic, and a clock generator. The core consists of an internal DAC, a reference voltage generation

circuit, a sampling / storage device, and a voltage comparator. The following supply voltages are required for an ADC: analog power supply 3.0 ... 3.6 V and digital power supply 0.9 - 1.1 V. The ADC can operate in standby mode, at which the reduced power consumption is realized. The device is made in accordance with the TSMSCMOP90nm technology.

Table 2- ADC characteristics.

Name of outputs	Direction	Purpose of outputs
En	I	Turn on the device :“ 1 ” on“ 0 ” off
input <7 : 0>	I	Input Bus
v12	I	Reference voltage (1.2V)
clk_50	I	Signal reference frequency 50 MHz
n_{reg}<2:0>	I	Register transform channel selection
Start	I	Conversion start signal
data <9:0>	O	Output Bus
datnum<9:0>	O	Test bus of the output
v_{dd33}	I/O	Analog power supply 3.3 V
V_{dd}	I/O	Supply voltage of digital blocks 1 V
G_{nda}	I/O	Zero potential analog block bus
G_{ndd}	I/O	Zero Capacity Digital Bus

Table 3- Dimensions of the ADC block

Size	Value	Unitof measurement
Height	145	mic
Width	308	mic

Table 4- Electrical specifications. The values of electrical parameters are given.

Parameter name	Desig nation	Con ditions	Value			Unit of measurement
			min	type	max	
1	2	3	4	5	6	7
Operating temperature range	T	-	-60	27	125	°C
Analog power supply voltage	V_{dd}	-	3,0	3,3	3,6	V
Digital power supply voltage	$V_{3.3dd}$	-	0,9	1,0	1,1	V

Digit	N	-	-	10	-	bit
Clocking frequency	F_{clk}	-	-	50	-	MHz
Data transfer rate	F_s	-	-	1	-	MSa/s
Bandwidth	F_b	-	-	0,5	-	MHz
Standby current	I_{st}	-	-	230	-	nA
Power consumption	P_{cn}	-	0,69	1,32	3,08	mWt
Real dynamic range	SFDR	50MHz	65	67	68	dB
High level input voltage	V_{ih}	For digital inputs	0,7	-	-	V
Low input voltage	V_{il}	For digital inputs	-	-	0,3	V

4.8 RAM

The program code for the Atmega8 microcontroller is schematically executed.The ATmega8K contains 8K bytes on – chip In- System Reprogrammable Flash memory for program storage. Since all AVR instructions are 16- or- 32- bites wide, the Flash is organized as 4K x 16 bites. For software security, the Flash program memory space is divided into two sections, Boot Program section and Application Program section.

The Flash memory has an endurance of at least 10,000 wire erase cycles. The ATmega8K Program Counter is12 bits wide, thus addressing the 4K Program memory locations.

4.9 Buffer

Data buffer (or just buffer) is a region of a physical memory storage used to temporarily store data while it is being moved from one place to another. However, a buffer may be used when moving data between processes within a computer. This is comparable to buffers in telecommunication. Buffers can be implemented in a fixed memory location in hardware or by using a virtual data buffer in software, pointing at a location in the physical memory. In all cases, the data stored in a data buffer are stored on a physical storage medium.

4.10 LCD display

LCD display indicates the process of loading signal data in the microcontroller. Melt's MT-16S2H LCD display for backlit text. The image is similar to the displays of old mobile phones like the Nokia 3310 or Siemens C35. The screen has 16 contacts for supplying power and interaction with the control electronics. To control the display output, it is reasonable to use only 6 of them.

The display is made on a chip compatible with HD44780, which is the standard for LCD screens. Specifications

- Power supply: 3.3—5 V
- Maximum current consumption: 1 mA
- Current consumption backlight: 100 mA
- Display: 2 lines of 16 characters each. The characters are displayed in a 5 × 8 dot matrix.
- Dimensions: 84 × 44 × 13 mm

4.11 Power Supply

Two bipolar power supplies with stabilized voltages of ± 5 and ± 12 V are selected for powering the device nodes. These sources must have sufficient power, to ensure their use for working with external load when various devices assembled on transistors, microchips and operational amplifiers will be setting up and testing. The power sources also produce reference voltages, the main purpose of which is to sets table reference voltages of direct current to different polarity, necessary for the operation of measuring transducers and powering measuring circuits with relatively low current consumption, for example, for calibrating a digital DC counter. Specifications:

- Output voltage, V- ±5 and ±12
- Load current, mA:
- For voltages - ±5 V- 800 mA
- For voltages - ±12V- 300 mA
- Voltage in stability current, %- 0,2
- Reference voltage, V- ±1
- Voltage stabilization factor -100 — 150

The power scheme of block unit is shown in Figure.1.AMS1117 AMS 1119 Diaphragm transistor circuits have been used to stabilize the input voltage.The main purpose of the above voltage surge protector is microcontrollers, digital counters, and so on. That is a standalone power supply which protects against a flawed signal from a logic microcircuit. AMS1117 AMS1119 Voltage Stabilizer Specifications.

The linear voltage stabilizes and the output voltage drops to a lesser degree. AMS1117AMS1119 are located in SOT 223. It is shown in Figure.2. The voltage stabilizer AMS1117 AMS1119's specifications:

- Maximum Output Current - 1 A
- Maximum input voltage 15 V
- Temperature range T= -20and 125^0C

In order to supply the power supply, the stable input voltage 5 and 8 V must be converted to 5 V and 12 V voltages.Because as the unit is a 14-digit counting unit, the power in avr8 microcontroller and display equipment needs to be met.

4.12 Software

In order to minimize distortion of the waveform when transmitting it via cable, it is desirable that the digitizer, and therefore the computer serving it, be in close proximity to the radiation detectors. As a rule, the presence of an operator near the detector during measurements is undesirable or, in principle, impossible (for example, if the installation is in the field of ionizing radiation). Therefore, the task of accumulating data in such conditions can be effectively solved only by two or more computers combined within a local computer network. At the same time, one of them performs the actual functions of data collection and experiment management, while the others serve as terminals for operators, provide their disk space for data storage and are engaged in preliminary data processing. Signal transmission in digital form by means of a local network and the Internet can be carried out at almost any distance without any distortion.

The main function of the accumulation of experimental data is the detection and maintenance of requests coming from the digitizer, transferring data from the internal memory of the digitizer to the computer's RAM, and storing this data on the hard disk. In addition, the program is responsible for the on-line monitoring of the quality of the typed information, the visualization of data, the resolution of regular emergency situations (for example, lack of free space on the hard disk) and providing the operator with the ability to quickly change the drive parameters.

Since digital spectrometry, unlike analog spectrometry, is associated with the accumulation of much larger amounts of experimental data, the accumulation programs, in the first place, require forward response and data storage. So with the accumulation from each event of two digital signals of 512 samples, each amount of information will correspond to a 1024-dimensional experiment with conventional ADCs! For an optimal solution of this problem, first of all, it is necessary to select the slowest stage on the way from the digitizer to the hard disk. Depending on the standard in which the digitizer is made, and the type of computer, this can be either a data bus or a write to a hard disk. So, when working with a digitizer made in the CAMAC standard, the process of transferring data over the bus imposes very severe restrictions on the speed of the entire system [6,13,14]. The main actions of a computer associated with the reception of information from the functional module are as follows. The module sets the request signal to the crate controller, the controller issues a computer interrupt signal. The computer processes the interrupt — sets its priority, interrupts the execution of the current program, remembers its characteristics, goes on to the module's maintenance program, and after receiving one data word returns to the previously interrupted program. The implementation of such a number of operations leads to the fact that the reception of one word of data from the register of a module via a program channel takes a long time, which can be several tens or even hundreds of microseconds. One of the ways to reduce the time of receiving information in a computer is to use block data

transfer. Block data exchange can be defined as the execution of a sequence of KAMAK single operations on sending data initiated by a single read or write command.

When working with digitizers with a bus in the PCI standard, the speed of data exchange between the digitizer and the computer's RAM can reach 100 Mb/s. In such conditions, the process of writing data to the hard disk becomes the limiting factor of the system speed. To reduce the impact of slow disk operations, which are detrimental to speed, multiple-tested recipes can be proposed to significantly improve the drive parameters. 1) Many models of digitizers are equipped with internal memory capable of storing several signals simultaneously. It is necessary to make the most of this memory. 2) As a drive, it is desirable to use a computer with large RAM. This memory can be used for buffering experimental data, which allows minimizing the frequency of accessing the hard disk. 3) It is necessary to write to the hard disk as much data as possible in one access. At the same time, not only time is saved on the disk search for free space, but the data are also less defragmented, which speeds up their subsequent reading and processing.

In some cases, it is very useful to be able to perform preliminary data processing. The solution of such urgent tasks as the removal of saturated and superimposed signals, control over the area and duration of signals is possible at the hardware level, but this leads to a significant complication of the logical scheme of event selection and, consequently, to a decrease in the reliability of the entire system. The same tasks can be solved by software.

All accumulation programs were written in C # and Borland C ++ languages. After the signal is read from the digitizer, it is subjected to preliminary, simplified processing on the control computer. In the event that a certain condition is met, it will be written to disk, if not, it will be deleted. Such a selection helps save disk space from knowingly useless information. This feature can be turned on or off by the operator at any time.

At the stage of setting up the spectrometer equipment, it is often necessary to carry out a visual control over the signals arriving at the input of the digitizer. Usually this procedure is carried out using an oscilloscope. However, the digitizer itself is essentially a digital oscilloscope. A small subroutine is capable of displaying a graphical representation of the readable signals on the display screen. There is a simple switching of viewing modes in which each signal is drawn, every fiftieth signal or a disabled graphics mode (used in data accumulation mode).

To achieve maximum automation and reduce the burden on the operator, the program provides for the possibility of solving some abnormal situations in a semi-automatic mode. In the configuration file, you can specify up to 5 discs on which data can be written sequentially. Moreover, these can be either different hard disks installed on the main control computer, or disks of other computers connected to the local area network. When filling the main (first in the list) disk, the program automatically redirects the output to the disk, which is next in the list.

During the experiments on charged particle accelerators, sometimes there are cases of a sharp decrease in the current on the target or its complete disappearance. This leads to the fact that in the accumulated data the background component will be noticeably increased. The accumulation program can automatically track the frequency of events received at the input of the digitizer and, depending on this, independently make some decisions. On the test case, under the control of the experimenter, it defines the “normal” load. After that, the operator sets the maximum deviation of the load, which is considered valid. If, in the absence of the operator, the frequency of arrival of events beyond the permissible boundaries occurs, the program will pause the recording of data, but will continue to monitor the loading at the input. If, after a break, the counting rate returns to normal, the accumulation of information will continue. During the work, the program creates a file - a log about events that occurred during its work. It reflects: the start time of work, the time of closing each experimental file, the time to transfer to another drive, the time of the start and end of the break caused by problems with the accelerator current, the time of the end of measurements.

Experience with the developed programs has shown that they are more adapted to work in a nuclear-physical experiment, they work much faster and more reliably and they are simpler to configure and control than the standard ones supplied by the manufacturer.

As noted earlier, the programs used in digital signal processing have a more complex structure than those used in analog processing. This is due to the fact that there is an additional block that is associated with obtaining information about the waveform, replacing the work of analog electronics. As a rule, this part of the program requires much more computational resources, as it is associated with complex manipulations with large amounts of data.

A large amount of computations that have to be made in digital signal processing leads to the fact that specific rounding errors may occur that are associated with the form of representation of different formats of numbers in a computer and which can accumulate in the process of repeatedly repeated mathematical operations.

In order to avoid loss of accuracy in calculations, it is necessary to adhere to well-known rules: first of all, perform operations on numbers that are comparable in order of magnitude, make wider use of special features of the translator to control rounding, choose the types of variables correctly in each case [19].

4.13 Spectrometric characteristics of detecting system

In most cases, two types of measurements are most significant: determining the energy of particles and measuring their flow. Sometimes it is necessary to register groups of particles of low intensity in the presence of a large number of other particles with very close energies.

For the most intense peaks (595 keV and 720 keV), the calibration of the channel of the measuring instrument was determined, and the width at half-height of the most intense peak was used to find the energy resolution in keV using the formula:

$$R_\beta = \sqrt{(\Delta E_0 N_n)^2 - E_{noise}^2} \quad ,$$

where ΔE_0 - the value of division of channel, N_n – number of channels at half height, E_{noise} – noise of installation.

The calculated energy resolution of ^{207}Bi for this detector is 19 keV. The theoretical resolution of the detector is determined by the noise of the detector and the energy of the ionizing radiation source.

$$E_\beta = \sqrt{(\Delta E_{noise})^2 (keV) + 1.5\ (MeV)}$$

For this detector, the calculation gives E_β ~ 15 keV.

The time constants of the forming circuit are set deliberately above the collection time in order to exclude the fluctuation of the pulse shape.

Spectrometric characteristics at room temperature were studied on these samples. The energy resolution was measured using a source of α particles of ^{239}Pu and β particles of ^{207}Bi. Amplitude spectra were recorded using a spectrometric tract.

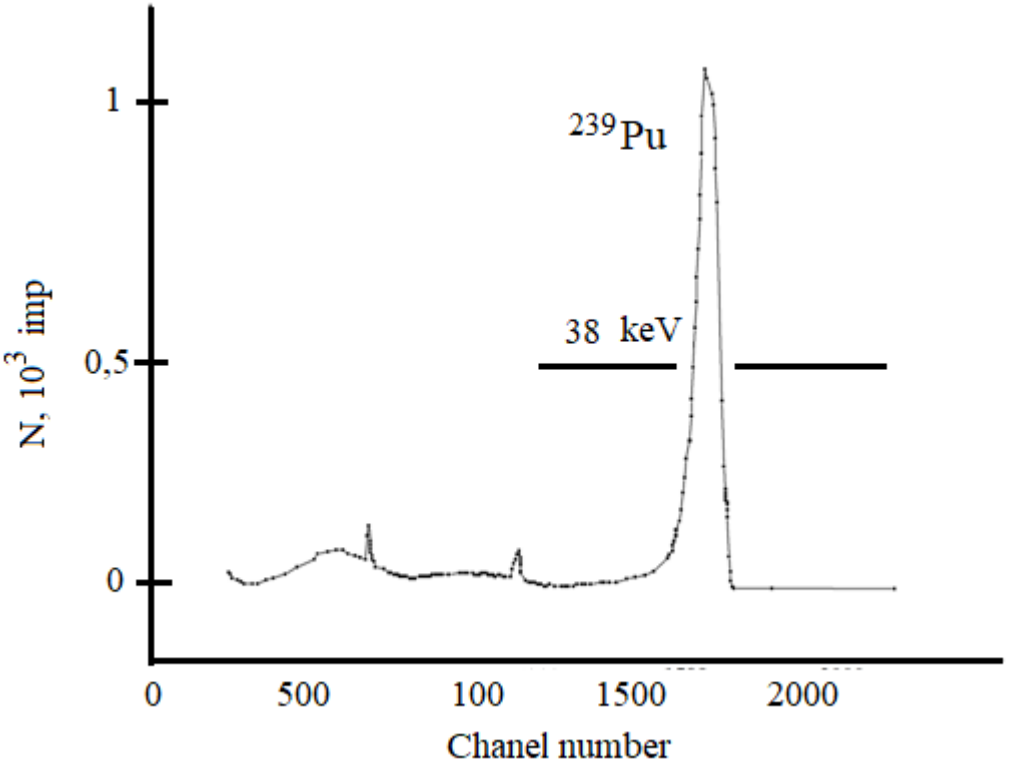

a)

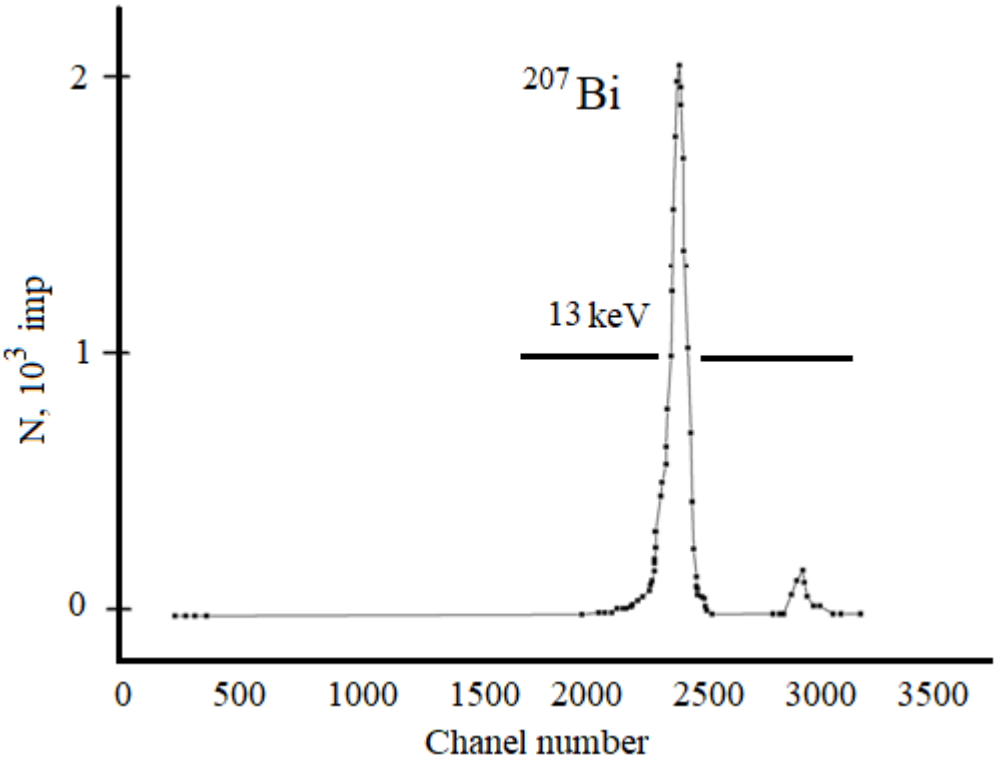

б)

Figure. 4.4. Energy spectra of the detecting system with use of a) α- particles ^{239}Pu and б) β- beta particles ^{207}Bi.

At the detector, the energy resolution along the 5157 keV line of the ^{239}Pu alpha radiation source was 38 keV. The energy equivalent of the noise in this case was equal to 20.6 keV and for β- particles of ^{207}Bi energy resolution is R_β= 13 keV. As shown in Figure. 4.4.

Consequently, a slight difference between the experimental E_β value and the theoretical value may be due to the fluctuation of energy loss in the detector input window, or the fluctuation of carrier collection efficiency associated with the above effects, in particular, the effects of photo-voltage pulse and the effect of elongation of the carrier path charge. Thus, the observed difference in E_β values (theoretical and experimental) is due to the influence of local inhomogeneities in the bulk of a semiconductor crystal.

CONCLUSION

In the work, it was improved the technological processes of mechanical and chemical processing of semiconductor wafers based on silicon of a large area. The optimal modes of diffusion of lithium ions in p-Si of large diameter are determined. It should be noted that with such heating of high silicon to a temperature above 400 ° C, which leads to a decrease in the lifetime of charge carriers decreases.

Correspondingly, the calculations and experimental data have shown that the optimal regime for lithium diffusion to obtain large-diameter detectors (≥110 mm) with a thickness of the sensitive region $W \geq 4mm$ is at a temperature $T = (450 \pm 20)\ ^0C$, t = 3 min, h_{Li} = (300 ± 10) mm. According to the results of the experimental diffusion profile, it can be seen that a mono- crystalline silicon obtained by the floating zone method is well diffusible. The penetration of lithium ions into a mono- crystalline silicon obtained by the Czochralski method has a peculiar slowed-down character in comparison with the crystal obtained by the floating zone method. This is due to a decrease in the effective diffusion coefficient due to the complex formation of Li- O in oxygen-containing silicon obtained by the Czochralski method.

For semiconductor detectors used for low -background installations, this result is very important because it opens up possibilities for improving their performance - increasing registration efficiency through the formation of precision diffusion of thin controlled "Dead Layers" and decreasing the slope of the counting characteristic, especially in the area of low operating voltages. And also, improves the energy resolution of a semiconductor detector.

According to the double-sided drift of lithium, it can be cancluded that the theoretical assumptions of this model are proposed on the basis of Pell's theory, in which lithium ions drift in the bulk of the crystal with the help of an applied external field from both flat ends of the crystal. The proposed theoretical model is based on the homogeneity of acceptor atoms in a crystal where can be a dynamic equilibrium in which lithium ions move uniformly in the depleted region, producing no net charge in the lithium concentration except in boundary. The experimentally obtained data is consistent with the theory.

Also, the electrophysical characteristics of the detectors obtained from two types of silicon were investigated in the work. As the obtained data show, Czochralski silicon well propagates the drift of lithium ions and has the most appropriate electrophysical characteristic.

For semiconductor detectors used for low-noise installations, this result is very important, since it opens up new possibilities for improving the registration efficiency due to the energy resolution and large dimensions of the detectors.

Designed amplifiers for the silicon detectors has a high speed (rise time not more than 5 nsec), low sensitivity to the magnitude of the input capacitance to ensure that, as a consequence, a low noise amplifier with the level of 0.43 $nV/Hz^{1/2}$ and its stability, as

well as the possibility of matching the impedance of the connected line and the amplifier input. The amplifier is operable at the output capacity of the signal source up to 1500 pF. Characteristics of the amplifier correspond to the world level. Comparison with some samples of current amplifiers, for example LeCroy TRA403, having an input impedance of 300 Ohms, rise time of 7 nsec and noise current (standard deviation) 35 na for the signal source capacitance of 10 pF, shows the correctness of the selected circuit solution.

It was shown that when choosing a digitizer as applied to the needs of a nuclear physics experiment, in contrast to classical applications, there are a number of features. The frequency and digit capacity of the digitizer, as well as the sample length, should be selected taking into account the physics of the processes occurring in the detector, and the peculiarities of the background conditions.

The software used both at the accumulation stage and in processing the measurement results has a number of features that are analyzed in this chapter.

Designed amplifiers for the silicon detectors has a high speed (rise time not more than 5 nsec), low sensitivity to the magnitude of the input capacitance to ensure that, as a consequence, a low noise amplifier with the level of 0.43 nV/Hz1/2 and its stability, as well as the possibility of matching the impedance of the connected line and the amplifier input. The amplifier is operable at the output capacity of the signal source up to 1500 pF. Characteristics of the amplifier correspond to the world level. Comparison with some samples of current amplifiers, for example LeCroy TRA403 [119], having an input impedance of 300 Ohms, rise time of 7 nsec and noise current (standard deviation) 35 nA for the signal source capacitance of 10 pF, shows the correctness of the selected circuit solution.

The use of the amplifier is also possible in silicon trigger systems, calorimetry, track and other silicon systems, when it is required to provide the above high parameters of the amplifier.

A Labview subroutine library has been developed, consisting of three blocks. 1) Subroutines that simulate the work of the most common electronic modules in experimental nuclear physics. 2) Subroutines based on classical algorithms. 3) General purpose subprograms.

REFERENCES

1. Dearnaley G., Northrop D. C. Semiconductor counters for nuclear radiation. – 1963.– Vol. 406. – №5. – pp. 336 – 348.

2. Stolyarova E. L. Semiconductor detectors of nuclear radiation // Soviet Physics Advantages. – 1964. – Vol. 6. – № 6. – pp.872 – 887.

3. Goulding F. S. Semiconductor detectors for nuclear spectrometry, I // Nuclear Instruments and Methods. – 1966. – Vol. 43. – № 1. – pp. 1 – 54.

4. Beams I. C. E. E. et al. STUDIES OF COLLIDING ELECTRON-ELECTRON, POSITRON-ELECTRON AND PROTON-PROTON BEAMS AT THE INSTITUTE FOR NUCLEAR PHYSICS, THE SIBERIAN BRANCH OF THE USSR ACADEMY OF SCIENCES // Proceedings. – USAEC Division of Technical Information Extension, 1963. – Vol. 157. – № 3. – pp. 334 – 363.

5. Goulding F. S., Stone Y. Semiconductor Radiation Detectors: Basic principles and some uses of a recent tool that has revolutionized nuclear physics are described // Science. – 1970. – Vol. 170. – № 3955. – pp. 280 – 289.

6. Sellin P. J. Recent advances in compound semiconductor radiation detectors // Nuclear Instruments and Methods in Physics Research Section A: Accelerators, Spectrometers, Detectors and Associated Equipment. – 2003. – Vol. 513. – №1 – 2. – pp. 332 – 339.

7. Lechner P. et al. Silicon drift detectors for high count rate X-ray spectroscopy at room temperature // Nuclear Instruments and Methods in Physics Research Section A: Accelerators, Spectrometers, Detectors and Associated Equipment. – 2001. – Vol. 458. – №1 – 2. – pp. 281 – 287.

8. Hess K. Advanced theory of semiconductor devices. New York, Publ., 2000. pp. 283 – 286.

9. Liu W. et al. Fundamentals of III-V Devices: HBTs, MESFETs, and HFETs/HEMTs. New York, Publ., 1999. pp. 151 – 158.

10. Akimov Y. K. Silicon radiation detectors // Instruments and Experimental Techniques. – 2007. – Vol. 50. – №1. – pp. 1 – 28.

11. Krammer M. Instrumentation at the LHC—The silicon tracking systems// Nuclear Instruments and Methods in Physics Research Section A: Accelerators, Spectrometers, Detectors and Associated Equipment. – 2013. – Vol. 699. – № 6 – pp. 134 – 138.

12. Peisert A. Silicon microstrip detectors // Instrumentation in High Energy Physics. Singapore, Publ., 1992. pp. 1 – 79.

13. Lindström G., Moll M., Fretwurst E. Radiation hardness of silicon detectors–a challenge from high-energy physics // Nuclear Instruments and Methods in Physics Research Section A: Accelerators, Spectrometers, Detectors and Associated Equipment. – 1999. – Vol. 426. – №1. – pp. 1 – 15.

14. Chaudhry R. et al. Surface barrier detectors from p-type Si. – Bhabha Atomic Research Centre. – 1971. – Vol. 4. – № 17. – pp. 3 – 8.

15. Scholze F. et al. Determination of the electron–hole pair creation energy for semiconductors from the spectral responsivity of photodiodes // Nuclear Instruments and Methods in Physics Research Section A: Accelerators, Spectrometers, Detectors and Associated Equipment. – 2000. – Vol. 439. – №2 – 3. – pp. 208 – 215.

16. Sze S. M., Ng K. K. Physics of semiconductor devices. – John Wiley sons, Hoboken, Publ.,2006. pp. 135 –150.

17. Haller E. E., Hansen W. L., Goulding F. S. Physics of ultra-pure germanium // Advances in Physics. – 1981. – Vol. 30. – №1. – pp. 93 – 138.

18. Rudakov V. I., Ovcharov V. V., Bashmakov A. V. Modeling diffusion of ion-implanted impurity in silicon under a temperature gradient // Micro-and Nanoelectronics 2003. – International Society for Optics and Photonics, 2004. – Vol. 5401. №15. – pp. 662 – 669.

19. Campbell J. L. et al. Simulations of Si (Li) x-ray detector response // X-Ray Spectrometry: An International Journal. – 2001. – Vol. 30. – №4. – pp. 230 – 241.

20. Drechsel J. et al. High efficiency organic solar cells based on single or multiple PIN structures // Thin Solid Films. – 2004. – Vol. 451. – №5. – pp. 515 – 517.

21. Delaney C. F. G., Finch E. C. Radiation detectors: physical principles and applications. Oxford University Press, New York, Publ., 1992. pp. 256 – 264.

22. Imamoto K., Yoshiba M., Iso F. Environment-conscious building materials comprising pulverized plaster board, fly ash and ground granulated blast-furnace slag // International Conference on Sustainable Construction Materials and Technologies, Proceedings of Special Sessions. – 2007. – Vol. 27. – № 1. – pp. 157 – 162.

23. Taguchi K. et al. An analytical model of the effects of pulse pileup on the energy spectrum recorded by energy resolved photon counting x-ray detectors // Medical physics. – 2010. – Vol. 37. – № 8. – pp. 3957 – 3969.

24. Wilford J. R., Bierwirth P. N., Craig M. A. Application of airborne gamma-ray spectrometry in soil/regolith mapping and applied geomorphology // AGSO Journal of Australian Geology and Geophysics. – 1997. – Vol. 17. – № 2. – pp. 201 – 216.

25. Kemmer J. Improvement of detector fabrication by the planar process // Nuclear Instruments and Methods in Physics Research Section A: Accelerators, Spectrometers, Detectors and Associated Equipment. – 1984. – Vol. 226. – № 1. – pp. 89 – 93.

26. Tremsin A. S. et al. Novel high-resolution readout for UV and x-ray photon counting detectors with microchannel plates // High Energy, Optical, and Infrared Detectors for Astronomy II. – International Society for Optics and Photonics. – 2006. – Vol. 6276. – № 16. – pp. 139 – 151.

27. Alice Collaboration. Performance of the ALICE Experiment at the CERN LHC // International Journal of Modern Physics. –2014. – Vol. 29. – №24. – pp. 3 – 10.

28. Anghinolfi F. et al. A 1006 element hybrid silicon pixel detector with strobed binary output // IEEE transactions on nuclear science. – 1992. – Vol. 39. – №4. – pp. 654 – 661.

29. Kemmer J. Fabrication of low noise silicon radiation detectors by the planar process // Nuclear Instruments and Methods. – 1980. – Vol. 169. – № 3. – pp. 499 – 502.

30. Patolsky F., Zheng G., Lieber C. M. Fabrication of silicon nanowire devices for ultrasensitive, label-free, real-time detection of biological and chemical species // Nature protocols. – 2006. – Vol. 1. – № 4. – pp. 1711 – 1724.

31. Desa M. K. M. et al. Silicon back contact solar cell configureuration: A pathway towards higher efficiency // Renewable and sustainable energy reviews. – 2016. – Vol. 60. – № 2. – pp. 1516 – 1532.

32. Wang Q. et al. Development of a fluorescence polarization immunoassay for the detection of melamine in milk and milk powder // Analytical and bioanalytical chemistry. – 2011. – Vol. 399. – № 6. – pp. 2275 – 2284.

33. Campbell M. et al. Detection of single electrons by means of a Micromegas-covered MediPix2 pixel CMOS readout circuit // Nuclear Instruments and Methods in Physics Research Section A: Accelerators, Spectrometers, Detectors and Associated Equipment. – 2005. – Vol. 540. – № 2 – 3. – pp. 295 – 304.

34. Piuz F. et al. The CsI-based ring imaging detector for the ALICE experiment: technical description of a large prototype // Nuclear Instruments and Methods in Physics Research Section A: Accelerators, Spectrometers, Detectors and Associated Equipment. – 1999. – Vol. 433. – № 1 – 2. – pp. 222 – 234.

35. Keil M. et al. Radiation damage effects in the NA60 silicon pixel detectors // Nuclear Instruments and Methods in Physics Research Section A: Accelerators, Spectrometers, Detectors and Associated Equipment. – 2005. – Vol. 552. – № 1 – 2. – pp. 239 – 243.

36. Freund H. P. et al. Theory of the free-electron laser based upon a coaxial hybrid wiggler // Nuclear Instruments and Methods in Physics Research Section A: Accelerators, Spectrometers, Detectors and Associated Equipment. – 1995. – Vol. 358. – № 1 – 3. – pp. 139 – 142.

37. Cattai A. et al. Dosimetry with micro strip gas chambers // Nuclear Instruments and Methods in Physics Research Section A: Accelerators, Spectrometers, Detectors and Associated Equipment. – 1995. – Vol. 367. – № 1 – 3. – pp. 62 – 65.

38. Gys T. et al. Latest results from the TORCH R&D Project // Nuclear Instruments and Methods in Physics Research Section A: Accelerators, Spectrometers, Detectors and Associated Equipment. – 2018. – Vol. 912. – № 3. – pp. 53 – 56.

39. Turqueti M. et al. Study of temperature dependence of bump bonding for the BTeV pixel detector // IEEE Transactions on Nuclear Science. – 2004. – Vol. 51. – № 5. – pp. 2161 – 2167.

40. Gemme C. et al. Study of indium bumps for the ATLAS pixel detector // Nuclear Instruments and Methods in Physics Research Section A: Accelerators,

Spectrometers, Detectors and Associated Equipment. – 2001. – Vol. 465. – № 1. – pp. 200 – 203.

41. Klaiber-Lodewigs J. M. et al. Evaluation of testing strategies for the radiation tolerant ATLAS n+-in-n pixel sensor // Nuclear Instruments and Methods in Physics Research Section A: Accelerators, Spectrometers, Detectors and Associated Equipment. – 2003. – Vol. 512. – № 1 – 2. – pp. 332 – 340.

42. Ta D. B. et al. Serial powering: Proof of principle demonstration of a scheme for the operation of a large pixel detector at the LHC // Nuclear Instruments and Methods in Physics Research Section A: Accelerators, Spectrometers, Detectors and Associated Equipment. – 2006. – Vol. 557. – № 2. – pp. 445 – 459.

43. Coluccia M. R. et al. Electrical characterization of irradiated prototype silicon pixel sensors for BTeV // 2002 IEEE Nuclear Science Symposium Conference Record. – IEEE, 2002. – Vol. 1. – № 5. – pp. 638 – 644.

44. Heijne E. H. M. et al. LHC1: A semiconductor pixel detector readout chip with internal, tunable delay providing a binary pattern of selected events // Nuclear Instruments and Methods in Physics Research Section A: Accelerators, Spectrometers, Detectors and Associated Equipment. – 1996. – Vol. 383. – № 1. – pp. 55 – 63.

45. Amendolia S. R. et al. A Ge-Si active target for the measurement of short lifetimes //Nuclear Instruments and Methods in Physics Research Section A: Accelerators, Spectrometers, Detectors and Associated Equipment. – 1984. – Vol. 226. – № 1. – pp. 78-81.

46. Akimov Y. K. Silicon radiation detectors // Instruments and Experimental Techniques. – 2007. – Vol. 50. – № 1. – pp. 1 – 28.

47. Ropotar I. An investigation of silicon pixel tracking detectors and their aplication in a prototype vertex telescope in the CERN NA50 heavy-ion experiment. – Wuppertal U., 2000. – pp. 34 – 39.

48. Amidei D. et al. The silicon vertex detector of the Collider Detector at Fermilab // Nuclear Instruments and Methods in Physics Research Section A: Accelerators, Spectrometers, Detectors and Associated Equipment. – 1994. – Vol. 350. – № 1 – 2. – pp. 73 – 130.

49. Anelli G. et al. The totem experiment at the cern large hadron collider // Journal of Instrumentation. – 2008. – Vol. 3. – № 8. – pp. 38 – 45.

50. Allport P. P. et al. FOXFET biassedmicrostrip detectors // Nuclear Instruments and Methods in Physics Research Section A: Accelerators, Spectrometers, Detectors and Associated Equipment. – 1991. – Vol. 310. – № 1 – 2. – pp. 155 – 159.

51. Abraamyan K. U. et al. The MPD detector at the NICA heavy-ion collider at JINR // Nuclear Instruments and Methods in Physics Research Section A: Accelerators, Spectrometers, Detectors and Associated Equipment. – 2011. – Vol. 628. – № 1. – pp. 99 – 102.

52. Sadrozinski H. F. W. Silicon microstrip detectors in high luminosity application // IEEE Transactions on Nuclear Science. – 1998. – Vol. 45. – № 3. – pp. 295 – 302.

53. Litke A. et al. A silicon strip vertex detector for the Mark II experiment at the SLAC linear collider // Nuclear Instruments and Methods in Physics Research. Section A, Accelerators, Spectrometers, Detectors and Associated Equipment. – 1988. – Vol. 265. – № 1 – 2. – pp. 93 – 98.

54. Picozza P. et al. PAMELA–A payload for antimatter matter exploration and light-nuclei astrophysics // Astroparticle physics. – 2007. – Vol. 27. – № 4. – pp. 296 – 315.

55. Michelson P. F. GLAST: A detector for high-energy gamma rays // Gamma-Ray and Cosmic-Ray Detectors, Techniques, and Missions. – International Society for Optics and Photonics, 1996. – Vol. 2806. – № 5. – pp. 31 – 41.

56. Kanbach G. et al. Development and calibration of the tracking Compton/Pair telescope MEGA // Nuclear Instruments and Methods in Physics Research Section A: Accelerators, Spectrometers, Detectors and Associated Equipment. – 2005. – Vol. 541. – № 1 – 2. – pp. 310 – 322.

57. Booth I. S., Mann R. B. Static and infalling quasilocal energy of charged and naked black holes // Physical Review D. – 1999. – Vol. 60. – № 12. – pp. 14 – 17.

58. Gruner S. M., Eikenberry E. F., Tate M. W. Comparison of X-ray detectors // International Tables for Crystallography Volume F: Crystallography of biological macromolecules. – Springer, Dordrecht, 2006. – Vol. 7. – № 1. – pp. 143 – 147.

59. Goldstein J. I. et al. Scanning electron microscopy and X-ray microanalysis. – Springer, Publ., 2017. pp. 302 – 322.

60. Landis D. A. et al. Transistor reset preamplifier for high rate high resolution spectroscopy // IEEE Transactions on Nuclear Science. – 1982. – Vol. 29. – № 1. – pp. 619 – 624.

61. Herrero M. The standard model // Techniques and Concepts of High Energy Physics X. – Springer, Dordrecht, Publ., 1999. pp. 1 – 59.

62. Scandale W., Prest M. Proposal of the CRYSTAL experiment. – 2008. – Vol. 335. – № 14. – pp. 9 – 18.

63. Spieler H. Semiconductor detector systems. – Oxford university press, Oxford, 2005. pp. 315 – 330.

64. Goulding, F. S., and D. A. Landis. Signal processing for semiconductor detectors. // IEEE Transactions on Nuclear Science. – 1982. – Vol. 29. – № 3. – pp. 1125 – 1141.

65. Granfors P. R., Aufrichtig R. Performance of a 41× 41cm2 amorphous silicon flat panel x-ray detector for radiographic imaging applications // Medical physics. – 2000. – Vol. 27. – № 6. – pp. 1324 – 1331.

66. Horisberger R., Pitzl D. A novel readout chip for silicon strip detectors with analog pipeline and digitally controlled analog signal processing // Nuclear Instruments and Methods in Physics Research Section A: Accelerators, Spectrometers, Detectors and Associated Equipment. – 1993. – Vol. 326. – № 1 – 2. – pp. 92 – 99.

67. Bingefors N. et al. A novel technique for fast pulse-shaping using a slow amplifier at LHC // Nuclear Instruments and Methods in Physics Research Section A: Accelerators, Spectrometers, Detectors and Associated Equipment. – 1993. – Vol. 326. – № 1 – 2. – pp. 112 – 119.

68. Valley G. C. Photonic analog-to-digital converters // Optics express. – 2007. – Vol. 15. – № 5. – pp. 1955 – 1982.

69. Alekseev E. N. et al. Possible detection of a neutrino signal on 23 February 1987 at the Baksan underground scintillation telescope of the Institute of Nuclear Research // JETP Lett. – 1987. – Vol. 45. № 7 – С. 739 – 744.

70. Beddar A. S., Mackie T. R., Attix F. H. Water-equivalent plastic scintillation detectors for high-energy beam dosimetry: I. Physical characteristics and theoretical considerations // Physics in Medicine & Biology. – 1992. – Vol. 37. – № 10. – pp. 1883 – 1886.

71. Kim J. et al. Multiphoton detection using visible light photon counter // Applied Physics Letters. – 1999. – Vol. 74. – № 7. – pp. 902 – 904.

72. Fossum E. R. CMOS image sensors: Electronic camera-on-a-chip // IEEE transactions on electron devices. – 1997. – Vol. 44. – № 10. – pp. 1689 – 1698.

73. Kleinfelder S. A. et al. A flexible 128 channel silicon strip detector instrumentation integrated circuit with sparse data readout // IEEE Transactions on Nuclear Science. – 1988. – Vol. 35. – № 1. – pp. 171 – 175.

74. J. Butler. Triggering and Data Acquisition General Considerations. // in Instrumentation in Elementary Particle Physics, AIP Conf. Proc. – 2003. Vol. 674. – № 3. – pp. 101 – 129.

75. Kondo T. et al. Construction and performance of the ATLAS silicon microstrip barrel modules // Nuclear Instruments and Methods in Physics Research Section A: Accelerators, Spectrometers, Detectors and Associated Equipment. – 2002. – Vol. 485. – № 1 – 2. – pp. 27 – 42.

76. Ikeda S. et al. Development of a real-time digital radiography system using a scintillator-type flat-panel detector // Medical Imaging 2001: Physics of Medical Imaging. – International Society for Optics and Photonics. – 2001. – Vol. 4320. – № 1. – pp. 516 – 524.

77. Grybos P., Szczygiel R. Pole-zero cancellation circuit with pulse pile-up tracking system for low noise charge-sensitive amplifiers // IEEE Transactions on Nuclear Science. – 2008. – Vol. 55. – № 1. – pp. 583 – 590.

78. Noulis T., Siskos S., Sarrabayrouse G. Noise optimised charge-sensitive CMOS amplifier for capacitive radiation detectors // IET circuits, devices & systems. – 2008. – Vol. 2. – № 3. – pp. 324 – 334.

79. Saukoski M. et al. Fully integrated charge sensitive amplifier for readout of micromechanical capacitive sensors // Circuits and Systems, 2005. ISCAS 2005. IEEE International Symposium on. – IEEE. – 2005. – Vol. 2. – № 4. – pp. 5377 – 5380.

80. Wang W. et al. Note: A charge sensitive spectroscopy amplifier for position sensitive micro-channel plate detectors // Review of Scientific Instruments. – 2014. – Vol. 85. – № 10. – 106104 p.

81. Chang Z. Y. and Sansen W. Effect of 1/f noise on the resolution of CMOS analog readout systems for microstrip and pixel detectors. // Nuclear Instruments and Methods. –2004. – Vol. 305. – № 3. – pp. 553 – 560.

82. Sansen W. M. C., Chang Z. Y. Limits of low noise performance of detector readout front ends in CMOS technology // IEEE transactions on circuits and systems. – 1990. – Vol. 37. – № 11. – pp. 1375 – 1382.

83. Kapnistis C., Misiakos K., Haralabidis N. Noise performance of pixel readout electronics using very small area devices in CMOS technology // Nuclear Instruments and Methods in Physics Research Section A: Accelerators, Spectrometers, Detectors and Associated Equipment. – 2001. – Vol. 458. – № 3. – pp. 729 – 737.

84. Hu Y. et al. A low-noise, low-power CMOS SOI readout front-end for silicon detector leakage current compensation with capability // IEEE Transactions on Circuits and Systems I: Fundamental Theory and Applications. – 2001. – Vol. 48. – № 8. – pp. 1022 – 1030.

85. Grybos P. et al. RX64DTH-a fully integrated 64-channel ASIC for a digital X-ray imaging system with energy window selection // IEEE transactions on nuclear science. – 2005. – Vol. 52. – № 4. – pp. 839 – 846.

86. Randazzo N. et al. Integrated front-end for a large strip detector with E,/spl Delta/E and position measurements // IEEE Transactions on Nuclear Science. – 1999. – Vol. 46. – № 5. – pp. 1300 – 1309.

87. Grybos P., Dabrowski W. Development of a fully integrated readout system for high count rate position-sensitive measurements of X-rays using silicon strip detectors // IEEE Transactions on Nuclear Science. – 2001. – Vol. 48. – № 3. – pp. 466 – 472.

88. Kapnistis C., Misiakos K., Haralabidis N. A small area charge sensitive readout chain with a dual mode of operation // Analog Integrated Circuits and Signal Processing. – 2001. – Vol. 27. – № 1 – 2. – pp. 39 – 48.

89. Stanton J. C. A low power low noise amplifier for a 128 channel detector read-out chip // IEEE Transactions on Nuclear Science. – 1989. – Vol. 36. – №. 1. – pp. 522 – 527.

90. Inubushi Y. et al. Determination of the pulse duration of an X-ray free electron laser using highly resolved single-shot spectra // Physical review letters. – 2012. – Vol. 109. – № 14. – 144801 p.

91. Feser M. et al. Integrating Silicon detector with segmentation for scanning transmission X-ray microscopy // Nuclear Instruments and Methods in Physics Research Section A: Accelerators, Spectrometers, Detectors and Associated Equipment. – 2006. – Vol. 565. – № 2. – pp. 841 – 854.

92. Chen P. et al. A time-to-digital-converter-based CMOS smart temperature sensor // IEEE Journal of Solid-State Circuits. – 2005. – Vol. 40. – № 8. – pp. 1642 – 1648.

93. Lee H. S., Sodini C. G. Analog-to-digital converters: Digitizing the analog world // Proceedings of the IEEE. – 2008. – Vol. 96. – № 2. – pp. 323 – 334.

94. Walden R. H. Analog-to-digital converter survey and analysis // IEEE Journal on selected areas in communications. – 1999. – Vol. 17. – № 4. – pp. 539 – 550.

95. Roberts G. W., Ali-Bakhshian M. A brief introduction to time-to-digital and digital-to-time converters // IEEE Transactions on Circuits and Systems II: Express Briefs. – 2010. – Vol. 57. – № 3. – pp. 153 – 157.

96. Wilkinson D. H. A stable ninety-nine channel pulse amplitude analyser for slow counting // Mathematical Proceedings of the Cambridge Philosophical Society. – Cambridge University Press. – 1950. – Vol. 46. – № 3. – pp. 508 – 518.

97. Azimov S.A., Muminov R.A., Bayzakov B.B., KarpovV.D., RadzhapovS.A., KhasanovD.K., YafasovA.YA. Poluprovodnikovyye detektory beta-izlucheniya bol'shoy ploshchadi. // Atomnayaenergiya. – 1986. – Vol. 60. – № 2. – pp. 144 – 146.

98. Miyachi T. et al. A thick and large active area Si (Li) detector // Japanese journal of applied physics. – 1988. – Vol. 27. – № 2. – 307 p.

99. PichuginI.G., TairovYu.M. Tekhnologiyapoluprovodnikovykhpriborov. – M.: Vysshayashk , 1984. – pp. 33 – 40.

100. Gorina S.N. Travleniye poluprovodnikov. – M.: Sb. Stat'i. Izd-vo Mir, 1965. – 380 p.

101. Boltaks B.I. Diffuziya v poluprovodnikakh – M.: Fizmatgiz, 1961. – 462 p.

102. Xogan R.A., Petirs N.J., Diffusion in oxygen in silicon. // J.Appl.Phys. –1959. – Vol. 30. – № 2. – 1627 p.

103. Radzhapov S.A. Issledovaniya osobennostey protsessa diffuzii litiya v kremnii vyrashchennogo metodom Chokhral'skogo. // UFZH. – Tashkent. – 2007. – Vol. 9. – № 3. – pp. 190 – 194.

104. Radzhapov S. A. Diffusion formation of the i region in Si (Li) detectors of nuclear radiation // Atomic Energy. – 2007. – Vol. 102. – № 6. – pp. 484 – 486.

105. Radzhapov S.A., Saymbetov A.K., Abdugafurov A.M. Osobennosti protsessa diffuzii litiya v Si (Li) detektorakh bol'shikh ploshchadey. // Fundamental'nyye i prikladnyye problemy fiziki poluprovodnikov: Tez.dokal. Mezhd. nauch. konf. 20-21 dekabrya 2005 goda. – Andizhan. – 2005. – Vol. 1. – № 300. – pp. 130 – 131.

106. Akimov Y.K., Kalinin A.I., Kushniruk V.R., Yungklaussen X. Poluprovodnikovyye detektory vybra chastits i ikh primeneniya. – M. – Atomizdat, 1967. – 253 p.

107. Radzhapov S.A. Osobennosti protsessa dreyfa ionov litiya v nizkoomnom kremnii bol'shogo diametra. // DAN RUz. – Tashkent. – 2007. – № 2. – pp. 17 – 21.

108. Azimov S.A., Muminov R.A., Shamirzayev S.K, Yafasov A.Y. Kremniy-litiyevyye detektory yadernogo izlucheniya. –Tashkent. – Fan, 1981. – 257 p.

109. Suarez F. F., Cusumano M. A., Fine C. H. An empirical study of manufacturing flexibility in printed circuit board assembly // Operations research. – 1996. – Vol. 44. – № 1. – pp. 223 – 240.

110. Huang K., Guo J., Xu Z. Recycling of waste printed circuit boards: A review of current technologies and treatment status in China // Journal of hazardous materials. – 2009. – Vol. 164. – № 2 – 3. – pp. 399 – 408.

111. Domingos P. Metacost: A general method for making classifiers cost-sensitive // KDD. – 1999. – Vol. 99. – № 3. – pp. 155 – 164.

112. Wego A., Richter S., Pagel L. Fluidic microsystems based on printed circuit board technology // Journal of Micromechanics and microengineering. – 2001. – Vol. 11. – № 5. – pp. 528.

113. Ball M. O., Magazine M. J. Sequencing of insertions in printed circuit board assembly // Operations Research. – 1988. – Vol. 36. – № 2. – pp. 192 – 201.

114. Ridenour J. A., Rundberg R. S. NSSC-LANL Keepin Nonproliferation Science Summer Program Silicon Drift Detectors: X-ray Spectroscopy. – Los Alamos National Lab. (LANL), Los Alamos, NM (United States), 2018. – 9 p.

115. Liu J. et al. Simulations of depleted CMOS sensors for high-radiation environments // Journal of Instrumentation. – 2017. – Vol. 12. – № 11. – 11013 p.

116. Muminov R. A., Radzhapov S. A., Saimbetov A. K. Developing Si (Li) nuclear radiation detectors by pulsed electric field treatment // Technical Physics Letters. – 2009. – Vol. 35. – № 8. – pp. 768 – 769.

117. Zhang J. et al. Towards Gotthard-II: development of a silicon microstrip detector for the European X-ray Free-Electron Laser // Journal of Instrumentation. – 2018. – Vol. 13. – № 1. – 1025 p.

118. Obertino M. M. Silicon sensor technologies for timing, 2017. – 3 p.

119. Muminov R. A., Radzhapov S. A., Saimbetov A. K. Silicon-lithium telescopic detector in one crystal // Atomic energy. – 2009. – Vol. 106. – № 2. – pp. 141 – 142.

120. Salim E. T. et al. Synthesis of Cadmium Oxide/Si Heterostructure for Two-Band Sensor Application // Iranian Journal of Science and Technology, Transactions A: Science. – 2018. – Vol. 11. – № 1. – pp. 1 – 7.

121. Muminov, R. A., A. K. Saymbetov, and Yo K. Toshmurodov. Special features of formation of high-performance semiconductor detectors based on αSi-Si (Li) heterostructures. // Instruments and Experimental Techniques. – 2013. – Vol. 56. – № 1. – pp. 32 – 33.

122. Ackermann K. H. et al. STAR detector overview // Nuclear Instruments and Methods in Physics Research Section A: Accelerators, Spectrometers, Detectors and Associated Equipment. – 2003. – Vol. 499. – № 2 – 3. – pp. 624 – 632.

123. Protic D., Krings T., Schleichert R. Development of double-sided microstructured Si (Li) detectors // IEEE Transactions on Nuclear Science. – 2002. – Vol. 49. – № 4. – pp. 1993 – 1998.

124. Mil'Vidsky M. G., Osvensky V. B., Shifrin S. S. Effect of doping on formation of dislocation structure in semiconductor crystals // Journal of Crystal Growth. – 1981. – Vol. 52. – № 2. – pp. 396 – 403.

125. Muminov R. A., Sambetov A.K., Japashov N.M., et al. Double Sided Diffusion and Drift of Lithium Ions on Large Volume Silicon Detector Structure // Journal of semiconductor technology and science. – 2017. – Vol. 17. – № 5. – pp. 591 – 596.

126. Comyn J. Introduction to polymer permeability and the mathematics of diffusion // Polymer permeability. – Springer, Dordrecht. – 1985. – Vol. 3. – № 2. – pp. 1 – 10.

127. Crank J. et al. The mathematics of diffusion. – Oxford university press, 1979. – 352 p.

128. Chapman S., Cowling T. G., Burnett D. The mathematical theory of non-uniform gases: an account of the kinetic theory of viscosity, thermal conduction and diffusion in gases. – Cambridge university press, 1990. – 382 p.

129. Chen C. M. et al. A Fourier method for the fractional diffusion equation describing sub-diffusion // Journal of Computational Physics. – 2007. – Vol. 227. – № 2. – pp. 886 – 897.

130. Malkovich, R. S. Matematika diffuzii v poluprovodnikakh. – SPb: Nauka, 1999. – 380 p.

131. Krasheninnikov A. V. When defects are not defects // Nature materials. – 2018. – Vol. 17. – № 9. – 757 p.

132. Khedhiri L. et al. Crystal structure, hirshfeld surface analysis, thermal behavior and spectroscopic investigations of a new organic cyclohexaphosphate,(C 10 H 15 N 2) 4 (Li) 2 (P 6 O 18)(H 2 O) 6 // Journal of Molecular Structure. – 2018. – Vol. 1171. – № 5. – pp. 429 – 437.

133. Pell E. M. Ion Drift in an n-p Junction // Journal of Applied Physics. – 1960. – Vol. 31. – № 2. – pp. 291 – 302.

134. Lehrer F. A., Reiss H. Details of Ion Drift in an n-p Junction // Journal of Applied Physics. – 1962. – Vol. 33. – № 7. – pp. 2353 – 2359.

135. Gibbons P. E., Iredale P. On the accuracy of acceptor compensation by lithium ion drift // Nuclear Instruments and Methods. – 1967. – Vol. 53. – № 1. – pp. 1 – 6.

136. Lauber A. On the theory of compensation in lithium drifted semiconductor detectors. – AB Atomenergi, 1969. – 356 p.

137. Luke P. N. et al. Recent developments in semiconductor gamma-ray detectors // Journal of radioanalytical and nuclear chemistry. – 2005. – Vol. 264. – № 1. – pp. 145 – 153.

138. Luke, Paul N., et al. Recent developments in semiconductor gamma-ray detectors. // Journal of radioanalytical and nuclear chemistry. – 2005. – Vol. 264. –№ 1. – pp. 145 – 153.

139. Shi W. et al. The PIN detector parallel application // Nuclear Electronics and Detection Technology. – 2007. – Vol. 27. – № 5. – pp. 908 – 910.

140. Protic D., Krings T., Schleichert R. Development of double-sided microstructured Si (Li) detectors // IEEE Transactions on Nuclear Science. – 2002. – Vol. 49. – № 4. – pp. 1993 – 1998.

141. N. M. Japashov, N. B. Kuttybay, M. K. Nurgaliyev. Readout electronics of detecting system based on silicon strip detectors // International Scientific Conference of Students and Young Scientists «Farabi Alemi», April 9- 12, 2018, Almaty, Kazakhstan, Book of Abstracts, ed. by A. E. Davletov. – 2018. – Vol. 4. –№ 1. – 316 p.

142. N. M. Japashov, Ye. Tulkibaiuly. Output signal characteristics of silicon strip detectors // International Scientific Conference of Students and Young Scientists «Farabi Alemi», April 9- 12, 2018, Almaty, Kazakhstan, Book of Abstracts, ed. by A. E. Davletov. – 2018. – Vol. 5. – № 3. – 317 p.

143. Saymbetov A. K., Japashov N.M., et al. Development of high sensitive silicon strip detectors of large sizes // Reports of The National Academy of Science of the Republic of Kazakhstan. – 2016. –Vol. 1. – № 305. – pp. 5 – 8.

144. Muminov R. A., Radzhapov S. A., Saimbetov A. K. Developing Si (Li) nuclear radiation detectors by pulsed electric field treatment // Technical Physics Letters. – 2009. – Vol. 35. – № 8. – pp. 768 – 769.

145. Muminov R. A., Saymbetov A.K., Japashov N.M., et al. High-sensing detecting systems for X-ray fluorescence spectrometer. // Bulletin of National Academy of sciences of the republic of Kazakhstan. – 2018. – Vol. 374. – № 4. – pp. 23 – 28.

146. Elbashir S. A. M. Differential Transforms Method Applied to Systems of ODEs, Fractional Integro-Differential and Volterra Integral Equations:diss. – University of Gezira, 2017. – 62 p.

147. N. Japashov, A. Saymbetov, R. Muminov, S. Radzhapov, Yo. Toshmurodov, B. Mukhametkali, N. Sissenov, N. Kuttybay, A. Mansurova. Development of silicon strip detectors of nuclear radiation with orthogonal field // Fourth International Conference on Radiation and Applications in Various Fields of Research, May 23- 27, 2016, Nis, Serbia, Book of Abstracts RAD Conference, ed. by Dr Dragan Mancic. – 2016. – Vol. 251. – № 2. – 184 p.

148. Saymbetov A. K., Japashov N.M., et al. Physical features of formation of silicon p-i-n detector structure // News of The National Academy of Science of the Republic of Kazakhstan Physico- Mathematical Series. – 2016. – Vol. 1. – № 305. – pp. 141 – 144.